Global OZone Chemistry And Related Datasets for the Stratosphere (GOZCARDS): methodology and sample results with a focus on HCl, H_2O, and O_3

L. Froidevaux[1], J. Anderson[2], H.-J. Wang[3], R. A. Fuller[1], M. J. Schwartz[1], M. L. Santee[1], N. J. Livesey[1], H. C. Pumphrey[4], P. F. Bernath[5], J. M. Russell III[2], and M. P. McCormick[2]

[1]Jet Propulsion Laboratory, California Institute of Technology, Pasadena, CA, USA

[2]Hampton University, Hampton, VA, USA

[3]Georgia Institute of Technology, Atlanta, GA, USA

[4]The University of Edinburgh, Edinburgh, UK

[5]Old Dominion University, Norfolk, VA, USA

Correspondence to: L. Froidevaux (lucienf@jpl.nasa.gov)

Abstract

We describe the publicly available data from the Global OZone Chemistry And Related Datasets for the Stratosphere (GOZCARDS) project, and provide some results, with a focus on hydrogen chloride (HCl), water vapor (H_2O), and ozone (O_3). This dataset is a global long-term stratospheric Earth System Data Record, consisting of monthly zonal mean time series starting as early as 1979. The data records are based on high quality measurements from several NASA satellite instruments and ACE-FTS on SCISAT. We examine consistency aspects between the various datasets. To merge ozone records, the time series are debiased relative to SAGE II values by calculating average offsets versus SAGE II during measurement overlap periods, whereas for other species, the merging derives from an averaging procedure during overlap periods. The GOZCARDS files contain mixing ratios on a common pressure/latitude grid, as well as standard errors and other diagnostics; we also present estimates of systematic uncertainties in the merged products. Monthly mean temperatures for GOZCARDS were also produced, based directly on data from the Modern-Era Retrospective analysis for Research and Applications.

The GOZCARDS HCl merged product comes from HALOE, ACE-FTS and lower stratospheric Aura MLS data. After a rapid rise in upper stratospheric HCl in the early 1990s, the rate of decrease in this region for 1997-2010 was between 0.4 and 0.7%/yr. On 6-8 yr timescales, the rate of decrease peaked in 2004-2005 at about 1%/yr, and has since levelled off, at ~0.5%/yr. With a delay of 6-7 years, these changes roughly follow total surface chlorine, whose behavior versus time arises from inhomogeneous changes in the source gases. Since the late 1990s, HCl decreases in the lower stratosphere have occurred with pronounced latitudinal variability at rates sometimes exceeding 1-2%/yr. Recent short-term tendencies of lower stratospheric and column HCl vary substantially, with increases from 2005-2010 for northern mid-latitudes and deep tropics, but decreases (increases) after 2011 at northern (southern) mid-latitudes.

For H_2O, the GOZCARDS product covers both stratosphere and mesosphere, and the same instruments as for HCl are used, along with UARS MLS stratospheric H_2O data (1991-1993). We display seasonal to decadal-type variability in H_2O from 22 years of data. In the upper mesosphere, the anti-correlation between H_2O and solar flux is now clearly visible over two full solar cycles. Lower stratospheric tropical H_2O has exhibited two periods of increasing values,

followed by fairly sharp drops (the well-documented 2000-2001 decrease and a recent drop in 2011-2013). Tropical decadal variability peaks just above the tropopause. Between 1991 and 2013, both in the tropics and on a near-global basis, H_2O has decreased by ~5-10% in the lower stratosphere, but about a 10% increase is observed in the upper stratosphere and lower mesosphere. However, such tendencies may not represent longer-term trends.

For ozone, we used SAGE I, SAGE II, HALOE, UARS and Aura MLS, and ACE-FTS data to produce a merged record from late 1979 onward, using SAGE II as the primary reference. Unlike the 2 to 3% increase in near-global column ozone after the late 1990s reported by some, GOZCARDS stratospheric column O_3 values do not show a recent upturn of more than 0.5 to 1%; long-term interannual column ozone variations from GOZCARDS are generally in very good agreement with interannual changes in merged total column ozone (Version 8.6) data from SBUV instruments..

A brief mention is also made of other currently available, commonly-formatted GOZCARDS satellite data records for stratospheric composition, namely those for N_2O and HNO_3.

1 Introduction

The negative impact of anthropogenic chlorofluorocarbon emissions on the ozone layer, following the early predictions of Molina and Rowland (1974), stimulated interest in the trends and variability of stratospheric ozone, a key absorber of harmful ultraviolet radiation. The discovery of the ozone hole in ground-based data records (Farman et al., 1985) and the associated dramatic ozone changes during southern hemisphere winter and spring raised the level of research and understanding regarding the existence of new photochemical processes (see Solomon, 1999). This research was corroborated by analyses of aircraft and satellite data (e.g., Anderson et al., 1989; Waters et al., 1993), and of independent ground-based data. Global total column ozone averages in 2006-2009 were measured to be smaller than during 1964-1980 by ~3%, and larger more localized decreases over the same periods reached ~6% in the southern hemisphere midlatitudes (WMO, 2011). Halogen source gas emissions have continued to decrease as a result of the Montreal Protocol and its amendments. Surface loading of total chlorine peaked in the early 1990s and subsequent decreases in global stratospheric HCl and ClO have been measured from satellite-based sensors (Anderson et al., 2000; Froidevaux et al., 2006;

Jones et al., 2011) as well as from the ground (e.g., Solomon et al., 2006, Kohlhepp et al., 2012). A slow recovery of the ozone layer towards pre-1985 levels is expected (WMO, 2011; 2014). High quality long-term datasets for ozone and related stratospheric species are needed to document past variability and to constrain global atmospheric models. The history of global stratospheric observations includes a large suite of satellite-based instruments, generally well-suited for the elucidation of long-term global change. A review of differences between past and ongoing satellite measurements of atmospheric composition has been the focus of the Stratosphere-troposphere Processes And their Role in Climate (SPARC) Data Initiative; results for stratospheric H_2O and O_3 intercomparisons have been described by Hegglin et al. (2013) and Tegtmeier et al. (2013), respectively, to be followed by a report on many other species. Systematic biases reported in these papers mirror past validation work.

Under the Global OZone Chemistry And Related Datasets for the Stratosphere (GOZCARDS) project, we have created monthly zonally averaged datasets of stratospheric composition on a common latitude/pressure grid, using high quality data from the following satellite instruments: the Stratospheric Aerosol and Gas Experiments (SAGE I and SAGE II), the Halogen Occultation Experiment (HALOE) which flew aboard the Upper Atmosphere Research Satellite (UARS), the UARS Microwave Limb Sounder (MLS), the Atmospheric Chemistry Experiment Fourier Transform Spectrometer (ACE-FTS) on SCISAT, and Aura MLS. Table 1 provides characteristics of the original datasets; validation papers from the instrument teams and other related studies give a certain degree of confidence in these data. However, the existence of validation references does not imply that there are no caveats or issues with a particular measurement suite. In this project, we have strived to optimize data screening and mitigate some undesirable features, such as the impact of outlier values or the effects of clouds or aerosols. All source data sets still have imperfections, but in creating the GOZCARDS Earth System Data Record (ESDR) we maintain the integrity of the original data and do not arbitrarily disregard data, nor do we typically attempt to fill in spatial or temporal gaps in the record.

Based on original profiles from the various instruments, GOZCARDS "source" monthly zonal mean values were derived. After data screening, monthly average profiles were created by vertical interpolation onto the GOZCARDS pressure levels, followed by binning and averaging

into monthly sets. In order to accomodate the lower vertical resolution of some limb viewers, such as UARS MLS, the GOZCARDS pressure grid was chosen as

$$p(i) = 1000 \times 10^{-\frac{i}{6}} (\text{hPa}) \quad (1)$$

with i varying from 0 to a product-dependent top; this grid width corresponds to ~2.7 km. The high resolution SAGE O_3 profiles were converted to mixing ratio versus pressure using their associated NCEP temperature profiles, and smoothed vertically onto this grid. Given the sampling of solar occultation instruments, which usually provide 15 sunrise and 15 sunset profiles in two narrow latitude bands every day (versus the denser sampling from MLS, with almost 3500 profiles/day), we used 10°-wide latitude bins (18 bins from 80°S-90°S to 80°N-90°N) to construct monthly zonal means. Next, we merged the GOZCARDS source data by computing average relative biases between source datasets during periods of overlap, and then adjusting each source dataset to a common reference to remove relative biases. Non-zero biases always exist between data from different instruments for various reasons, such as systematic errors arising from the signals or the retrieved values, different vertical resolutions, or sampling effects. Toohey et al. (2013) studied sampling biases from a large suite of satellite-based stratospheric profiling instruments, based on simulations using fully-sampled model abundance averages versus averages of output sampled at sub-orbital locations. Larger sampling errors arise from occultation than from emission measurements, which often sample thousands of profiles per day. Toohey et al. (2013) found that sampling biases reach 10-15%, notably at high latitudes with larger atmospheric variability. Sofieva et al. (2014) have also discussed sampling uncertainty issues for satellite ozone datasets.

We have observed very good correlations between GOZCARDS and other long-term ozone data, such as the Stratospheric Water vapor and OzOne Satellite Homogenized (SWOOSH) data (S. Davis, personal communication, 2012) and homogenized Solar Backscatter Ultraviolet (SBUV) data. Dissemination of trend results arising from analyses of GOZCARDS and other merged ozone datasets was planned as part of WMO (2014) and the SI^{2}N (Stratospheric Processes And their Role in Climate (SPARC), International Ozone Commission (IOC), Integrated Global Atmospheric Chemistry Observations (IGACO-O_3), and the Network for the Detection of Atmospheric Composition Change (NDACC)) initiative. Profile trend results have been provided by Tummon et al. (2015), Harris et al. (2015), as well as Nair et al. (2013, 2015).

This paper starts with a discussion of data screening issues (Sect. 2 and Appendix A), and then describes the GOZCARDS data production methodology, followed by some atmospheric results for HCl (Sect. 3), H_2O (Sect. 4), and O_3 (Sect. 5). We provide specific diagnostics that indicate generally good correlations and small relative drifts between the source datasets used to create the longer-term GOZCARDS merged time series. Section 6 briefly mentions GOZCARDS N_2O and HNO_3, as well as temperatures derived from Modern-Era Retrospective analysis for Research and Applications (MERRA) fields. The version of GOZCARDS described here is referred to as ESDR version 1.01 or ev1.01.

2 GOZCARDS source data and data screening

Data provenance information regarding the various measurements used as inputs for GOZCARDS is provided in Appendix A (Sect. A.1).

2.1 GOZCARDS data screening and binning

The screening of profiles for GOZCARDS has largely followed guidelines recommended by the various instrument teams and/or relevant publications, and we have documented these issues and procedures in Appendix A (Table A1). Unless otherwise noted, we only provide monthly means constructed from 15 or more (good) values in a given latitude/pressure bin. For ACE-FTS data, we also found it necessary to remove occasional large outlier values that could significantly impact the monthly zonal means. Our outlier screening removed values outside 2.5 times the standard deviation, as measured from the medians in each latitude/pressure bin, for each year of data. This was deemed close to optimum by comparing results to Aura MLS time series, which typically are not impacted by large outliers, and to ACE-FTS zonal means screened (in a slightly different way) by the ACE-FTS instrument team. Up to 5% of the profile values in each bin in any given month were typically discarded as a result, but the maximum percentage of discarded values can be close to 10% for a few months of ACE-FTS data, depending on year and species. Moreover, because of poor ACE-FTS sampling, the threshold for minimum number of good ACE-FTS values determining a monthly zonal mean was allowed to be as low as 10 for mid- to high latitudes, and as low as 6 for low latitudes (bins centered from 25°S to 25°N). Zonal mean data from ACE-FTS become too sparse in some years if such lower threshold values are not

used. Finally, no v2.2 ACE-FTS data are used after September 2010 (or after December 2009 for ozone) because of a data processing problem that affected this data version; a newly reprocessed ACE-FTS dataset was not available before we made the GOZCARDS data public.

Placing profiles on a common pressure grid is straightforward when pressures are present in the original files, as is the case for most data used here. Also, the vertical resolutions are similar for most of the instruments used for GOZCARDS. The UARS MLS, HALOE, and Aura MLS native pressure grids are either the same as or a superset of the GOZCARDS pressure grid, so these datasets were readily sampled for the construction of monthly means. For ACE-FTS, pressures are provided along with the fixed altitude grid, and we used linear interpolation versus log(pressure) to convert profiles to the GOZCARDS grid. More details are provided later for SAGE I and SAGE II O_3, for which density versus altitude is the native representation.

The binning of profiles occurs after the screened values are averaged (in each latitude/pressure bin). Note that for the species discussed here, sunset and sunrise occultation values in the same latitude bin during a given month are averaged together. Negative monthly means are set to -999.0 in the GOZCARDS files; while negative mixing ratios smaller (in absolute value) than the associated standard errors can in theory be meaningful, negative monthly means are unlikely to be very useful scientifically. Quantities other than mixing ratios are provided in the netCDF GOZCARDS files, which are composed of one set of individual yearly files for all source datasets, and one set of yearly files for the merged products. The main quantities are monthly averages, plus standard deviations and standard errors. The GOZCARDS source files also provide the number of days sampled each month as well as minimum and maximum values for the source datasets. Other information includes average solar zenith angles and local solar times for individual sources. Finally, formulae for monthly standard deviations of the merged data are given in Appendix A, where sample time series of the standard deviations and standard errors (not systematic errors) for both source and merged data are also shown.

3 GOZCARDS HCl

3.1 GOZCARDS HCl source data records

We used HCl datasets from HALOE, ACE-FTS and Aura MLS to generate the monthly zonal mean source products for GOZCARDS HCl. In addition to the procedures mentioned before, a first-order aerosol screening was applied to the HALOE HCl profiles: all HCl values at and below a level where the 5.26 μm aerosol extinction exceeds 10^{-3} km^{-1} were excluded. Regarding Aura MLS HCl, Froidevaux et al. (2008a) found anomalously high values versus aircraft data at 147 hPa at low latitudes; these values are not used in the production of the merged HCl product. Also, the ongoing standard MLS HCl product is retrieved using band 14 rather than band 13, which targeted HCl for the first 1.5 years after launch, but started deteriorating rapidly after Feb. 2006. As the remaining lifetime for band 13 is expected to be short, this band has been turned on only for a few days since Feb. 2006. MLS HCl data are not recommended for trend analyses at pressures < 10 hPa. However, for pressures ≥ 10 hPa, band 14 HCl is deemed robust, because of the broader emission line in this region, in comparison to the measurement bandwidth.

Past validation studies have compared MLS HCl (v2.2), ACE-FTS (v2.2) and HALOE (v19) datasets using coincident pairs of profiles; such work was described by Froidevaux et al. (2008a) for MLS HCl validation and by Mahieu et al. (2008) for ACE-FTS HCl validation. The MLS version 3.3/3.4 HCl data used here (see Livesey et al., 2013) compare quite well with v2.2 HCl (average relative biases are within 5%). HALOE HCl values were found to be biased low by ~10-15% relative to both MLS and ACE-FTS, especially in the upper stratosphere; this low bias versus other (balloon- and space-based) measurements had been noted in past HALOE validation studies (Russell et al., 1996). Also, HALOE (v19) and ACE-FTS (v2.2) HCl data tend to lose sensitivity and reliability for pressures less than ~0.4 hPa.

3.2 GOZCARDS HCl merged data records

Although Aura MLS HCl data for pressures less than 10 hPa do not contribute to the time dependence of the merged HCl product, the 2004-2005 absolute Aura HCl measurements in this region are used to compute the offsets for the ACE-FTS and HALOE zonal mean source data in a consistent manner versus pressure. Figure 1 illustrates the merging process for HCl at 32 hPa

for the 45°S latitude bin (covering 40°S-50°S). Given that there exists very little overlap between the three sets of measurements in the same months in 2004 and 2005, especially in the tropics, a simple 3-way averaging of the datasets would lead to significant data gaps. Our methodology is basically equivalent to averaging all three datasets during this period, and we use Aura MLS as a transfer dataset. This was done by first averaging ACE-FTS and Aura MLS data, where the datasets overlap, and then including the third dataset (HALOE) into the merging process with the temporary merged data. As the HALOE HCl values are generally lower than both the MLS and ACE-FTS values, the merged HCl dataset is generally further away from HALOE than it is from either ACE-FTS or Aura MLS. The top left panel in Fig. 1 shows GOZCARDS source data for HALOE, ACE-FTS, and Aura MLS during the overlap period, from August 2004 (MLS data start) through November 2005 (HALOE data end). The top right panel illustrates the result of step 1 in the merging procedure, with the temporary merged data values (orange) resulting from the adjustment of ACE-FTS and Aura MLS values to the mean reference (black dashed line); this reference is simply the average of the two series for all months when both values exist. The middle left panel shows step 2, namely the values (brown) obtained from merging HALOE values with the temporary merged values from step 1; the temporary merged values are weighted by 2/3 and HALOE values by 1/3 (giving the black dashed line as mean reference), so this is equivalent to averaging the three datasets with a weight of 1/3 each. A simple mathematical description of the above procedure is provided in Appendix A. The middle right panel shows the source data along with the final merged values during the overlap period, whereas the bottom panel shows the full time period, after the additive offsets are applied to the whole source series, thus removing relative biases; the three adjusted series are then averaged together wherever overlap exists, to obtain the final merged dataset. We tested this procedure by using one or the other of the two occultation data as the initial one (for step 1) and the results were not found to differ appreciably. We also found that the use of multiplicative adjustments generally produces very similar results as additive offsets. Some issues were found on occasion with multiplicative offsets, when combining very low mixing ratios, but additive offsets can also have drawbacks if the merged values end up being slightly negative, notably as a result of changes that modify the already low HCl values during Antarctic polar winter. This occurs on occasion as additive offsets tend to be weighted more heavily by larger mixing ratios found during non-winter seasons; as a

result, we decided not to offset lower stratospheric HCl source datasets in the polar winter at high latitudes for any of the years. Further specifics and procedural details regarding the merging of HCl data are summarized in Appendix A.

In Fig. 2, we display the offsets that were applied to the three HCl source datasets as a result of the merging process in each latitude/pressure bin; a positive value means that a dataset is biased low relative to the reference mean and needs to be increased by the offset value. These offsets show that in general, ACE-FTS and Aura MLS HCl values were adjusted down by 0.1-0.2 ppbv (a decrease of about 2-10%), while HALOE HCl was adjusted upward by 0.2-0.4 ppbv. Offset values tend to be fairly constant with latitude and the sum of the offsets equals zero. The generally homogeneous behaviour versus latitude is a good sign, as large discontinuities would signal potential issues in the merging (e.g., arising from large variability or lack of sufficient statistics). Figure S1 provides more detailed examples of upper and lower stratospheric offsets versus latitude, including standard errors based on the variability in the offsets during the overlap period (error bars provide an indication of robustness). Another indication of compatibility between datasets is provided by a comparison of annual cycles. Figure S2 provides average annual cycle amplitudes obtained from simple regression model fits to HALOE, ACE-FTS, and Aura MLS series over their respective periods. While there are a few regions where noise or spikes exist (mainly for ACE-FTS), large annual amplitudes in the polar regions occur in all time series; this arises from HCl decreases in polar winter, followed by springtime increases.

A more detailed analysis of interannual variability and trend consistency is provided from results in Fig. 3, which shows an example of ACE-FTS and Aura MLS time series. We have used coincident points from these time series to compare the deseasonalized anomalies (middle panel in Fig. 3) from both instrument series; correlation coefficient values (R values) are also computed. Very good correlations are obtained and no significant trend difference between the anomalies (bottom panel in Fig. 3) exists for ACE-FTS versus Aura MLS HCl. A view of these correlations and drifts at all latitudes/pressures is provided in Fig. 4, where the top panel gives R values for deseasonalized anomalies, and the bottom panel gives the ratio of the difference trends over the error in these trends. The results in Fig. 4 confirm that there are significant trend differences between the upper stratospheric HCl time series from ACE-FTS and Aura MLS (as a reminder, we did not use Aura MLS HCl for pressures less than 10 hPa). Fig. 4 also shows very

low correlation coefficients from the deseasonalized HCl series in the uppermost stratosphere, because Aura MLS HCl exhibits unrealistically flat temporal behavior, whereas ACE-FTS HCl varies more. In the lower stratosphere, there is generally good agreement between the ACE-FTS and Aura MLS HCl time series, with R values typically larger than 0.7 and difference trend to error ratios smaller than 1.5. The few low R values for 100 hPa at low latitudes likely reflect more infrequent ACE-FTS sampling and some (possibly related) outlier data screening issues.

Figure S3 illustrates GOZCARDS merged 46 hPa HCl variations versus time; there is clearly a much more complete global view (with no monthly gaps) after the launch of Aura MLS. Gaps at low latitudes in 1991 and 1992 are caused by post-Pinatubo aerosol-related issues in the HALOE record, and gaps in later years arise from the decrease in coverage from UARS. In the upper stratosphere, there are more gaps compared to 10 hPa and below, as a result of the much poorer tropical coverage from ACE-FTS and the elimination of MLS data in this region.

An indication of systematic errors in the merged values is given by the range of available monthly mean source data. For each bin, we compute the ranges of monthly means above and below the merged values that include 95% of the available source data monthly means. These error bars are not usually symmetric about the merged values, especially if one dataset is biased significantly more than others, in a relative sense. We did not have enough datasets here to consider a more statistical approach (such as the standard deviations among source datasets). Figure 5 shows the result of such a systematic error calculation at 46 hPa for the 35°S latitude bin. The lower shaded region range gives the lower bound, determined by HALOE data, and the upper limit of the grey shading originates from ACE-FTS data. Figure 6 shows contour plots of these estimated systematic errors in HCl. These are fairly conservative error bars; however, even the source data averages at the 95% boundaries have their own systematic errors (rarely smaller than 5%), so our estimates do not really encompass all error sources. Error bars representing a range within which 95% of the source data values reside (see Figs. 5 and 6) can be a useful guide for data users or model comparisons; alhough this is not an official product, users can readily calculate such ranges (or we can provide these values).

3.3 GOZCARDS HCl sample results and discussion

Stratospheric HCl is important because it is the main reservoir of gaseous chlorine and it can be used to follow the chlorine budget evolution over the past decades. This includes a significant increase before the mid-1990s as a result of anthropogenic chlorofluorocarbon (CFC) production, followed by a slower decrease as a result of the Montreal Protocol and subsequent international agreements to limit surface emissions that were correctly predicted to be harmful to the ozone layer (Molina and Rowland, 1974; Farman et al., 1985).

In Fig. 7, we provide an overview of the HCl evolution since 1991, based on GOZCARDS average merged HCl for 3 different latitude regions at 4 pressure levels, from the upper stratosphere to the lower stratosphere. In the upper stratosphere (at 0.7 hPa shown here), the rapid early rise in HCl was followed by a period of stabilization (1997-2000) and subsequent decreases. Rates of decrease for stratospheric HCl and total chlorine have been documented using satellite-based upper stratospheric abundances, which tend to follow tropospheric source gas trends with a time delay of order 6 years, with some uncertainties in the modeling of this time delay and related age of air issues (Waugh et al., 2001; Engel et al., 2002; Froidevaux et al., 2006). As summarized in WMO (2011), the average rate of decrease in stratospheric HCl has typically been measured at -0.6 %/yr to -0.9 %/yr, in reasonable agreement with estimated rates of change in surface total chlorine; see also the HCl upper stratospheric results provided by Anderson et al. (2000) for HALOE, Froidevaux et al. (2006) for the one and a half year band 13 Aura MLS data record, and Jones et al. (2011) and Brown et al. (2011) for a combination of HALOE and ACE-FTS datasets. The WMO (2011) summary of trends also includes results from column HCl data at various NDACC Fourier transform infrared (FTIR) measurement sites; see Kohlhepp et al. (2012) for a comprehensive discussion of ground-based results, showing some scatter as a function of latitude. Figure 7 demonstrates that a global-scale decline in mid- to lower stratospheric HCl is visible since about 1997. We also notice that at 68 hPa in the tropics, the long-term rate of change appears to be near-zero or slightly positive. In addition, there are shorter-term periods in recent years when an average increasing "trend" would be inferred rather than a decrease; in particular, see the northern hemisphere from 2005 through 2012 at 32 hPa.

We created deseasonalized GOZCARDS merged monthly zonal mean HCl data at different latitudes and we show in Fig. 8 the linear rate of change that results from simple fits through

such series. The long-term trends (1997 - 2013 for lower and 1997 - 2010 for upper stratosphere) are generally negative and between about -0.5%/yr (upper stratosphere) and -1%/yr (lower stratosphere). Some separation between northern and southern hemisphere results is observed in the lower stratosphere, with less negative trends in the northern hemisphere. Also, the scatter increases from 68 hPa to 100 hPa, where some positive trends occur at low latitudes; however, we have less confidence in the 100 hPa results, given the larger scatter and errors (and smaller abundances) in that region. Without trying to assign exact linear trends from these simple analyses, we observe considerable latitudinal variability in lower stratospheric HCl short-term behavior, especially after 2005. Such lower stratospheric changes in HCl have been captured in column HCl FTIR data (Mahieu et al., 2013, 2014). The latter reference shows that total column (FTIR) results and GOZCARDS lower stratospheric HCl trends agree quite well, and the authors imply that a relative slowdown in the northern hemispheric circulation is responsible for observed recent changes in the lower stratosphere. However, we note (Fig. 7) that changes in lower stratospheric HCl appear to be fairly short-term in nature, with an apparent reversal in behavior occurring at both northern and southern midlatitudes since 2011 (e.g., at 32 hPa). Lower stratospheric changes are distinct from the upper stratospheric long-term decrease, which we expect to continue, as long as the Montreal Protocol and its amendments are followed and total surface chlorine keeps decreasing.

In Figure 9, we provide simple rates of upper and lower stratospheric change in HCl for 6-yr sliding time periods (e.g., a 2004 value means a 2001-2006 average) for various latitudes. These results indicate that there has been an acceleration in the rate of decrease of upper stratospheric HCl between 2000 and 2004, followed by a period with somewhat smaller rates of change. This is roughly in agreement with curves showing the rates of change for surface total chlorine based on National Oceanic and Atmospheric Administration (NOAA) surface data (Montzka et al., 1999), as shown in Fig. 9 (top panel) with the Earth System Research Laboratory Global Monitoring Division data, time shifted by 6 or 7 years to account for transport delays into the upper stratosphere. Chlorine source gases have indeed shown a reduction in their rate of decrease during the second half of the past decade, as discussed by Montzka et al. (1999) and summarized in WMO (2011, 2014). Reasons include the initial rapid decrease in methyl chloroform, slower rates of decrease from the sum of CFCs in recent years, and increases in

hydrochlorofluorocarbons (HCFCs). The lower stratospheric HCl behavior in Fig. 9 (bottom panel) shows rates of change in partial column density between 68 hPa and 10 hPa. These changes show more variability with latitude than in the upper stratosphere for short (6-yr) time periods, and a hemispheric asymmetry exists, peaking in 2009, when positive tendencies are seen in the northern hemisphere, as opposed to decreases in the south (Mahieu et al., 2014). These results do not depend much on whether 6-yr or 8-yr periods (not shown) are used, but longer periods smooth out the rates of change; interannual variations, such as those arising from the quasi-biennial oscillation (QBO), will affect short-term results. Temporal patterns in the upper and lower stratosphere are qualitatively similar, and rates of change in surface emissions will impact both regions, but carefully disentangling this from changes in dynamics or in other species (e.g., CH_4) that can affect chlorine partitioning will require more analyses and modeling.

4 GOZCARDS H_2O

4.1 GOZCARDS H_2O source data records

We used water vapor datasets from HALOE, UARS MLS, ACE-FTS, and Aura MLS to generate the monthly zonal mean source products for GOZCARDS H_2O. In addition to the data screening procedures mentioned in Appendix A, we screened HALOE H_2O data for high aerosol extinction values, closely following the screening used for merged H_2O in the Stratospheric Water vapor and OzOne Satellite Homogenized (SWOOSH) dataset (S. Davis, personal communication, 2012). This method (see Fig. S4) screens out anomalous HALOE H_2O values that occurred mainly in 1991-1992, when the aerosol extinction near 22 hPa exceeded $5x10^{-4}$ km^{-1}; for pressure levels at and below 22 hPa, we have excluded the corresponding H_2O values. While this method may exclude some good data points, the lowest values (< 3 ppmv) do get screened out; such outliers are not corroborated by 22 hPa UARS MLS data (with most values > 3 ppmv). Also, for upper mesospheric HALOE data, care should be taken during high latitude summer months, as no screening was applied for the effect of polar mesospheric clouds (PMCs). High biases (by tens of percent) in H_2O above ~70 km have been shown to occur as a result of PMCs in the HALOE field of view (McHugh et al., 2003). Indeed, monthly means larger than 8-10 ppmv are observed in GOZCARDS H_2O merged data and in HALOE source data for pressures less than ~0.03 hPa. A more recent HALOE data version (V20 or VPMC) could be used to

largely correct such PMC-related effects, although this was not implemented for GOZCARDS H_2O. Aura MLS and ACE-FTS measurements, obtained at longer wavelengths than those from HALOE, do not yield such large H_2O values; a rough threshold of 8.5 ppmv could also be used (by GOZCARDS data users) to flag the pre-2005 merged dataset.

UARS MLS stratospheric H_2O for GOZCARDS was obtained from V6 (or V600) H_2O data. This data version is identical to the original prototype (named V0104) from Pumphrey (1999), who noted that UARS MLS H_2O often exhibits drier values (by 5-10%) than HALOE H_2O (see also Pumphrey et al., 2000). The resulting UARS MLS H_2O source data span the period from Sep. 1991 through April, 1993; a significant fraction of this dataset in the tropics at 100 hPa is flagged bad, as a result of diminishing sensitivity.

Summarizing past validation results, SPARC WAVAS (2000) analyses pointed out the existence of a small low bias in HALOE stratospheric H_2O versus most other measurements, except for UARS MLS. Lambert et al. (2007) showed agreement within 5-10% between Aura MLS version 2.2 H_2O and other data, including ACE-FTS H_2O. From the mid-stratosphere to the upper mesosphere, excellent agreement between ground-based data from the Water Vapor Millimiter-wave Spectrometer and H_2O profiles from Aura MLS and ACE-FTS has been demonstrated by Nedoluha et al. (2007, 2009, 2011). Changes from MLS v2.2 to v3.3 led to an increase of 0.2-0.3 ppmv in stratospheric H_2O (Livesey et al., 2013). Recent comparisons by Hurst et al. (2014) of MLS v3.3 H_2O data versus Cryogenic Frost point Hygrometer time series above Boulder show excellent overall agreement, indicating that systematic uncertainties for lower stratospheric MLS data may be as low as ~5%; this reinforces MLS H_2O validation work by Read et al. (2007) and Voemel et al. (2007). Aura MLS stratospheric H_2O v3.3 values are slightly larger (by up to ~5%) than the multi-instrument average from a number of satellite datasets, as discussed in satellite intercomparisons by Hegglin et al. (2013), who observed only small disagreements in interannual variations from various series for pressures less than 150 hPa.

4.2 GOZCARDS H_2O merged data records

The merging process for H_2O is nearly identical to the method used for HCl. The main difference is an additional step that merges UARS MLS data with the already combined datasets from HALOE, ACE-FTS, and Aura MLS, by simply adjusting UARS MLS values to the average of

429 the previously merged series during the early (1991-1993) overlap period; see Fig. S5 for an
430 illustration. Typically, this requires an upward adjustment of UARS MLS H_2O data, as these
431 values are biased low versus most other datasets; nevertheless, the short but global record from
432 UARS MLS helps to fill the time series. After considering the channel drift issues for SAGE II
433 H_2O (and following past advice from the SAGE II team itself), we decided to use caution and did
434 not include that dataset for GOZCARDS, as trend results could be affected. Other minor
435 procedural merging details or issues for H_2O are included in the Supplement. Also, data users
436 should be aware of anomalous effects arising in merged average series from non-uniform
437 latitudinal sampling when no MLS data exist, in regions with large latitudinal gradients, as for
438 H_2O at 147 hPa, the largest pressure for merged GOZCARDS H_2O. Latitudinal averages can be
439 biased in certain months and month-to-month variability is increased because of relatively poor
440 global sampling (in this region) prior to Aug. 2004, after which Aura MLS data are used.
441 In Fig. 10, we display the average offsets that were applied to the four H_2O source datasets;
442 these offsets follow previously known relative data biases. For example, low biases in UARS
443 MLS H_2O, especially in the mesosphere, were discussed by Pumphrey (1999) and the UARS
444 MLS offsets (see Fig. 10) correct that dataset upward. The application of offsets derived for
445 HALOE and UARS MLS raises the H_2O time series from these instruments, whereas negative
446 offsets lower the H_2O source data from ACE-FTS and Aura MLS. As we found for HCl, the
447 offset values generally display small variations versus latitude and are therefore fairly stable
448 systematic adjustments to the time series. Figure S6 displays the amplitudes of the fitted annual
449 cycles for HALOE, ACE-FTS, and Aura MLS. As for HCl, similar patterns emerge for these
450 datasets. Wintertime descent into the polar vortex regions is responsible for large annual cycles
451 at high latitudes, especially in the mesosphere; also, the seasonal impact of dehydration in the
452 lower stratospheric Antarctic region causes a large annual cycle in Aura MLS high southern
453 latitude data. Figure 11 provides some statistical information, as done for HCl in Sect. 3.2,
454 regarding the correlations and trend differences between ACE-FTS and Aura MLS. There are a
455 few regions with noisier relationships. While slow increases in H_2O are generally observed by
456 both instruments in the stratosphere and mesosphere, the tropical region near 0.1 hPa shows a
457 slight decreasing trend for the ACE-FTS points, thus leading to larger discrepancies; it is not
458 clear what the source of these discrepancies is. While the tropical ACE-FTS data are generally

459 sampled with a significantly lower temporal frequency, the same applies for all pressure levels;
460 however, a few outlier points can have a much larger impact when sampling is poorer. There are
461 also a few other spots, such as near 65°S and 65°N and near 5 hPa, with a large drift in the
462 difference time series; this may be caused by a combination of poorer sampling by ACE-FTS
463 and higher atmospheric variability, which can lead to more scatter. At the highest latitudes in the
464 lower stratosphere, the observed slope differences are more within error bars, but the larger
465 variability means that a longer record is needed to determine if the time series trend differently.
466 The merged dataset tends to be much closer to Aura MLS in terms of trends because there are
467 many more months of Aura MLS than ACE-FTS data; the overall impact of
468 ACE-FTS data on the merged H_2O series is fairly small.
469 Figure S7 provides a visual representation of the merged GOZCARDS H_2O fields at
470 3 hPa and 68 hPa, respectively. Well-known features are displayed in these plots, given the good
471 global coverage in the post-2004 period in particular. In the upper stratosphere, descent at high
472 latitudes during the winter months leads to larger H_2O values, and low latitude QBO features are
473 also observed. In the lower stratosphere, one observes dehydration evidence at high southern
474 latitudes in the winter months, as well as a low latitude seasonal "tape recorder" signal; this
475 phenomenon is driven by tropopause temperatures and has been measured in satellite data since
476 the early 1990s (Mote et al., 1996; Pumphrey, 1999). A vertical cross-section of this lower
477 stratospheric tropical (20°S to 20°N) tape recorder in GOZCARDS merged H_2O for 1991-2013
478 is shown in Fig. 12; periods of positive anomalies alternate with negative anomalies, including
479 the post-2000 lows, as well as the most recent decreases in 2012-2013 (see also next section).
480 As we discussed for HCl, we have estimated systematic errors for the merged H_2O product.
481 This is illustrated by the contour plots in Fig. 13; these ranges encompass at least 95% of the
482 monthly mean source data values from HALOE, UARS MLS, ACE-FTS, and Aura MLS above
483 or below the merged series. These errors typically span 5 to 15% of the mean between 100 and
484 0.1 hPa; errors larger than 30% exist in the tropical upper troposphere (147 hPa), and large
485 values in the upper mesosphere arise from the low bias in UARS MLS H_2O.

4.3 GOZCARDS H_2O sample results and discussion

Stratospheric H_2O variations have garnered attention because of the radiative impacts of water vapor in the UTLS and the connection to climate change (Solomon et al., 2010), as well as the stratospheric chemical significance of H_2O oxidation products. Individual water vapor datasets have been used here to produce a merged stratospheric H_2O record spanning more than two decades. We do not attempt here to characterize trends or to imply that recent tendencies will carry into the next decade or two. Rather, as variability is also of interest to climate modelers, we focus here on observed decadal-type (longer-term) variability in stratospheric water vapor.

Figure 14 illustrates monthly, annual, and longer-term changes in stratospheric water vapor, based on GOZCARDS merged H_2O; this shows the well-known H_2O minimum in the lower tropical stratosphere as well as an increases in the upper stratosphere (as a result of methane oxidation). As we know from past studies (e.g., Randel et al., 2004), medium- to long-term changes in H_2O are large-scale in nature. However, lower stratospheric H_2O variations are more accentuated at low latitudes, in comparison to near-global (60°S-60°N) results. It has long been known (e.g., from the *in situ* balloon-borne measurements of Kley et al., 1979) that the hygropause is typically located a few km higher than the thermal tropopause. We observe that the tropical stratosphere is drier at 68 hPa than at 100 hPa (near the tropopause). According to the 22-year GOZCARDS data record, annually-averaged H_2O values in the tropics (20°S-20°N) have varied between about 3.2 and 4.2 ppmv at 68 hPa. The rapid drop between 2000 and 2001 is observed at 100 and 68 hPa, with some dilution of this effect at higher altitudes. There is a clear difference in long-term behavior between the upper stratosphere, where changes in methane should have the clearest influence, and the lower stratosphere, where cold point temperatures and dynamical changes have a significant impact. To first-order, the last few years show ~10% larger values in the upper stratosphere than in the early 1990s, while the opposite holds in the lowest stratospheric region, where a decrease of order 10% is observed over the same period. Figure 14 also shows that month-to-month and seasonal variations are usually somewhat larger than the long-term changes in the lower stratosphere, most notably at 100 hPa.

In order to provide longer-term variability diagnostics for water vapor, we show in Fig. 15 the minimum to maximum spread in annual averages (tropics and mid-latitudes) from Fig. 14 for the 22-yr period. We observe that the tropical variability is largest just above the tropopause (here

this means at the 68 hPa GOZCARDS level), where it reaches ~27% (1 ppmv). Such diagnostics of variability should be useful for comparisons to various chemistry climate models.

The longer-term variability in water vapor increases above the stratopause and reaches close to 30% in the uppermost mesosphere, as seen in Fig. 16(a); this plot shows the monthly and annual near-global (60°S-60°N) H_2O variations at 0.01 hPa. Large seasonal changes in this region are driven by vertical advection associated with the mesospheric circulation, with each hemisphere's summertime peaks contributing to the maxima (two per year) in these near-global averages; such seasonal variations were compared to model results by Chandra et al. (1997), based on the first few years of HALOE H_2O data. The strong upper mesospheric variability in annual-mean H_2O is known from previous studies of ground-based and satellite H_2O data (Chandra et al., 1997; Nedoluha et al., 2009; Remsberg, 2010), and this region is where the solar (Lyman α) influence on H_2O is strongest. Figure 16(b) displays the near-global variations in annual upper mesospheric H_2O from 0.1 to 0.01 hPa. We clearly see increased variability in the uppermost mesosphere, and decreases in the mixing ratios as a result of H_2O photodissociation.

5 GOZCARDS ozone

A number of discussions relating to signs of ozone recovery have been presented before (Newchurch et al., 2003; Wohltmann et al., 2007; Yang et al., 2008; Jones et al., 2009; Hassler et al., 2011; Salby et al., 2011, 2012; Ziemke and Chandra, 2012; Gebhardt et al., 2014; Kuttipurath et al., 2013; Kirgis et al., 2013; Nair et al., 2013, 2015; Shepherd et al., 2014, Frith et al., 2014). While there are some indications of small increases in O_3 in the past 10-15 years, further confirmation of an increase in global O_3 and its correlation with column increases is needed in order to more clearly distinguish between long-term forcings, notably from the 11-yr solar cycle, slow changes in halogen source gases, temperature changes, and shorter-term variability. Continuing, good long-term ozone datasets are clearly needed for such studies.

5.1 GOZCARDS ozone source data records

We used ozone datasets from SAGE I, SAGE II, HALOE, UARS MLS, ACE-FTS, and Aura MLS to generate the monthly zonal mean source products for GOZCARDS. Due to time constraints, we did not use the newer SAGE II version 7 ozone (see Damadeo et al., 2013) as part of the GOZCARDS merged dataset. Our studies indicate that there are systematic

differences of only a few percent between SAGE II V6.2 and V7 O_3 on their native coordinates (number density versus altitude). However, these 2 versions exhibit some differences if the data are converted to mixing ratios on pressure surfaces. These differences result mainly from different temperatures (and their trends) between MERRA and analyses from the National Centers for Environmental Prediction (NCEP), used by SAGE II V7 and V6.2 retrievals, respectively. The main differences between MERRA and NCEP temperatures occur in the upper stratosphere for time periods before 1989 and after mid-2000 (see further details in Sect. 5.2).

5.1.1 Treatment of SAGE ozone profiles

Both SAGE I and SAGE II used solar occultations during satellite sunrise and sunset to measure vertical profiles of ozone, along with other composition data and aerosol extinction (McCormick et al., 1989; Cunnold et al., 1989). It takes about 1 month for SAGE I and II to provide near global coverage (about 80°N to 80°S), with some dependence on season. The SAGE I measurements started in February 1979 and stopped in November 1981, while SAGE II provided data between October 1984 and August 2005. In the middle of July 2000, SAGE II had a problem in its azimuth gimbal system. Although this was corrected by November 2000, the instrument operation was switched to a 50% duty cycle, with either sunrise or sunset occultations occurring in monthly alternating periods, until the end of the mission.

It is known that there were altitude registration errors in SAGE I (V5.9) data (Veiga et al., 1995; Wang et al., 1996). To correct this problem, an empirical altitude correction method based on Wang et al. (1996) had been applied to SAGE I (V5.9) data; these corrected SAGE I V5.9 profiles, which had been evaluated in previous trend studies (e.g. SPARC, 1998; WMO, 2003), were used to create the GOZCARDS SAGE I product (denoted as version V5.9_rev). We did not use reprocessed version 6.1 SAGE I data (L. W. Thomason, personal communication, 2012) because the altitude registration problems had not been completely fixed and new altitude correction criteria should be derived and validated.

Ozone data screening details for the original SAGE I and SAGE II datasets are provided in Appendix A. The number density profiles were converted to mixing ratios on pressure levels by using NCEP temperature and pressure data provided with each profile. Derived ozone profiles were then interpolated to fixed pressure levels on the following grid:

574 $$p(i) = 1000 \times 10^{-\frac{i}{30}} (\text{hPa}) \quad i = 0, 1, 2, ... \qquad (2)$$

575 Ozone values at each of the 5 levels centered on every GOZCARDS pressure level were then
576 averaged (weighted by pressure) to derive mixing ratios at each GOZCARDS pressure level. By
577 doing this, the SAGE profiles were smoothed to a vertical resolution comparable to that of the
578 other satellite instruments used in this GOZCARDS work. Monthly zonal means were then
579 computed for the SAGE ozone datasets on the GOZCARDS-compatible grid.

580 **5.1.2 Comparisons of ozone zonal means**

581 Ozone differences between SAGE II and other satellite data are shown in Fig. S8. Zonal mean
582 differences between SAGE II and HALOE are generally within 5% for 1.5 to 68 hPa at mid-
583 latitudes, and for 1.5 to 46 hPa in the tropics; relative biases are larger outside those ranges and
584 increase to ~10% near the tropopause and also near 1 hPa. This good level of agreement was
585 demonstrated in the past (e.g., SPARC, 1998). SAGE II data show better agreement with UARS
586 and Aura MLS in the upper stratosphere and lower mesosphere, within 5% up to 0.68 hPa and
587 for latitudes outside the polar regions. Aura MLS O_3 compares better with SAGE II data than
588 does UARS MLS in the tropics for pressures larger than 68 hPa; the high bias in UARS MLS O_3
589 at 100 hPa has been discussed previously (Livesey et al., 2003). There are no months that include
590 both SAGE II and ACE-FTS data in the northern hemisphere tropics (see the gap in Fig. S8,
591 bottom right panel), largely due to the poorer coverage from ACE-FTS in the tropics. ACE-FTS
592 O_3 shows the largest positive bias (greater than 10%) with respect to SAGE II, for pressures less
593 than 1.5 hPa. The high bias in upper stratospheric ACE-FTS ozone has been mentioned in past
594 validation work using ACE-FTS data (e.g., Froidevaux et al., 2008b; Dupuy et al., 2009). The
595 biases shown here are also consistent with recent O_3 intercomparison studies from a
596 comprehensive array of satellite instruments by Tegtmeier et al. (2013). It has been known for
597 some time that the HALOE and SAGE II ozone datasets, which govern the main variations of the
598 GOZCARDS merged ozone values before 2005, agree quite well (within 5%) in absolute value,
599 and also in terms of temporal trends (Nazaryan et al., 2005), and versus ozonesondes (mostly
600 above ~20 km or ~50 hPa). Larger percentage differences occur in the lowest region of the
601 stratosphere at low latitudes, and especially in the upper troposphere, where HALOE values
602 become significantly smaller than SAGE II data, which are already biased low (by ~50%) versus

603 sondes (Wang et al., 2002); see also Morris et al. (2002), as well as results of SAGE II and
604 HALOE comparisons versus solar occultation UV-Visible spectrometer measurements from long
605 duration balloons (Borchi et al., 2005). We should note here that in this GOZCARDS merging
606 work, we have largely avoided the upper tropospheric region.

607 Zonal mean differences between SAGE II and Aura MLS show some latitudinal structure
608 between 1 and 3 hPa, with larger (5-10%) biases in the southern hemisphere, especially for 0 to
609 30°S (see Fig. S8). There are no such features between SAGE II and HALOE or UARS MLS.
610 We found that this results from anomalous NCEP temperatures after 2000, which affect SAGE II
611 data converted from number density/altitude to GOZCARDS VMR/pressure coordinates.
612 Figure 17 shows an example of the ozone series from SAGE II and other satellite data for 10°S to
613 20°S from 1 to 6.8 hPa. At 1 hPa, the SAGE II ozone values (converted to mixing ratios) drift
614 relative to HALOE and are elevated after mid-2000; this can be attributed to abnormal NCEP
615 temperature trends compared to MERRA and HALOE during the same time period (for detailed
616 views, see Figs. S9 and S10). Similar features are found down to pressures near 3 hPa. These
617 issues relating to anomalous upper stratospheric NCEP temperature trends were noted by
618 McLinden et al. (2009). Because such artifacts are confirmed by using either MERRA or
619 HALOE temperatures, we decided not to include in the merging process any SAGE II O_3 values
620 after June 30, 2000 for pressures equal to or less than 3.2 hPa. SAGE II ozone is not significantly
621 affected by the conversion to mixing ratio/pressure coordinates at 4.6 and 6.8 hPa (Fig. 17).

622 ## 5.2 GOZCARDS ozone merged data records

623 ### 5.2.1 Methodology for GOZCARDS merged ozone

624 Ozone measurements from SAGE I, SAGE II, HALOE, UARS MLS, Aura MLS and ACE-FTS,
625 were used to establish a near-continuous monthly zonal mean record from late 1979 through
626 2012 for the GOZCARDS merged O_3 product (ESDR version 1.01). The SAGE II dataset was
627 used as a reference standard, since it has the longest period of measurements and has been
628 extensively validated. A GOZCARDS ozone merged data record is constructed by combining
629 these measurements after removing systematic biases with respect to SAGE II. This is done by
630 applying additive offsets to all other instrument series, as determined from average differences

between monthly zonal means and SAGE II during overlap time periods. The merged data are then derived by averaging all available adjusted datasets. Because there are gaps in overlap between SAGE II and ACE-FTS monthly mean data in some latitudes (Fig. S7), and as SAGE II ozone VMRs obtained from the vertical grid transformation were affected by anomalous NCEP temperatures after mid-2000 for pressures smaller than or equal to 3.2 hPa, a two-step approach is used to generate the merged product. First, SAGE II data are used as reference for pressures larger than 3.2 hPa to adjust HALOE, UARS MLS and Aura MLS based on overlapping months between 1991 and Nov. 2005; see the method overview schematic in Fig. 18. For $p \leq 3.2$ hPa, SAGE II O_3 is still used as a reference through June 2000, and HALOE and UARS MLS data are adjusted accordingly. This eliminates the effect of anomalous NCEP temperatures on SAGE II ozone and leads to more accurate offsets based on HALOE values, after they have been adjusted to SAGE II. Adjusted HALOE data (HALOE* in Fig. 18) are then used as a reference to derive estimated offsets for Aura MLS O_3, using the overlap period with HALOE from Aug. 2004 to Nov. 2005. In step 2, a new reference value is derived by averaging all available data from SAGE II, HALOE*, UARS MLS* and Aura MLS*. This value is used to adjust ACE-FTS ozone based on all overlapping months between March 2004 and Nov. 2005. By including Aura MLS in the dataset created in step 1, we obtain more complete spatial and temporal coverage than possible with SAGE II and HALOE, and ensure that there are overlapping months between this combined dataset and ACE-FTS source data. At the end of step 2, the final merged ozone is derived by averaging the temporary merged dataset from step 1 with the adjusted ACE-FTS data.

5.2.2 Further considerations regarding GOZCARDS merged ozone data

Even in the absence of diurnal variations, measurements from occultation sensors can yield larger sampling errors than those from densely-sampled emission measurements (Toohey et al., 2013). Diurnal changes in ozone can affect data comparisons and could impact data merging. Recently, Sakazaki et al. (2013) presented diurnal changes measured by the Superconducting Submillimeter-Wave Limb-Emission Sounder (SMILES) and Parrish et al. (2014) analyzed ground-based microwave O_3 profile variations versus local time in conjunction with satellite data. Ozone diurnal variations range from a few percent in the lower stratosphere to more than 10% in the upper stratosphere and lower mesosphere (see also Ricaud et al., 1996; Haefele et al., 2008; Huang et al., 2010). SAGE II and other occultation instruments observe ozone at local

661 sunrise or sunset, and the retrieved values are generally closer to nighttime values in the upper
662 stratosphere and mesosphere. To characterize systematic differences between satellite data,
663 coincident profiles with small differences in space and time are most often used; an example of
664 mean differences and standard deviations between SAGE II and Aura MLS using both
665 coincident profile and zonal mean methods is provided in Fig. S11. SAGE II and coincident
666 Aura MLS nighttime O_3 values agree within ~5% between 0.46 and 100 hPa, except in the
667 tropical lower stratosphere where comparisons are noisier. Differences between zonal mean
668 SAGE II and Aura MLS data are very close to differences from averaged coincident values,
669 except for pressures less than 2 hPa, where differences increase from a few to ~10% at 0.3 hPa,
670 consistent with what one expects from the diurnal cycle. Although zonal mean differences are
671 likely to be less representative of "true" differences, by combining SAGE II with Aura MLS data
672 adjusted by zonal mean biases, we provide a series adjusted to the average of sunrise and sunset,
673 as measured by SAGE II. If Aura MLS data were adjusted by biases obtained using the
674 coincident method, an upper stratospheric offset of more than several percent and artificial trends
675 due to such a diurnal cycle effect could be introduced. The use of long-term datasets with
676 consistent sampling should be an advantage for trend detection, even in a region with diurnal
677 changes. Also, our avoidance of SAGE II upper stratospheric O_3 after mid-2000 mitigates
678 potential artifacts arising from changing SAGE II sunrise/sunset sampling patterns over time.

679 Figure 19 displays the average ozone offsets obtained from the biases relative to SAGE II. A
680 high bias in upper stratospheric ACE-FTS O_3 relative to other datasets is evident from the
681 negative ACE-FTS offsets (as large as 25%). Most of the other instrument offsets are in the 5-
682 10% range; lowering O_3 from UARS MLS, HALOE, and Aura MLS in the lower mesosphere is
683 required to match SAGE II. Sampling differences and data sparseness may be mostly responsible
684 for larger offsets at high latitudes; in these regions, the merged data are less amenable to long-
685 term analyses because of data gaps and larger variability (especially prior to 2004).

686 As shown in the Supplement (Fig. S12), we observe strong similarities (e.g., peaks at
687 midlatitudes near 10 and 1.5 hPa) in the O_3 annual cycle amplitude patterns from SAGE II,
688 HALOE, ACE-FTS, and Aura MLS over their respective measurement periods. Middle
689 stratospheric peaks are a result of the annual cycle in oxygen photolysis, whereas temperature
690 variations drive the annual cycle in the upper stratosphere (Perliski et al., 1989). This sort of

691 comparison provides some reassurance regarding the consistency of various datasets. Figure 20
692 provides diagnostics similar to those given for HCl and H_2O, namely correlation coefficients and
693 significance ratios for the slopes of the deseasonalized anomaly time series from SAGE II versus
694 HALOE as well as from ACE-FTS versus Aura MLS (for 1992 through 1999, and 2005 through
695 2009, respectively). These diagnostic results for ACE-FTS and Aura MLS are of a quality that is
696 comparable to the HALOE/SAGE II results; poorer fits occur mostly at high latitudes and in the
697 upper stratosphere. Poorer correlations at upper altitude appear largely tied to a decrease in the
698 amount of valid data in this region (especially at high latitudes), coupled with a relatively small
699 variability. For regions with poorer agreement between ACE-FTS and Aura MLS, we often see
700 small variability in the series from Aura MLS but larger changes (scatter) in the ACE-FTS series.
701 Larger differences in trends between SAGE II and HALOE were noted by Nazaryan et al. (2005)
702 at low latitudes near 50 km; this is also indicated by our simple linear fits (not shown here) to the
703 GOZCARDS source datasets from these two instruments and the existence of poorer agreements
704 in Fig. 20 for the slope of the difference series in that region. The existence of good correlations
705 in interannual ozone variations between a large number of satellite measurements was discussed
706 by Tegtmeier at el. (2013). Regarding temporal drifts, Nair et al. (2012) have shown that small
707 drifts (mostly within about ±0.5%/yr for the 20-35 km region) exist between most of the datasets
708 from six ozone lidar sites and coincident HALOE, SAGE II, and Aura MLS measurements;
709 similar results were obtained by Kirgis et al. (2013). Other recent studies (in particular, by
710 Hubert et al., 2015) corroborate the very good stability of the datasets used for GOZCARDS,
711 which relies most heavily on O_3 data from SAGE II and Aura MLS. While we feel justified in
712 the use of the longer-term time series chosen for GOZCARDS O_3, data users should still note the
713 existence of a few regions with poorer correlations or trend agreement (and, therefore, larger
714 uncertainties) between different satellite ozone datasets, as indicated in Fig. 20. Long-term
715 merged datasets from GOZCARDS and other sources should undergo continued scrutiny from
716 the community, as done recently for trends by Tummon et al. (2015) and Harris et al. (2015).
717 Sample cross-sectional views of two slices through the GOZCARDS merged O_3 field are
718 provided in the Supplement (Fig. S13). Figure 21 shows estimated systematic errors from our
719 calculation of the 95% ranges for the monthly mean source data used here, both above and below
720 the merged values. In this case, as SAGE II is used as a reference dataset, the applied offsets

(Fig. 20) correlate quite well with this plot depicting the ranges about SAGE II values. Minimum error bars can be slightly lower than 5% for the middle stratosphere at low latitudes, where ozone values are largest. This view of systematic error bars is consistent with results by Tegtmeier et al. (2013), based on the larger set of data analyzed for the SPARC Data Initiative. They also found that the regions with lowest errors (scatter) are in the middle stratosphere at low to mid-latitudes, where most monthly mean satellite data fit within ±5% of the multi-instrument mean.

5.3 GOZCARDS ozone sample results and discussion

Nair et al. (2013) used regression analyses to compare profile trend results from GOZCARDS merged O_3 at northern midlatitudes versus a combined O_3 dataset from lidar and coincident satellite data at the Observatoire de Haute Provence (OHP), France. They showed that good consistency exists for the decreasing ozone time period, from the early 1980s to 1997, and for the upper stratospheric increase since 1997, but some differences exist in the lower stratosphere during this second time period, when the GOZCARDS results show a near-zero trend in comparison to small positive trends from the combined (and more localized) dataset. The above results for the declining time period agree broadly with earlier work (for the 1979-1997 period) by Jones et al. (2009). Gebhardt et al. (2014) analyzed ozone profile trends from SCIAMACHY on ENVISAT, and compared this to trends from Aura MLS, Optical Spectrograph and InfraRed Imager System (OSIRIS) on the Odin satellite, and sondes; their results include the detection of localized ozone increases in the mid-stratosphere at low latitudes; see also Bourassa et al. (2014), who analyzed merged SAGE II and (OSIRIS) observations for 1984-2013, as well as results from Kyrölä et al. (2013) on combined SAGE II and Global Ozone Monitoring by Occultation of Stars (GOMOS) records for 1984-2012, and Eckert et al. (2014), who investigated ENVISAT MIPAS trends for 2002-2012. The shortness of data records since 1997, coupled with relative variability and potential drifts between various measurements may explain some differences in recent trend results, notably for the post-1997 period. More comprehensive analyses from the SI^2N initiative have focused on an intercomparison of profile changes from a variety of datasets, including GOZCARDS and other merged records (Tummon et al., 2015; Harris et al., 2015).

Here, we investigate ozone column results for the stratosphere, based on the global GOZCARDS data, in light of other column ozone datasets, including the work by Ziemke and

750 Chandra (2012), hereafter referenced as ZC12. These authors analyzed total column and
751 stratospheric column data from satellites, and their analyses yielded a rather strong near-global
752 (60°S-60°N) average ozone increase since 1998. Their stratospheric columns depend on the
753 convective-cloud differential (CCD) method and use Total Ozone Mapping Spectrometer
754 (TOMS) and Ozone Monitoring Instrument (OMI) column data over convective clouds near the
755 tropopause (see also Ziemke et al., 2005). In Fig. 22, we compare changes in 60°S-60°N ZC12
756 column ozone data (J. Ziemke, personal communication, 2013) to changes in GOZCARDS O_3
757 columns above 68 hPa for that region; note that GOZCARDS values do not provide for a
758 continuous long-term time series down to pressures of 100 hPa or more in the SAGE I years
759 (1979-1981). To eliminate biases between stratospheric columns as calculated using the CCD
760 methodology and the GOZCARDS fixed bottom pressure approach, we reference all
761 stratospheric columns to the 1980 total column value. These column series include SAGE I data
762 and are linearly interpolated between 1981 and 1984, when no GOZCARDS source datasets
763 exist. We observe that relative changes in GOZCARDS columns follow the ZC12 curves within
764 a few DU in the downward phase until about 1992, but the 1992-1997 decrease in total columns
765 does not compare very well. Some of this discrepancy may occur because total columns capture
766 a stronger decrease from levels below 68 hPa, not fully represented in GOZCARDS. Focusing on
767 the late period (from Aura MLS and ACE-FTS), we also show the GOZCARDS columns above
768 68 hPa, referenced to 2007 instead of 1980. There is a good match in the variations between
769 GOZCARDS and ZC12 columns during 2005-2010, in agreement with the fact that very good
770 correlations were obtained by ZC12 between Aura MLS columns and stratospheric column data
771 from the CCD technique. ZC12 values for stratospheric and total columns are in good agreement,
772 although the stratospheric values have gaps when not enough data were present for near-global
773 estimates. The increase in ZC12 data from 1997 to 1998 is not matched very well by
774 GOZCARDS; this is also true if we remove the 11-yr solar cycle from both datasets (not shown
775 here), as done by ZC12. However, the interannual changes in GOZCARDS columns are in better
776 agreement with near-global total column variations in the Merged Ozone (Version 8.6) Dataset
777 obtained from the suite of SBUV instruments (McPeters et al., 2013, Frith et al., 2014), as shown
778 in Fig. 22. Discrepancies between the GOZCARDS and total column data (SBUV or TOMS) are
779 largest between 1992 and 1997; this could be related to some issues in this portion of the

GOZCARDS ozone data record or to the somewhat less robust SBUV data in this period, resulting from SBUV satellite orbits closer to the terminator (e.g., see Frith et al., 2014) and/or from total column errors introduced by Mount Pinatubo aerosols (e.g., Bhartia et al., 1993, Torres and Bhartia, 1995). Discrepancies between the various column results in Fig. 22 could also arise from differences in ozone column calculations or coverage because of different methodologies, grids, or sampling to properly determine near-global results. We also note that recent analyses by Shepherd et al. (2014), who used a chemistry-climate model constrained by meteorology to investigate causes of long-term total column O_3 variations, show a partial return, in 2010, towards 1980 ozone column values, but not nearly as much as implied by ZC12. Long-term halogen source gas reductions that have occurred since the mid-1990s should only lead to column ozone increases of a few DU since 1997 (Steinbrecht et al., 2011).

6 Other GOZCARDS data records

We now briefly mention the N_2O, HNO_3, and temperature GOZCARDS records that were part of the delivery for public dissemination in 2013. For N_2O and HNO_3, the somewhat simpler merging procedure consisted of averaging the source datasets from ACE-FTS and Aura MLS over the overlap time period (Aug. 2004 through Sep. 2010) to obtain the additive offsets for each of the two individual records. We then simply used the correspondingly-adjusted and averaged series to create the merged results; this procedure is the same as we described for the first step in the HCl (or H_2O) merging process.

6.1 N_2O

This data set starts in August 2004, when the Aura MLS data record began; the only dataset after Sep. 2010 is the Aura MLS N_2O (version 3.3) data record. Because of degradation in the main target MLS N_2O band (near 640 GHz) after the first few months of 2013, the N_2O standard MLS product is being reprocessed for the whole Aura MLS period using an alternate measurement band; currently, there are no official GOZCARDS N_2O data after 2012.

Excellent agreement (mostly within 5%) exists between stratospheric ACE-FTS and Aura MLS N_2O profiles (see Lambert et al., 2007; Strong et al., 2008; Livesey et al., 2013). Plots showing the average offsets applied to both MLS and ACE-FTS N_2O series as a function of

808 latitude and pressure are provided in Fig. S14. These plots are in agreement (in magnitude and in
809 sign) with the above-referenced studies; the two datasets yield typical offsets (one half of the
810 average differences) of less than 5%. Also, very good temporal agreement between these two
811 time series (for 2004-2010) is illustrated by the quality of the N_2O diagnostic information
812 displayed in Fig. S15, showing generally highly correlated fields and insignificant drifts.
813 Figure 23 shows sample contour plots for the N_2O merged field (2004-2012); as seen from the
814 bottom panel (100 hPa), wintertime descent brings low N_2O values down at high latitudes inside
815 the polar vortices. N_2O is a conserved tracer in the lower stratosphere and its variations near the
816 tropopause have implications regarding age of air. Variations in upper stratospheric N_2O are
817 clearly affected by seasonal and dynamical effects; this is evident from the striking semi-annual,
818 annual and QBO-related patterns displayed in Fig. 23 for the 6.8 hPa level (top panel).

819 ## 6.2 HNO_3

820 As for N_2O, we merged the HNO_3 data from ACE-FTS (version 2.2) and Aura MLS (version
821 3.3) from Aug. 2004 onward, and included only the adjusted MLS dataset after Sep. 2010. The
822 average offsets applied to MLS and ACE-FTS time series as a function of latitude and pressure
823 for HNO_3 are provided in Fig. S16. The typical offsets (one half of the average differences) for
824 HNO_3 are less than ~10% (and less than 0.5 ppbv). Despite somewhat larger percent absolute
825 differences than for N_2O between Aura MLS and ACE-FTS HNO_3, there is very good agreement
826 as a function of time between these two datasets in the stratosphere. This is illustrated by the
827 HNO_3 diagnostic information provided in Fig. S17; the poorest correlations are obtained at or
828 below the tropical tropopause.

829 Comparisons of v3.3 Aura MLS and v2.2 ACE-FTS nitric acid profiles have shown good
830 agreement (see also Livesey et al., 2013), as the MLS HNO_3 v3.3 values are now generally larger
831 than in v2.2, for which validation results were provided by Santee et al. (2007). Wolff et al.
832 (2008) also compared MLS (v2.2) and ACE-FTS (v2.2) coincident profiles, and obtained similar
833 results; in addition, they demonstrated that very good agreement exists between the HNO_3
834 profiles from ACE-FTS and coincident profiles from MIPAS on Envisat. Also, comparisons
835 between Aura MLS HNO_3 (v3.3) profiles and wintertime HNO_3 profiles retrieved by a Ground-

based Millimeter-wave Spectrometer (GBMS) in Thule, Greenland, during the first 3 months of 2010, 2011, and 2012 show agreement mostly within 10-15% (Fiorucci et al., 2013).

Figure 24 (top two panels) displays the HNO_3 fields at 46 hPa from the UARS MLS period (1991-1997) as well as from the 2004-2013 period, for which a merged GOZCARDS product was produced, based on Aura MLS and ACE-FTS source datasets. Also shown (bottom two panels) are time series for 45°N and 32 hPa from both these periods; the bottom right panel includes the source and merged time series. We have performed additional investigations (not shown here) which lead us to believe that small upward adjustments to the UARS MLS HNO_3 values (by about 10%) are needed to better cross-correlate these datasets across the two distinct time periods; such relative biases are within the expected systematic errors. This is based on a consideration of ground-based Fourier Transform infrared column HNO_3 data covering the full time period, as well as past GBMS HNO_3 profile retrievals. Also, Aura MLS and ACE-FTS HNO_3 data match ground-based and other correlative data quite well, and typically better than the intrinsically poorer quality UARS MLS HNO_3 data. However, obtaining an optimum global set of adjustments for the UARS MLS nitric acid field will be limited by the number of sites with such ground-based data as well as by the different vertical resolutions for these datasets versus MLS. More collaborative work regarding such analyses is needed in order to find the optimum adjustments to help tie together these two time periods for this species. Although we did not deliver the UARS MLS HNO_3 source data files for GOZCARDS, we could provide these monthly zonal mean series upon request, keeping the above caveats in mind.

6.3 Temperature

Finally, in terms of the initial set of delivered GOZCARDS products, and for the convenience of stratospheric composition data users, we have used temperatures (T) from the Modern-Era Retrospective Analysis for Research and Applications (MERRA) to produce a monthly mean GOZCARDS temperature data set from 1979 onward. MERRA is a NASA Goddard reanalysis (Rienecker et al., 2011) for the satellite era using Goddard Earth Observing System Data Assimilation System version 5 (GEOS-5); T is from the DAS 3d analyzed state MAI6NVANA, version 5.2 files (such as MERRA300.prod.assim.inst6_3d_ana_Nv.20110227.hdf). Data from four daily MERRA files (for 00, 06, 12, and 18 hr UT) were averaged to provide daily mean

865 temperature fields (appropriate for a mean time of 09 hr). Vertical interpolation was performed
866 onto the GOZCARDS pressure grid, which, for temperature, covers 30 pressures levels from
867 1000 hPa to 0.0147 hPa. Averaged values were stored for the 10° GOZCARDS latitude bins, and
868 daily results were binned to create the GOZCARDS monthly temperature data set (version 1.0).

869 ## 7 Summary and conclusions

870 We have reviewed the GOZCARDS project's production of merged data records of stratospheric
871 composition, mainly for HCl, H_2O, and O_3, using carefully screened satellite data, starting in
872 1979 with SAGE I and continuing through Aura MLS and ACE-FTS data periods. The source
873 data have a high degree of maturity and we have reinforced our confidence in their usefulness
874 through investigations of various diagnostics (offsets, annual cycles, correlations and trend
875 differences of deseasonalized series). These records are publicly available as GOZCARDS
876 ESDR version 1.01 and can be referenced using DOI numbers (Froidevaux et al., 2013b,
877 Anderson et al., 2013, and Wang et al., 2013, for the above species, respectively). The other
878 GOZCARDS data records also have references, namely Schwartz et al. (2013) for the MERRA-
879 based temperature records, and Froidevaux et al. (2013c, 2013d) for N_2O and HNO_3,
880 respectively. Table 2 provides a summary of the GOZCARDS monthly mean datasets. Yearly
881 netCDF files are available for public access (http://mirador.gsfc.nasa.gov). The merging
882 methodology follows from a determination of mean biases (for each pressure level and 10°
883 latitude bin) between monthly mean series, based on the overlap periods. For ozone, SAGE II
884 data are the chosen reference, whereas for other species, the merging basis is equivalent to an
885 average of the datasets during the periods of overlap. The merged data files contain the average
886 offset values applied to each source data time series, along with standard deviations and standard
887 errors. The GOZCARDS README document (Froidevaux et al., 2013a) provides more details
888 about data file quantities, including local time and solar zenith angle information, and a list of
889 days with available data. We also display here estimated systematic errors about the merged
890 values; we find that mixing ratio errors are typically within 5% to 15% and are consistent with
891 the magnitude of observed relative biases.

892 The GOZCARDS HCl merged record in the upper stratosphere enables long-term tracking of
893 changes in total stratospheric chlorine. The long-term increase in HCl prior to the late 1990s, and

894 the subsequent gentler decrease in the 21st century, are delayed manifestations of changes in the
895 sum of the surface source gas abundances as a result of regulations from the Montreal Protocol
896 and its amendments. From 1997 to 2010, the average rate of change in upper stratospheric HCl
897 (50°S to 50°N) was about -0.4 to -0.7%/yr (with the smaller rates of decrease after 2003). In the
898 lower stratosphere, where Aura MLS data are weighted heavily, recent short-term variations
899 have shown a flattening out and, in particular for northern midlatitudes and at 50-70 hPa for the
900 deep tropics, a significant reversal and increasing trend (see also Mahieu et al., 2014), compared
901 to the decrease from the late 1990s to about 2004. However, lower stratospheric HCl tendencies
902 appear to be reversing again in recent years (2011-2014), with decreases at northern
903 midlatitudes and some increasing tendencies at southern midlatitudes. In the future, we expect to
904 see long-term global HCl decreases in both the upper and lower stratosphere.

905 For water vapor, we have used data from the same instruments as for HCl, with the same
906 methodology, except for the addition of 1991-1993 UARS MLS data. The H_2O data record
907 shows large mesospheric variations that are anti-correlated with the solar flux over the past two
908 11-yr solar cycles. Net long-term trends in lower stratospheric H_2O are quite small if one
909 considers the past 22 years, but there has been considerable interannual variability, including the
910 steep drop from 2000 to 2001, as mentioned in past work. While H_2O tendencies have been
911 generally positive after 2001, the 68 and 100 hPa levels show some steep decreases (by 0.5-0.8
912 ppmv) from 2011 to 2013 (see also Urban et al., 2014). Over the past 22 years, long-term global
913 H_2O increases of order 10% are observed in the upper stratosphere and lower mesosphere,
914 whereas a decrease of nearly 10% has occurred in the lower stratosphere (near 70-100 hPa).
915 However, there is no regular monotonic change on decadal timescales, especially in the tropical
916 lower stratosphere, where fairly sharp decreases followed by steadier increases may be a
917 recurrent pattern (see also Fueglistaler, 2012); this complicates the detection of any small
918 underlying trend. As one might expect from the well-documented temperature influence on the
919 tropical lower stratosphere, H_2O variability (based on maximum minus minimum yearly
920 averages) is largest in the tropics and just above the tropopause. More accurate studies of
921 seasonal to decadal water vapor variability will be enabled by continuing such merged H_2O
922 datasets in the future. A reduction in model spread for stratospheric H_2O is likely easier to

923 achieve than tighter upper tropospheric model results; for the upper troposphere, see the
924 data/model comparisons (H_2O and ice water content) by Jiang et al. (2012).

925 For ozone, we have used measurements from SAGE I, SAGE II, HALOE, UARS MLS, Aura
926 MLS and ACE-FTS to produce a merged record starting in 1979, after adjusting the series to
927 SAGE II. We observed temporal drifts in the SAGE II series, after conversion to the
928 GOZCARDS mixing ratio/pressure grid, as a result of the NCEP temperature data used in this
929 conversion, mostly in the upper stratosphere after June 2000 (see also McLinden et al., 2009). To
930 mitigate this issue, we used HALOE upper stratospheric O_3 as a reference for July 2000 to
931 November 2005, after adjusting the HALOE series to SAGE II. The resulting GOZCARDS
932 merged O_3 data for northern midlatitudes have been used in regression analyses (Nair et al.,
933 2013) to reveal decreases in the whole stratosphere for 1984-1996. Nair et al. (2015) extended
934 this work and found increasing trends in upper stratospheric GOZCARDS O_3 since 1997, but no
935 significant positive trends in the lower stratosphere. Other studies of GOZCARDS O_3 profile
936 trends have been discussed as part of the WMO (2014) and SI^2N assessments (Tummon et al.,
937 2015; Harris et al., 2015). Here, we looked at the consistency of column data between
938 stratospheric GOZCARDS O_3 and work by Ziemke and Chandra (2012), who noted that a fairly
939 rapid change (“recovery’’) in near-global ozone columns from TOMS and OMI could be inferred
940 since the mid-1990s. We show that the similarly analyzed GOZCARDS column data does not
941 show an upturn of more than 0.5-1% since that period. Reasons for these differences could
942 include data coverage or merging-related issues in either dataset, or inaccuracies in globally-
943 averaged stratospheric columns. A recent global total ozone study (Shepherd et al., 2014) also
944 points to less of a return towards 1980 levels than implied by ZC12.

945 We also briefly described the creation of N_2O and HNO_3 GOZCARDS data records, based on
946 Aura MLS and ACE-FTS. The agreement between these two instruments’ datasets for these
947 species was shown to be generally very good. For HNO_3, UARS MLS HNO_3 source datasets in
948 the GOZCARDS format are available from the authors. However, a small upward adjustment (of
949 order 10%) to the UARS MLS values is likely needed based on our preliminary work comparing
950 these series to HNO_3 column results from FTIR measurements. More detailed work should help
951 determine if global adjustments can indeed be made to UARS MLS HNO_3 data; lacking this, one

should ensure that error bars reflect likely biases that can affect the continuity between HNO_3 datasets before and after 2000, given the multi-year gap in satellite coverage for this species.

There is a Supplement related to this article.

Acknowledgements. Work at JPL was performed under contract with the National Aeronautics and Space Administration (NASA). We dedicate this work to the memory of Professor Derek Cunnold (Georgia Institute of Technology) who was a member of the original NASA MEaSUREs (Making Earth System Data Records for Use in Research Environments) GOZCARDS proposal. The GOZCARDS data generation could not have been possible without the past work from instrument teams for SAGE I, SAGE II, HALOE, UARS MLS, Aura MLS, and ACE-FTS, and related data usage documentation. At JPL, we thank Joe Waters for his leadership role in making MLS instruments and datasets possible and Bill Read for his key role; thanks to Vince Perun for MERRA-related work, and to Brian Knosp and Robert Thurstans for database and computer management assistance. We also thank Kaley Walker and Ashley Jones for comments regarding ACE-FTS data, Gloria Manney and William Daffer for help in making the original ACE-FTS data profiles available, and Joe Zawodny and Larry Thomason for their contributions and comments regarding SAGE data. We acknowledge the work of the GMAO team responsible for MERRA data used to generate the GOZCARDS temperatures, specifically, Steven Pawson and Jianjun Jin for discussions and cross-checks regarding temperature data. We acknowledge Jerry Ziemke for the ozone column data (from Ziemke and Chandra, 2012), and Sean Davis for discussions on data usage and screening, and the creation of long-term series. For early HNO_3-related work connecting ground-based data to MLS datasets, we thank Giovanni Muscari and Irene Fiorucci. We are thankful for the NOAA Earth System Research Laboratory (ESRL) Global Monitoring Division (GMD) website information and data on total surface chlorine. We obtained solar flux data for the Ottawa/Penticton sites from the NOAA National Geophysical Data Center (NGDC) website (www.ngdc.noaa.gov), for which we also acknowledge the National Research Council of Canada. We thank the reviewers for their constructive comments and Michel Van Roozendael for useful discussions (notably related to ozone column comparisons).

References

Anderson, J. G., Brune, W. H., and Proffitt, M. H.: Ozone destruction by chlorine radicals within the Antarctic vortex: The spatial and temporal evolution of $ClO-O_3$ anticorrelation based on in situ ER-2 data, J. Geophys. Res., 94, 11,465-11,479, 1989.

Anderson, J., Russell, J. M., Solomon, S., and Deaver, L. E.: HALOE confirmation of stratospheric chlorine decreases in accordance with the Montreal Protocol, J. Geophys. Res., 105, 4483-4490, 2000.

Anderson, J., Froidevaux, L., Fuller, R. A., Bernath, P. F., Livesey, N. J., Pumphrey, H. C., Read, W. G., and Walker, K. A.: GOZCARDS Merged Data for Water Vapor Monthly Zonal Means on a Geodetic Latitude and Pressure Grid, version 1.01, Greenbelt, MD, USA: NASA Goddard Earth Science Data and Information Services Center, accessible from doi:10.5067/MEASURES/GOZCARDS/DATA3003, 2013.

Barath, F., Chavez, M. C., Cofield, R. E., Flower, D. A., Frerking, M. A., Gram, M. B., Harris, W. M., Holden, J. R., Jarnot, R. F., Kloezeman, W. G., Klose, G. J., Lau, G. K., Loo, M. S., Maddison, B. J., Mattauch, R. J., McKinney, R. P., Peckham, G. E., Pickett, H. M., Siebes, G., Soltis, F. S., Suttie, R. A., Tarsala, J. A., Waters, J. W., and Wilson, W. J.: The Upper Atmosphere Research Satellite Microwave Limb Sounder Experiment, J. Geophys. Res., 98, 10751-10762, 1993.

Bernath, P. F., McElroy, C. T., Abrams, M. C., Boone, D., Butler, M., Camy-Peyret, C., Carleer, M., Clerbaux, C., Coheur, P.-F., Colin, R., DeCola, P., DeMaziere, M., Drummond, J. R., Dufour, D., Evans, W. F. J., Fast, H., Fussen, D., Gilbert, K., Jennings, D. E., Llewellyn, E. J., Lowe, R. P., Mahieu, E., McConnell, J. C., McHugh, M., McLeod, S. D., Michaud, R., Midwinter, C., Nassar, R., Nichitiu, F., Nowlan, C., Rinsland, C. P., Rochon, Y. J., Rowlands, N., Semeniuk, K., Simon, P., Skelton, R., Sloan, J. J., Soucy, M.-A., Strong, K., Tremblay, P., Turnbull, D., Walker, K. A., Walkty, I., Wardle, D. A., Wehrle, V., Zander, R., and Zou, J.: Atmospheric Chemistry Experiment (ACE): Mission overview, Geophys. Res. Lett., 32, L15S01, doi:10.1029/2005GL022386, 2005.

Bhatt, P. P., Remsberg, E. E., Gordley, L. L., McInerney, J. M., Brackett, V. G., and Russell, III, J. M.: An evaluation of the quality of Halogen Occultation Experiment ozone profiles in the lower stratosphere, J. Geophys. Res., 104 (D8), 9261-9275, 1999.

1008 Bhartia, P. K., Herman, J., and McPeters, R. D.: Effect of Mount Pinatubo aerosols on total ozone
1009 measurements from Backscatter Ultraviolet (BUV) experiments, J. Geophys. Res., 98 (D10), 18547-
1010 18554, doi:10.1029/93JD01739, 1993.

1011 Borchi, F., Pommereau, J.-P., Garnier, A., and Pinharanda, M.: Evaluation of SHADOZ sondes, HALOE
1012 and SAGE II ozone profiles at the tropics from SAOZ UV-Vis remote measurements onboard long
1013 duration balloons, Atmos. Chem. Phys., 5, 1381-1397, doi:10.5194/acp-5-1381-2005, 2005.

1014 Bourassa, A. E., Degenstein, D. A., Randel, W. J., Zawodny, J. M., Kyrölä, E., McLinden, C. A., Sioris,
1015 C. E., and Roth, C. Z., Trends in stratospheric ozone derived from merged SAGE II and Odin-OSIRIS
1016 satellite observations, Atmos. Chem. Phys., 14, 6983-6994, doi:10.5194/acp-14-6983-2014, 2014.

1017 Brown, A. T., Chipperfield, M. P., Boone, C., Wilson, C., Walker, K. A., and Bernath, P.: Trends in
1018 atmospheric halogen containing gases since 2004, J. Quant. Spec. Rad. Trans., 112, 2552-2566,
1019 doi:10.1016/j.jqsrt.2011.07.005, 2011.

1020 Chandra, S., Jackman, C. H., Fleming, E. L., and Russell, J. M.: The seasonal and long term changes in
1021 mesospheric water vapor, Geophys. Res. Lett., 24, No. 6, 639-642, 1997.

1022 Chu, W. P., and McCormick, M. P.: Inversion of Stratospheric Aerosol and Gaseous Constituents From
1023 Spacecraft Solar Extinction Data in the 0.38-1.0 μm Wavelength Region, Appl. Opt., 18, No. 9, 1404-
1024 1413, 1979.

1025 Cunnold, D. M., Chu, W. P., Barnes, R. A., McCormick, M. P., and Veiga, R. E.: Validation of SAGE II
1026 ozone measurements, J. Geophys. Res., 94, 8447–8460, 1989.

1027 Damadeo, R. P., Zawodny, J. M., Thomason, L. W., and Iyer, N.: SAGE version 7.0 algorithm:
1028 application to SAGE II, Atmos. Meas. Tech., 6, 3539-3561, doi:10.5194/amt-6-3539-2013, 2013.

1029 Dupuy, E., Walker, K. A., Kar, J., Boone, C. D., McElroy, C. T., Bernath, P. F.,
1030 Drummond, J. R., Skelton, R., McLeod, S. D., Hughes, R. C., Nowlan, C. R., Dufour, D. G., Zou, J.,
1031 Nichitiu, F., Strong, K., Baron, P., Bevilacqua, R. M., Blumenstock, T., Bodeker, G. E., Borsdorff, T.,
1032 Bourassa, A. E., Bovensmann, H., Boyd, I. S., Bracher, A., Brogniez, C., Burrows, J. P., Catoire, V.,
1033 Ceccherini, S., Chabrillat, S., Christensen, T., Coffey, M. T., Cortesi, U., Davies, J., De Clercq, C.,
1034 Degenstein,D. A., De Maziere, M., Demoulin, P., Dodion, J., Firanski, B., Fischer, H., Forbes, G.,
1035 Froidevaux, L., Fussen, D., Gerard, P., Godin-Beekmann, S., Goutail, F., Granville, J., Griffith, D.,

Haley, C. S., Hannigan, J. W., Hopfner, M., Jin, J. J., Jones, A., Jones, N. B., Jucks, K., Kagawa, A., Kasai, Y., Kerzenmacher, T. E., Kleinbohl, A., Klekociuk, A. R., Kramer, I., Kullmann, H., Kuttippurath, J., Kyrölä, E., Lambert, J.-C., Livesey, N. J., Llewellyn, E. J., Lloyd, N. D., Mahieu, E., Manney, G. L., Marshall, B. T., McConnell, J. C., McCormick, M. P., McDermid, I. S., McHugh, M., McLinden, C. A., Mellqvist, J., Mizutani, K., Murayama, Y., Murtagh, D. P., Oelhaf, H., Parrish, A., Petelina, S. V., Piccolo, C., Pommereau, J.-P., Randall, C. E., Robert, C., Roth, C., Schneider, M., Senten, C., Steck, T., Strandberg, A., Strawbridge, K. B., Sussmann, R., Swart, D. P. J., Tarasick, D. W., Taylor, J. R., Tetard, C., Thomason, L. W., Thompson, A. M., Tully, M. B., Urban, J., Vanhellemont, F., Vigouroux, C., von Clarmann, T., von der Gathen, P., von Savigny, C., Waters, J. W., Witte, J. C., Wolff, M., and Zawodny, J. M.: Validation of ozone measurements from the Atmospheric Chemistry Experiment (ACE), Atmos. Chem. Phys., 9, 287–343, doi:10. 5194/acp-9-287-2009, 2009.

Eckert, E., von Clarmann, T., Kiefer, M., Stiller, G. P., Lossow, S., Glatthor, N., Degenstein, D. A., Froidevaux, L., Godin-Beekmann, S., Leblanc, T., McDermid, S., Pastel, M., Steinbrecht, W., Swart, D. P. J., Walker, K. A., and Bernath, P. F.: Drif-corrected trends and periodic variations in MIPAS IMK/IAA ozone measurements, Atmos. Chem. Phys., 14, 2571-2589, doi:10.5194/acp-14-2571-2014, 2014.

Engel, A., Strunk, M., Muller, M., Haase, H.-P., Poss, C., Levin, I., and Schmidt, U.: The temporal development of total chlorine in the high latitude stratosphere based on reference distributions of mean age derived from CO_2 and SF_6, J. Geophys. Res., 107, 4136, doi:10.1029/2001JD000584, 2002.

Farman, J. C., Gardiner, B. G., and Shanklin, J. D.: Large losses of total ozone in Antarctica reveal seasonal ClOx/NOx interaction, Nature, 315, 207-210, 1985.

Fiorucci, I., Muscari, G., Froidevaux, L., and Santee, M. L.: Ground-based stratospheric O_3 and HNO_3 measurements at Thule, Greenland: an intercomparison with Aura MLS observations, Atmos. Meas. Tech., 6, 2441–2453, doi:10.5194/amt-6-2441-2013, 2013.

Frith, S. M., Kramarova, N. A., Stolarski, R. S., McPeters, R. D., Bhartia, P. K., and Labow, G. J.: Recent changes in total column ozone based on the SBUV Version 8.6 Merged Ozone Data Set, J. Geophys. Res., 119, 9735-9751, doi:10.1029/2014JD021889, 2014.

Froidevaux, L., Livesey, N. J., Read, W. G., Salawitch, R. J., Waters, J. W., Drouin, B., MacKenzie, I. A., Pumphrey, H. C., Bernath, P., Boone, C., Nassar, R., Montzka, S., Elkins, J., Cunnold, D., and Waugh, D.: Temporal decrease in upper atmospheric chlorine, Geophys. Res. Lett., 33, L23813, doi:10.1029/2006GL027600, 2006.

Froidevaux, L., Jiang, Y. B., Lambert, A., Livesey, N. J., Read, W. G., Waters, J. W., Fuller, R. A., Marcy, T. P., Popp, P. J., Gao, R. S., Fahey, D. W., Jucks, K. W., Stachnik, R. A., Toon, G. C., Christensen, L. E., Webster, C. R., Bernath, P. F., Boone, C. D., Walker, K. A., Pumphrey, H. C., Harwood, R. S., Manney, G. L., Schwartz, M. J., Daffer,W.H., Drouin, B. J., Cofield, R. E., Cuddy, D. T., Jarnot, R. F., Knosp, B. W., Perun, V. S., Snyder, W. V., Stek, P. C., Thurstans, R. P., and Wagner, P. A.: Validation of Aura Microwave Limb Sounder HCl measurements, J. Geophys. Res., 113, doi:10.1029/2007JD009025, D15S25, 2008a.

Froidevaux, L., Jiang, Y. B., Lambert, A., Livesey, N. J., Read, W. G., Waters, J. W., Browell, E. V., Hair, J. W., Avery, M. A., McGee, T. J., Twigg, L. W., Sumnicht, G. K., Jucks, K. W., Margitan, J. J., Sen, B., Stachnik, R. A., Toon, G. C., Bernath, P. F., Boone, C. D., Walker, K. A., Filipiak, M. J., Harwood, R. S., Fuller, R. A., Manney, G. L., Schwartz, M. J., Daffer,W.H., Drouin, B. J., Cofield, R. E., Cuddy, D. T., Jarnot, R. F., Knosp, B. W., Perun, V. S., Snyder, W. V., Stek, P. C., Thurstans, R. P., and Wagner, P. A.: Validation of Aura Microwave Limb Sounder stratospheric and mesospheric ozone measurements, J. Geophys. Res., 113, doi:10.1029/2007JD008771, D15S20, 2008b.

Froidevaux, L., Fuller, R., Schwartz, M., Anderson, J., and Wang, R.: README Document for the Global OZoneChemistry And Related trace gas Data records for the Stratosphere (GOZCARDS) project, Goddard Earth Sciences Data and Information Services Center (GES DISC), http://disc.gsfc.nasa.gov, NASA Goddard Space Flight Center, Code 610.2, Greenbelt, MD 20771 USA, 2013a.

Froidevaux, L., Anderson, J., Fuller, R. A., Bernath, P. F., Livesey, N. J., Russell III, J. M., and Walker, K.A.: GOZCARDS Merged Data for Hydrogen Chloride Monthly Zonal Means on a Geodetic Latitude and Pressure Grid, version 1.01, Greenbelt, MD, USA: NASA Goddard Earth Science Data and Information Services Center, accessible from doi:10.5067/MEASURES/GOZCARDS/DATA3002, 2013b.

Froidevaux, L., Fuller, R. A., Lambert, A., Livesey, N. J., Bernath, P. F., Livesey, N. J., and Walker, K.A.: GOZCARDS Merged Data for Nitrous Oxide Monthly Zonal Means on a Geodetic Latitude and Pressure Grid, version 1.01, Greenbelt, MD, USA: NASA Goddard Earth Science Data and Information Services Center, accessible from doi:10.5067/MEASURES/GOZCARDS/DATA3013, 2013c.

Froidevaux, L., Fuller, R. A., Santee, M. L., Manney, G. L., Livesey, N. J., Bernath, P. F., and Walker, K.A.: GOZCARDS Merged Data for Nitric Acid Monthly Zonal Means on a Geodetic Latitude and Pressure Grid, version 1.01, Greenbelt, MD, USA: NASA Goddard

Earth Science Data and Information Services Center, accessible from doi:10.5067/MEASURES/GOZCARDS/DATA3008, 2013d.

Fueglistaler, S.: Step-wise changes in stratospheric water vapor? J. Geophys. Res., 117, D13302, doi:10.1029/2012JD017582, 2012.

Gebhardt, C., Rozanov, A., Hommel, R., Weber, M., Bovensmann, H., Burrows, J. P., Degenstein, D., Froidevaux, L., and Thompson, A. M.: Stratospheric ozone trends and variability as seen by SCIAMACHY from 2002 to 2012, Atmos. Chem. Phys., 14, 831–846, doi:10.5194/acp-14-831-2014, 2014.

Haefele, A., Hocke, K., Kampfer, N., Keckhut, P., Marchand, M., Bekki, S., Morel, B., Egorova, T., and Rozanov, E.: Diurnal changes in middle atmospheric H_2O and O_3: Observations in the Alpine region and climate models, J. Geophys. Res., 113, D17303, doi:10.1029/2008JD009892, 2008.

Harris, N. R. P., Hassler, B., Tummon, F., Bodeker, G. E., Hubert, D., Petropavlovskikh, I., Steinbrecht, W., Anderson, J., Bhartia, P. K., Boone, C. D., Bourassa, A., Davis, S. M., Degenstein, D., Delcloo, A., Frith, S. M., Froidevaux, L., Godin-Beekmann, S., Jones, N., Kurylo, M. J., Kyrölä, E., Laine, M., Leblanc, S. T., Lambert, J.-C., Liley, B., Mahieu, E., Maycock, A., de Maziere, M., Parrish, A., Querel, R., Rosenlof, K. H., Roth, C., Sioris, C., Staehelin, J., Stolarski, R. S., Stubi, R., Tamminen, J., Vigouroux, C., Walker, K., Wang, H. J., Wild, J., and Zawodny, J. M.: Past changes in the vertical distribution of ozone - Part 3: Analysis and interpretation of trends, Atmos. Chem. Phys., in press, 2015.

Hassler, B., Bodeker, G. E., Solomon, S., and Young, P. J.: Changes in the polar vortex: Effects on Antarctic total ozone observations at various stations, Geophys. Res. Lett., 38, L01805, doi:10.1029/2010GL045542, 2011.

Hegglin, M. I., Tegtmeier, S., Anderson, J., Froidevaux, L., Fuller, R., Funke, B., Jones, A., Lingenfelser, G., Lumpe, J., Pendlebury, D., Remsberg, E., Rozanov, A., Toohey, M., Urban, J., von Clarmann, T., Walker, K. A., Wang, R., and Weigel, K.: SPARC Data Initiative: Comparison of water vapor climatologies from international satellite limb sounders, J. Geophys. Res. Atmos., 118, 11,824–11,846, doi: 10.1002/jgrd.50752, 2013.

Hervig, M., and McHugh, M.: Cirrus detection using HALOE measurements, Geophys. Res. Lett., 26, No. 6, 719-722, 1999.

1126 Huang, F. T., Mayr, H. G., Russell III, J. M., and Mlynczak, M. G.: Ozone diurnal variations in the
1127 stratosphere and lower mesosphere, based on measurements from SABER on TIMED,
1128 J. Geophys. Res., 115, D24308, doi:10.1029/2010JD014484, 2010.

1129 Hubert, D., et al., Ground-based assesment of the bias and long-term stability of fourteen limb and
1130 occultation ozone profile data records, Atmos. Meas. Tech., in review, 2015.

1131 Hurst, D. F., Lambert, A., Read, W. G., Davis, S. M., Rosenlof, K. H., Hall, E. G., Jordan, A. F., and
1132 Oltmans, S. J.: Validation of Aura Microwave Limb Sounder stratospheric water vapor measurements by
1133 the NOAA frost point hygrometer, J. Geophys. Res. Atmos., 119, 1612-1625,
1134 doi:10.1002/2013JD020757, 2014.

1135 Jiang, J. H., Su, H., Zhai, C., Perun, V. S., Del Genio, A., Nazarenko, L. S., Donner, L. J., Horowitz, L.,
1136 Seman, C., Cole, J., Gettelman, A., Ringer, M. A., Rotstayn, L., Jeffrey, S., Wu, T., Brient, F., Dufresne,
1137 J.-L., Kawai, H., Koshiro, T., Watanabe, M., L'Écuyer, T. S., Volodin, E. M., Iversen, T., Drange, H.,
1138 Mesquita, M. D. S., Read, W. G., Waters, J. W., Tian, B., Teixeira, J., and Stephens, G. L.: Evaluation of
1139 cloud and water vapor simulations in CMIP5 climate models using NASA "A-Train" satellite
1140 observations, J. Geophys. Res., 117, D14105, doi:10.1029/2011JD017237, 2012.

1141 Jones, A., Urban, J., Murtagh, D. P., Eriksson, P., Brohede, S., Haley, C., Degenstein, D., Bourassa, A.,
1142 von. Savigny, C., Sonkaew, T., Rozanov, A., Bovensmann, H., and Burrows, J.: Evolution of
1143 stratospheric ozone and water vapour time series studied with satellite measurements, Atmos. Chem.
1144 Phys., 9, 6055-6075, doi:10.5194/acp-9-6055-2009, 2009.

1145 Jones, A., Urban, J., Murtagh, D. P., Sanchez, C., Walker, K. A., Livesey, N. J., Froidevaux, L., and
1146 Santee, M. L.: Analysis of HCl and ClO time series in the upper stratosphere using satellite data sets,
1147 Atmos. Chem. Phys., 11, 5321-5333, doi:10.5194/acp-11-5321-2011, 2011.

1148 Kirgis, G., Leblanc, T., McDermid, I. S., and Walsh, T. D.: Stratospheric ozone interannual variability
1149 (1995–2011) as observed by Lidar and Satellite at Mauna Loa Observatory, HI and Table Mountain
1150 Facility, CA, Atmos. Chem. Phys., 13, 5033–5047, doi:10.5194/acp-13-5033-2013, 2013.
1151
1152 Kley, D., Stone, E. J., Henderson, W. R., Drummond, J. W., Harrop, W. J., Schmeltekopf, A. L.,
1153 Thompson, T. L., and Winkler, R. H.: In Situ Measurements of the Mixing Ratio of Water Vapor in the
1154 Stratosphere, J. Atmos. Sci., 36, 2513-2524, 1979.
1155

Kohlhepp, R., Ruhnke, R., Chipperfield, M. P., De Maziere M., Notholt, J., Barthlott, S., Batchelor, R. L., Blatherwick, R. D., Blumenstock, T., Coffey, M. T., Demoulin, P., Fast, H., Feng, W., Goldman, A., Griffith, D. W. T., Hamann, K., Hannigan, J. W., Hase, F., Jones, N. B., Kagawa, A., Kaiser, I., Kasai, Y., Kirner, O., Kouker, W., Lindenmaier, R., Mahieu, E., Mittermeier, R. L., Monge-Sanz, B., Morino, I., Murata, I., Nakajima, H., Palm, M., Paton-Walsh, C., Raffalski, U., Reddmann, T., Rettinger, M., Rinsland, C. P., Rozanov, E., Schneider, M., Senten, C., Servais, C., Sinnhuber, B.-M., Smale, D., Strong, K., Sussmann, R., Taylor, J. R., Vanhaelewyn, G., Warneke, T., Whaley, C., Wiehle, M., and Wood, S. W.: Observed and simulated time evolution of HCl, $ClONO_2$, and HF total column abundances, Atmos. Chem. Phys., 12, 3527–3557, doi:10.5194/acp-12-3527-2012, 2012.

Kuttippurath, J., Lefevre, F., Pommereau, J.-P., Roscoe, H. K., Goutail, F., Pazmino, A., and Shanklin, J. D.: Antarctic ozone loss in 1979–2010: first sign of ozone recovery, Atmos. Chem. Phys., 13, 1625–1635, doi:10.5194/acp-13-1625-2013, 2013.

Kyrölä, E., Laine, M., Sofieva, V., Tamminen, J., Päivärinta, S.-M., Tukiainen, S., Zawodny, J., and Thomason, L.: Combined SAGE II-GOMOS ozone profile data set for 1984-2011 and trend analysis of the vertical distribution of ozone, Atmos. Chem. Phys., 13, 10,645-10,658, doi:10.5194/acp-13-10645-2013, 2013.

Lambert, A., Read, W. G., Livesey, N. J., Santee, M. L., Manney, G. L., Froidevaux, L., Wu, D. L., Schwartz, M. J., Pumphrey, H. C., Jimenez, C., Nedoluha, G. E., Cofield, R. E., Cuddy, D. T., Daffer, W. H., Drouin, B. J., Fuller, R. A., Jarnot, R. F., Knosp, B. W., Pickett, H. M., Perun, V. S., Snyder, W. V., Stek, P. C., Thurstans, R. P., Wagner, P. A., Waters, J. W., Jucks, K. W., Toon, G. C., Stachnik, R. A., Bernath, P. F., Boone, C. D., Walker, K. A., Urban, J., Murtagh, D., Elkins, J. W., and Atlas, E.: Validation of the Aura Microwave Limb Sounder stratospheric water vapour and nitrous oxide measurements, J. Geophys. Res., 112, D24S36, doi:10.1029/2007JD008724, 2007.

Livesey, N. J., Read, W. J., Froidevaux, L., Waters, J. W., Santee, M. L., Pumphrey, H. C., Wu, D. L., Shippony, Z., and Jarnot, R. F.: The UARS Microwave Limb Sounder version 5 dataset: Theory, characterization and validation, J. Geophys. Res., 108 (D13), 4378, doi:10.1029/2002JD002273, 2003.

Livesey, N. J., Read, W. G., Froidevaux, L., Lambert, A., Manney, G. L., Pumphrey, H. C., Santee, M. L., Schwartz, M. J., Wang, S., Cofield, R. E., Cuddy, D. T., Fuller, R. A., Jarnot, R. F., Jiang, J. H., Knosp, B. W., Stek, P. C., Wagner, P. A., and Wu, D. L.: EOS MLS Version 3.3/3.4 Level 2 data quality

and description document, Tech. rep., Jet Propulsion Laboratory, available from http://mls.jpl.nasa.gov/, 2013.

Mahieu, E., Duchatelet, P., Demoulin, P., Walker, K. A., Dupuy, E., Froidevaux, L., Randall, C., Catoire, V., Strong, K., Boone, C. D., Bernath, P. F., Blavier, J.-F., Blumenstock, T., Coffey, M., DeMaziere, M., Griffith, D., Hannigan, J., Hase, F., Jones, N., Jucks, K. W., Kagawa, A., Kasai, Y., Mebarki, Y., Mikuteit, S., Nassar, R., Notholt, J., Rinsland, C. P., Robert, C., Schrems, O., Senten, C., Smale, D., Taylor, J., Tetard, C., Toon, G. C., Warneke, T., Wood, S. W., Zander, R., and Servais, C.: Validation of ACE-FTS v2.2 measurements of HCl, HF, CCl_3F and CCl_2F_2 using space-, balloon- and ground-based instrument observations, Atmos. Chem. Phys., 8, 6199-6221, doi:10.5194/acp-8-6199-2008, 2008.

Mahieu, E., Zander, R., Bernath, P. F., Boone, C. D., and Walker, K. A.: Recent trend anomaly of hydrogen chloride (HCl) at northern mid-latitudes derived from Jungfraujoch, HALOE, and ACE-FTS infrared solar observations, in: The Atmospheric Chemistry Experiment ACE at 10: a solar occultation anthology, Bernath, P. (Ed.), Deepak Publishing, Hampton, VA, 239-249, 2013.

Mahieu, E., Chipperfield, M. P., Notholt, J., Reddmann, T., Anderson, J., Bernath, P. F., Blumenstock, T., Coffey, M. T., Dhomse, S. S., Feng, W., Franco, B., Froidevaux, L., Griffith, D. W. T., Hannigan, J. W., Hase, F., Hossaini, R., Jones, N. B., Morino, I., Murata, I., Nakajima, H., Palm, M., Paton-Walsh, C., Russell III, J. M., Schneider, M., Servais, C., Smale, D., and Walker, K. A.: Recent Northern Hemisphere stratospheric HCl increase due to atmospheric circulation changes, Nature, 515, 104-107, doi:10.1038/nature13857, 2014.

McCormick, M. P., Zawodny, J. M., Veiga, R. E., Larsen, J. C., and Wang, P. H.: An overview of SAGE-I and II ozone measurements, Planetary and Space Science, 37, No. 12, 1567-1586, 1989.

McHugh, M., Hervig, M., Magill, B., Thompson, R. E., Remsberg, E., Wrotny, J., and Russell, J. M.: Improved mesospheric temperature, water vapor, and polar mesospheric cloud extinctions from HALOE, Geophys. Res. Lett., 30, 8, doi: 10.1029/2002GL016859, 2003.

McLinden, C. A., Tegtmeier, S., and Fioletov, V.: Technical Note: A SAGE-corrected SBUV zonal-mean ozone data set, Atmos. Chem. Phys., 9, 7963–7972, doi:10.5194/acp-9-7963-2009, 2009.

McPeters, R. D., Bhartia, P. K., Haffner, D., Labow, G. J. and Flynn, L.: The v8.6 SBUV Ozone Data Record: An Overview, J. Geophys. Res., 118, 8032-8039, doi:10.1002/jgrd.50597, 2013.

1214 Molina, M. J., and Rowland, F. S.: Stratospheric sink for chlorofluoromethane: chlorine atom-catalyzed
1215 destruction of ozone, Nature, 249, 810-812, 1974.

1216 Montzka, S. A., Butler, J. H., Elkins, J. W., Thompson, T. M., Clarke, A. D., and Lock, L. T.: Present
1217 and future trends in the atmospheric burden of ozone-depleting halogens, Nature, 398, 690-694,
1218 doi:10.1038/19499, 1999.

1219 Morris, G. A., Gleason, J. F., Russell III, J. M., Schoeberl, M. R., and McCormick, M. P.: A comparison
1220 of HALOE V19 with SAGE II V6.00 ozone observations using trajectory mapping, J. Geophys. Res.,
1221 107, D13, 4177, doi:10.1029/2001JD000847, 2002.

1222 Mote, P. W., Rosenlof, K. H., McIntyre, M. E., Carr, E. S., Gille, J. C., Holton, J. R., Kinnersley, J. S.,
1223 Pumphrey, H. C., Russell III, J. M., and Waters, J. W.: An atmospheric tape recorder: The imprint of
1224 tropical tropopause temperatures on stratospheric water vapor,
1225 J. Geophys. Res., 101, 3989–4006, 1996.

1226 Nair, P. J., Godin-Beekmann, S., Froidevaux, L., Flynn, L. E., Zawodny, J. M., Russell III, J. M.,
1227 Pazmino, A., Ancellet, G., Steinbrecht, W., Claude, H., Leblanc, T., McDermid, S., van Gijsel, J. A. E.,
1228 Johnson, B., Thomas, A., Hubert, D., Lambert, J.-C., Nakane, H., and Swart, D. P. J.: Relative drifts and
1229 stability of satellite and ground-based stratospheric ozone profiles at NDACC lidar stations, Atmos.
1230 Meas. Tech., 5, 1301–1318, doi: 10.5194/amt-5-1301-2012, 2012.

1231 Nair, P. J., Godin-Beekmann, S., Kuttippurath, J., Ancellet, G., Goutail, F., Pazmiño, A., Froidevaux, L.,
1232 Zawodny, J. M., Evans, R. D., Wang, H.-J., Anderson, A., and Pastel, M.: Ozone trends derived from the
1233 total column and vertical profiles at a northern mid-latitude station, Atmos. Chem. Phys., 13, 10373–
1234 10384, doi:10.5194/acp-13-10373-2013, 2013.
1235
1236 Nair , P. J., Froidevaux, L., Kuttippurath, J., Zawodny, J. M., Russell III, J. M., Steinbrecht, W., Claude,
1237 H., Leblanc, T., van Gijsel, J. A. E., Johnson, B., Swart, D. P. J., Thomas, A., Querel, R., Wang, R., and
1238 Anderson, J.: Subtropical and midlatitude ozone trends in the stratosphere: Implications for recovery, J.
1239 Geophys. Res., 120, 7247-7257, doi:10.1002/2014JD022371, 2015.

1240 Nazaryan, H., McCormick, M. P., and Russell III, J. M.: New studies of SAGE II and HALOE ozone
1241 profile and long-term change comparisons, J. Geophys. Res., 110, D09305, doi:10.1029/2004JD005425,
1242 2005.

1243 Nedoluha, G. E., Gomez, R. M., Hicks, B. C., Bevilacqua, R. M., Russell III, J. M.,

1244 Connor, B. J., and Lambert, A.: A comparison of middle atmospheric water vapor as measured by
1245 WVMS, EOS-MLS, and HALOE, J. Geophys. Res., 112, D24S39, doi:10.1029/2007JD008757, 2007.
1246
1247 Nedoluha, G. E., Gomez, R. M., Hicks, B. C., Wrotny, J. E., Boone, C., and Lambert, A.: Water vapor
1248 measurements in the mesosphere from Mauna Loa over solar cycle 23, J. Geophys. Res., 114, D23303,
1249 doi:10.1029/2009JD012504, 2009.
1250
1251 Nedoluha, G., Gomez, R. M., Hicks, B. C., Helmboldt, J., Bevilacqua, R. M., and Lambert, A.: Ground-
1252 based microwave measurements of water vapor from the midstratosphere to the mesosphere, J. Geophys.
1253 Res., 116, D02309, doi:10.1029/2010JD014728., 2011.
1254
1255 Newchurch, M. J., Yang, E. S., Cunnold, D. M., Reinsel, G. C., Zawodny, J. M., and
1256 Russell III, J. M.: Evidence for slowdown in stratospheric ozone loss: First stage of ozone recovery, J.
1257 Geophys. Res., 108, D16, doi:10.1029/2003JD003471, 2003.

1258 Parrish, A., Boyd, I. S., Nedoluha, G. E., Bhartia, P. K., Frith, S. M., Kramarova, N. A.,
1259 Connor, B. J., Bodeker, G. E., Froidevaux, L., Shiotani, M., and Sakazaki, T.: Diurnal variations of
1260 stratospheric ozone measured by ground-based microwave remote sensing at the Mauna Loa NDACC
1261 site: measurement validation and GEOSCCM model comparison, Atmos. Chem. Phys., 7255-7272,
1262 doi:10.5194/acp-14-7255-2014, 2014.

1263 Perliski, L. M., Solomon, S., and London, J.: On the interpretation of seasonal variations of stratospheric
1264 ozone, Planet. Space Sci., 37, 12, 1527-1538, 1989.

1265 Pumphrey, H. C.: Validation of a new prototype water vapor retrieval for UARS MLS,
1266 J. Geophys. Res, 104 (D8), 9399–9412, doi:10.1029/1998JD200113, 1999.

1267 Pumphrey, H. C., Clark, H. L., and Harwood, R. S.: Lower stratospheric water vapor measured by UARS
1268 MLS, Geophys. Res. Lett., 27, 1691–1694, doi:10.1029/1999GL011339, 2000.

1269 Randel, W. J., Wu, F., Oltmans, S. J., Rosenlof, K., and Nedoluha, G. E.: Interannual changes of
1270 stratospheric water vapor and correlations with tropical tropopause temperatures, J. Atmos. Sci., 61,
1271 2133–2148, 2004.
1272
1273 Read, W. G., Lambert, A., Bacmeister, J., Cofield, R. E., Chris- tensen, L. E., Cuddy, D. T., Daffer, W.
1274 H., Drouin, B. J., Fetzer, E., Froidevaux, L., Fuller, R., Herman, R., Jarnot, R. F., Jiang, J. H., Jiang, Y.

1275 B., Kelly, K., Knosp, B. W., Kovalenko, L. J., Livesey, N. J., Liu, H.-C., Manney, G. L., Pickett, H. M.,
1276 Pumphrey, H. C., Rosenlof, K. H., Sabounchi, X., Santee, M. L., Schwartz, M. J., Snyder, W. V., Stek, P.
1277 C., Su, H., Takacs, L. L., Thurstans, R. P., Voemel, H., Wagner, P. A., Waters, J. W., Web- ster, C. R.,
1278 Weinstock, E. M., and Wu, D. L.: Aura Microwave Limb Sounder upper tropospheric and lower
1279 stratospheric H_2O and relative humidity with respect to ice validation, J. Geophys. Res., 112, D24S35,
1280 doi:10.1029/2007JD008752, 2007.
1281
1282 Read, W. G., Schwartz, M. J., Lambert, A., Su, H., Livesey, N. J., Daffer, W. H., and
1283 Booe, C. D.: The roles of convection, extratropical mixing, and in-situ freeze-drying in the Tropical
1284 Tropopause Layer, Atmos. Chem. Phys., 8, 6051–6067, doi:10.5194/acp-8-6051-2008, 2008.
1285
1286 Remsberg, E.: Observed seasonal to decadal scale responses in mesospheric water vapor,
1287 J. Geophys. Res., 115, D06306, doi:10.1029/2009JD012904, 2010.
1288
1289 Ricaud, P., de La Noë, J., Connor, B. J., Froidevaux, L., Waters, J. W., Harwood, R. S., MacKenzie, I. A.,
1290 and Peckham, G. E.: Diurnal variability of mesospheric ozone as measured by the UARS microwave limb
1291 sounder instrument: Theoretical and ground-based validations, J. Geophys. Res., 101 (D6), 10,077–
1292 10,089, doi:10.1029/95JD02841, 1996.
1293
1294 Rienecker, M., Suarez, M. J., Gelaro, R., Todling, R., Bacmeister, J., Liu, E., Bosilovich, M. G.,
1295 Schubert, S. D., Takacs, L., Kim, G.-K., Bloom, S., Chen, J., Collins, D., Conaty, A.,
1296 da Silva, A., Gu, W., Joiner, J., Koster, R. D., Lucchesi, R., Molod, A., Owens, T., Pawson, S., Pegion,
1297 P., Redder, C. R., Reichle, R., Robertson, J., F. R., Ruddick, A. G., Sienkiewicz, M., and Woollen, J.:
1298 MERRA: NASA's Modern-Era Retrospective Analysis for Research and Applications, J. Climate, 24,
1299 3624–3648, doi:10.1175/JCLI-D-11-00015.1, 2011.
1300
1301 Russell III, J. M., Gordley, L. L., Park, J. H., Drayson, S. R., Hesketh, D. H., Cicerone, R. J., Tuck, A. F.,
1302 Frederick, J. E., Harries, J. E., and Crutzen, P.: The Halogen Occultation Experiment, J. Geophys. Res.,
1303 98, 10777-10797, 1993.

1304 Russell III, J. M., Deaver, L. E., Luo, M., Park, J. H., Gordley, L. L., Tuck, A. F., Toon, G. C., Gunson ,
1305 M. R., Traub, W. A., Johnson, D. G., Jucks, K. W., Murcray, D. G., Zander, R.,
1306 Nolt, I. G., and Webster, C. R.: Validation of hydrogen chloride measurements made by the Halogen

Occultation Experiment from the UARS platform, J. Geophys. Res., 101 (D6), 10,151– 10,162, 1996.

Sakazaki, T., Fujiwara, M., Mitsuda, C., Imai, K., Manago, N., Naito, Y., Nakamura, T., Akiyoshi, H., Kinnison, D., Sano, T., Suzuki, M., and Shiotani, M.: Diurnal ozone variations in the stratosphere revealed in observations from the Superconducting Submillimeter-Wave Lime-Emission Sounder (SMILES) on board the International Space Station (ISS), J. Geophys. Res. Atmos., 118, 2991-3006, doi:10.1002/jgrd.50220, 2013.

Santee, M. L., Lambert, A., Read, W. G., Livesey, N. J., Cofield, R. E., Cuddy, D. T., Daffer, W. H., Drouin, B. J., Froidevaux, L., Fuller, R. A., Jarnot, R. F., Knosp, B. W., Manney, G. L., Perun, V. S., Snyder, W. V., Stek, P. C., Thurstans, R. P., Wagner, P. A., Waters, J. W., Muscari, G., de Zafra, R. L., Dibb, J. E., Fahey, D. W., Popp, P. J., Marcy, T. P., Jucks, K. W., Toon, G. C., Stachnik, R. A., Bernath, P. F., Boone, C. D., Walker, K. A.,

Urban, J., and Murtagh, D.: Validation of the Aura Microwave Limb Sounder HNO_3 measurements, J. Geophys. Res., 112, D24S40, doi:10.1029/2007JD008, 2007.

Salby, M., Titova, E., and Deschamps, L.: Rebound of Antarctic ozone, Geophys. Res. Lett., 38, L09702, doi:10.1029/2011GL047266, 2011.

Salby, M. L., Titova, E. A., and Deschamps, L.: Changes of the Antarctic ozone hole: Controlling mechanisms, seasonal predictability, and evolution, J. Geophys. Res., 117, D10111, doi:10.1029/2011JD016285, 2012.

Schwartz, M. J., Froidevaux, L., Fuller, R. A., and Pawson, S.: GOZCARDS Merged Data for Temperature Monthly Zonal Means on a Geodetic Latitude and Pressure Grid, version 1.01, Greenbelt, MD, USA: NASA Goddard Earth Science Data and Information Services Center, accessible from doi:10.5067/MEASURES/GOZCARDS/DATA3023, 2013.

Shepherd, T. G., Plummer, D. A., Scinocca, J. F., Hegglin, M. I., Fioletov, V. E., Reader, M. C., Remsberg, E., von Clarmann, T., and Wang, H. J.: Reconciliation of halogen-induced ozone loss with the total-column ozone record, Nature Geoscience, 7, 443-449, doi:10.1038/NGEO2155, 2014.

Solomon P. M., Barrett, J., Mooney, T., Connor, B., Parrish, A., and Siskind, D. E.: Rise and decline of active chlorine in the stratosphere, Geophys. Res. Lett., 33, L18807, doi:10.1029/2006GL027029, 2006.

1336 Sofieva, V. F., Kalakoski, N., Päivärinta, S.-M., Tamminen, J., Laine, M., and Froidevaux, L.: On
1337 sampling uncertainty of satellite profile ozone measurements, Atmos. Meas. Tech., 7, 1891–1900,
1338 doi:10.5194/amt-7-1891-2014, 2014.

1339 Solomon, S.: Stratospheric ozone depletion: A review of concepts and history, Rev. Geophys., 37, 275–
1340 316, doi:10.1029/1999RG900008, 1999.

1341 Solomon, S., Rosenlof, K., Portmann, R., Daniel, J., Davis, S., Sanford, T., and Plattner, G.-K.:
1342 Contributions of Stratospheric Water Vapor to Decadal Changes in the Rate of Global Warming, Science,
1343 237, 1219-1223, doi:10.1126/science.1182488, 2010.

1344 SPARC: Assessment of Trends in the Vertical Distribution of Ozone, edited by N. Harris, R. Hudson and
1345 C. Phillips, SPARC/IOC/GAW, SPARC Rep. 1, WMO Ozone Res. Monit. Project Rep. 43, 1998.

1346 SPARC WAVAS: Assessment of upper tropospheric and stratospheric water vapour, World Climate
1347 Research Programme, WCRP-113, WMO/TD-No.1043, 261-264, 2000.

1348 Steinbrecht, W., Koehler, U., Claude, H., Weber, M., Burrows, J. P., and van der A, R. J.: Very high
1349 ozone columns at northern mid latitudes in 2010, Geophys. Res. Lett., 38, L06803,
1350 doi:10.1029/2010GL046634, 2011.

1351 Strong, K., Wolff, M. A., Kerzenmacher, T. E., Walker, K. A., Bernath, P. F., Blumenstock, T., Boone,
1352 C., Catoire, V., Coffey, M., De Maziere, M., Demoulin, P., Duchatelet, P., Dupuy, E., Hannigan, J.,
1353 Hopfner, M., Glatthor, N., Griffith, D. W. T., Jin, J. J., Jones, N., Jucks, K., Kuellmann, H., Kuttippurath,
1354 J., Lambert, A., Mahieu, E., McConnell, J. C., Mellqvist, J., Mikuteit, S., Murtagh, D. P., Notholt, J.,
1355 Piccolo, C., Raspollini, P., Ridolfi, M., Robert, C., Schneider, M., Schrems, O., Semeniuk, K., Senten, C.,
1356 Stiller, G. P., Strandberg, A., Taylor, J., Tetard, C., Toohey, M., Urban, J., Warneke, T., and Wood, S.:
1357 Validation of ACE-FTS N_2O measurements, Atmos. Chem. Phys., 8, 4759-4786, doi:10.5194/acp-8-
1358 4759-2008, 2008.

1359 Tegtmeier, S., Hegglin, M. I., Anderson, J., Bourassa, A., Brohede, S., Degenstein, D., Froidevaux, L.,
1360 Fuller, R., Funke, B., Gille, J., Jones, A., Kasai, Y., Krüger, K., Kyrölä, E., Lingenfelser, G., Lumpe, J.,
1361 Nardi, B., Neu, J., Pendlebury, D., Remsberg, E., Rozanov, A., Smith, L., Toohey, M., Urban, J., von
1362 Clarmann, T., Walker, K. A., and Wang, H. J.: The SPARC Data Initiative: A comparison of ozone
1363 climatologies from international satellite limb sounders, J. Geophys. Res. Atmos., 118, 12,229–12,247,
1364 doi: 10.1002/2013JD019877, 2013.

Toohey, M., Hegglin, M. I., Tegtmeier, S., Anderson, J., Añel, J. A., Bourassa, A., Brohede, S., Degenstein, D., Froidevaux, L., Fuller, R., Funke, B., Gille, J., Jones, A., Kasai, Y., Krüger, K., Kyrölä, E., Neu, J. L., Rozanov, A., Smith, L., Urban, J., von Clarmann, T., Walker, K. A., and Wang, R.: Characterizing sampling bias in the trace gas climatologies of the SPARC Data Initiative, J. Geophys. Res. Atmos., 118, 11,847–11,862, doi: 10.1002/jgrd.5087, 2013.

Torres, O., and Bhartia, P. K.: Effect of stratospheric aerosol on ozone profile from BUV measurements, Geophys. Res. Lett., 22(3), 235-238, doi:10.1029/94GL02994, 1995.

Tummon, F., Hassler, B., Harris, N. R. P., Staehelin, J., Steinbrecht, W., Anderson, J., Bodeker, G. E., Bourassa, A., Davis, S. M., Degenstein, D., Frith, S. M., Froidevaux, L., Kyrölä, E., Laine, M., Long, C., Penckwitt, A. A., Sioris, C. E., Rosenlof, K. H., Roth, C., Wang, H.-J., and Wild, J.: Intercomparison of vertically resolved merged satellite ozone data sets: interannual variability and long-term trends, Atmos. Chem. Phys., 15, 3021-3043, doi: 10.5194/acp-15-3021-2015, 2015.

Urban, J., Lautié, N., Murtagh, D. P., Eriksson, P., Kasai, Y., Lossow, S., Dupuy, E., de LaNoë, J., Frisk, U., Olberg, M., Flochmoën, E. Le., and Ricaud, P.: Global observations of middle atmospheric water vapour by the Odin satellite: An overview, Planet. Space Sci., 55, 9, 1093-1102, 2007.

Urban, J., Lossow, S., Stiller, G., and Read, W.: Another drop in water vapor, EOS Transactions, American Geophysical Union, 95, 27, 245-252, doi:10.1002/2014EO270001, 2014.

Veiga, R.E., Cunnold, D. M., Chu, W. P., and McCormick, M. P.: Stratospheric Aerosol and Gas Experiments I and II comparisons with ozonesondes. J. Geophys. Res., 100 (D5), 9073-9090, doi:10.1029/94JD03251, 1995.

Voemel, H., Barnes, J. E., Forno, R. N., Fujiwara, M., Hasebe, F., Iwasaki, S., Kivi, R., Komala, N., Kyrölä, E., Leblanc, T., Morel, B., Ogino, S.-Y., Read, W. G., Ryan, S. C., Saraspriya, S., Selkirk, H., Shiotani, M., Valverde Canossa, J., and Whiteman, D. N.: Validation of Aura Microwave Limb Sounder water vapor by balloon-borne Cryogenic Frost point Hygrometer measurements, J. Geophys. Res., 112, D24S37, doi:10.1029/2007JD008698, 2007.

Wang, H. J., Cunnold, D. M., and Bao, X.: A critical analysis of Stratospheric Aerosol and Gas Experiment ozone trends J. Geophys. Res., 101 (D7), 12495-12514, doi:10.1029/96JD00581, 1996.

1393 Wang, H. J., Cunnold, D. M., Thomason, L. W., Zawodny, J. M., and Bodeker, G. E.: Assessment of
1394 SAGE version 6.1 ozone data quality, J. Geophys. Res., 107 (D23),
1395 doi: 10.1029/2002JD002418, 2002.

1396 Wang, H. J., Cunnold, D. M., Trepte, C., Thomason, L. W., and Zawodny, J. M.: SAGE III solar ozone
1397 measurements: Initial results, Geophys. Res. Lett., 33, L03805, doi:10.1029/2005GL025099, 2006.

1398 Wang, R., Froidevaux, L., Anderson, J., Fuller, R. A., Bernath, P. F., McCormick, M. P., Livesey, N. J.,
1399 Russell III, J. M., Walker, K. A., and Zawodny, J. M.: GOZCARDS Merged Data for Ozone Monthly
1400 Zonal Means on a Geodetic Latitude and Pressure Grid,version 1.01, Greenbelt, MD, USA: NASA
1401 Goddard Earth Science Data and Information Services Center, accessible from
1402 doi:10.5067/MEASURES/GOZCARDS/DATA3006, 2013.

1403 Waters, J. W., Microwave limb sounding, in Atmospheric Remote Sensing by Microwave Radiometry,
1404 ed. by M. Janssen, chap. 8, John Wiley, New York, 1993.

1405 Waters, J. W., Froidevaux, L., Read, W. G., Manney, G. L., Eslon, L. S., Flower, D. A., Jarnot, R. F., and
1406 Harwood, R. S.: Stratospheric ClO and ozone from the Microwave Limb Sounder on the Upper
1407 Atmosphere Research Satellite, Nature, 362, 597-602, 1993.

1408 Waters, J. W., Froidevaux, L., Harwood, R. S., Jarnot, R. F., Pickett, H. M., Read, W. G., Siegel, P. H.,
1409 Cofield, R. E., Filipiak, M. J., Flower, D. A., Holden, J. R., Lau, G. K., Livesey, N. J., Manney, G. L.,
1410 Pumphrey, H. C., Santee, M. L., Wu, D. L., Cuddy, D. T., Lay, R. R., Loo, M. S., Perun, V. S., Schwartz,
1411 M. J., Stek, P. C., Thurstans, R. P., Boyles, M. A., Chandra, S., Chavez, M. C., Chen, G.-S., Chudasama,
1412 B. V., Dodge, R., Fuller, R. A., Girard, M. A., Jiang, J. H., Jiang, Y., Knosp, B. W., LaBelle, R. C., Lam,
1413 J. C., Lee, K. A., Miller, M., Oswald, J. E., Patel, N. C., Pukala, D. M., Quintero, O., Scaff, D. M.,
1414 Snyder, W. V., Tope, M. C., Wagner, P. A., and Walch, M. J.: The Earth Observing System Microwave
1415 Limb Sounder (EOS MLS) on the Aura satellite, IEEE Trans. Geosci. Remote Sens., 44 (5), 1075–1092,
1416 doi:10.1109/TGRS.2006.873771, 2006.

1417 Waugh, D. W., Considine, D. B., and Fleming, E. L.: Is Upper Stratospheric Chlorine Decreasing as
1418 Expected?, Geophys. Res. Lett., 28(7), 1187–1190, doi:10.1029/2000GL011745, 2001.

1419 WMO (World Meteorological Organization): Scientific Assessment of Ozone Depletion: 2002, Global
1420 Ozone Research and Monitoring Project – Report No. 47, Geneva, Switzerland, 2003.

1421 WMO (World Meteorological Organization), Scientific Assessment of Ozone Depletion: 2010, Global
1422 Ozone Research and Monitoring Project – Report No. 52, Geneva, Switzerland, 2011.

WMO (World Meteorological Organization), Scientific Assessment of Ozone Depletion: 2014, Global Ozone Research and Monitoring Project – Report No. 55, Geneva, Switzerland, 2014.

Wohltmann, I., Lehmann, R., Rex, M., Brunner, D., and Mader, J.A.: A process-oriented regression model for column ozone, J. Geophys. Res., 112, D12304, doi:10.1029/2006JD007573, 2007.

Wolff, M. A., Kerzenmacher, T., Strong, K., Walker, K. A., Toohey, M., Dupuy, E., Bernath, P. F., Boone, C. D., Brohede, S., Catoire, V., von Clarmann, T., Coffey, M., Daffer, W. H., De Maziere, M., Duchatelet, P., Glatthor, N., Griffith, D. W. T., Hannigan, J., Hase, F., Hopfner, M., Huret, N., Jones, N., Jucks, K., Kagawa, A., Kasai, Y., Kramer, I., Kullmann, H., Kuttippurath, J., Mahieu, E., Manney, G., McElroy, C. T., McLinden, C., Mebarki, Y., Mikuteit, S., Murtagh, D., Piccolo, C., Raspollini, P., Ridolfi, M., Ruhnke, R., Santee, M., Senten, C., Smale, D., Tetard, C., Urban, J., and Wood, S.: Validation of HNO_3, $ClONO_2$, and N_2O_5 from the Atmospheric Chemistry Experiment Fourier Transform Spectrometer (ACE-FTS), Atmos. Chem. Phys., 8, 3529–3562, doi:10.5194/acp-8-3529-2008, 2008.

Yang, E.-S., Cunnold, D. M., Newchurch, M. J., Salawitch, R., McCormick, J. M. P., Russell III, J. M., Zawodny, J. M., and Oltmans, S. J.: First stage of Antarctic ozone recovery, J. Geophys. Res., 113, D20308, doi:10.1029/2007JD009675, 2008.

Ziemke, J. R., and Chandra, S.: Development of a climate record of tropospheric and stratospheric column ozone from satellite remote sensing: evidence of an early recovery of global stratospheric ozone, Atmos. Chem. Phys., 12, 5737-5753, doi:10.5194/acp-12-5737-2012, 2012.

Ziemke, J. R., Chandra, S., and Bhartia, P. K.: A 25-year data record of atmospheric ozone from TOMS Cloud Slicing: Implications for trends in stratospheric and tropospheric ozone, J. Geophys. Res., 110, D15105, doi:10.1029/2004JD005687, 2005.

Appendix A

A.1. GOZCARDS data provenance

The general origin of the datasets is summarized here. Data coverage from limb sounders (including the instruments used here) is displayed nicely in the work by Toohey et al. (2013).

SAGE I

SAGE I was launched February 18, 1979, aboard the Applications Explorer Mission-B (AEM-B) satellite. SAGE I was a sun photometer using solar occultation (Chu and McCormick, 1979), and it collected a global database for nearly three years on stratospheric aerosol, O_3, and NO_2. For more information, the reader is referred to http://sage.nasa.gov/SAGE1.

SAGE II

SAGE II was launched aboard the Earth Radiation Budget Satellite (ERBS) in October 1984 and its data gathering period ended in August 2005. During each sunrise and sunset, SAGE II measured stratospheric aerosols, O_3, NO_2, and H_2O via solar occultation. This long dataset has proven very valuable in determining past ozone trends. For more information on and data access to the (V6.2) dataset used for GOZCARDS, the reader is referred to http://sage.nasa.gov/SAGE2.

HALOE

Since its launch on September 12, 1991 from the Space Shuttle Discovery until November 2005, UARS HALOE collected profiles of atmospheric composition and temperature. HALOE (Russell et al., 1993) used solar occultation to measure vertical profiles of O_3, HCl, HF, CH_4, H_2O, NO, NO_2, temperature, aerosol extinction, and aerosol composition and size distribution. More information and access to the HALOE data can be obtained from http://haloe.gats-inc.com and http://disc.sci.gsfc.nasa.gov/UARS/data-holdings/HALOE. For GOZCARDS purposes, we have used Version 19 HALOE netCDF data files available at http://haloe.gats-inc.com.

UARS MLS

This instrument observed the Earth's limb in microwave emission using three radiometers, at frequencies near 63, 183 and 205 GHz (Waters, 1993; Barath et al., 1993), providing unique

daily global information on stratospheric ClO, along with other profiles, including O_3, H_2O, HNO_3, temperature, and cloud ice water content. The stratospheric H_2O data ceased on April 15, 1993, after the failure of the 183 GHz radiometer. After March 15, 1994, measurements became increasingly sparse in order to conserve the life of the MLS antenna scan mechanism and UARS power. Data exist until July 28, 1999, although for GOZCARDS, only data through mid-June 1997 are used, as data sparseness and degradation of the 63 GHz radiometer led to less 'trend-quality' data after this. Sampling patterns follow the alternating yaw cycles imposed on MLS by the precessing UARS orbit; MLS measurements were obtained continuously for all latitudes between 34°S and 34°N, with higher latitudes covered in either the northern or southern hemisphere with a roughly 36-day cycle. Livesey et al. (2003) provide more information on the UARS MLS instrument, retrievals, and results. For data access, the reader is directed to the relevant Goddard Earth Sciences and Information Services Center (GES DISC) data holdings at http://disc.sci.gsfc.nasa.gov/UARS/data-holdings/MLS. L3AT data files were used as the basis for the production of the GOZCARDS UARS MLS monthly source datasets.

ACE-FTS

ACE-FTS is the primary instrument onboard the SCISAT satellite, launched on August 12, 2003. It is a high spectral resolution (0.02 cm^{-1}) Michelson interferometer operating from 2.2 to 13.3 μm (750-4400 cm^{-1}); see Bernath et al. (2005) for an overview of the ACE mission. The instrument can simultaneously measure temperature and many trace gases (including all the species mentioned here for GOZCARDS), thin clouds, and aerosols, using the solar occultation technique. ACE-FTS data version 2.2, along with the version 2.2 update for ozone, were used here for GOZCARDS. For access to the public ACE-FTS datasets, with a routine measurement start date of March 2004, the reader is directed to http://www.ace.uwaterloo.ca.

Aura MLS

MLS is one of four instruments on NASA's Aura satellite, launched on July 15th 2004. Aura MLS is a greatly enhanced version of the UARS MLS experiment, providing better spatial coverage, vertical resolution, and vertical range, along with more continuous data over its lifetime (and with ongoing measurements at the time of writing). The instrument includes

radiometers at 118, 190, 240, and 640 GHz, and a 2.5 THz module (Waters et al., 2006). Aura MLS provides measurements of many chemical species, cloud ice, temperature and geopotential height. Continuous measurements have been obtained since August 2004, with the exception of OH, for which sparser measurements exist since August 2010, in order to preserve the life of the THz module. For more information and access to the Aura MLS datasets, the reader is referred to http://disc.sci.gsfc.nasa.gov/Aura/data-holdings/MLS. For GOZCARDS, we use the currently recommended Aura MLS data versions (version 2.2/2.3 for ozone and 3.3/3.4 for other species).

A.2. Calculation details for the iterative merging procedure

Given three time series, the merging procedure that we use first combines two out of the three time series, $y_1(i)$ and $y_2(i)$ (where index i represents time for each monthly mean value in a given latitude/pressure bin). We first obtain the temporary merged series $m_1(i)$ via:

$$m_1(i) = (1/2)\,(y_1(i) + y_2(i)) \quad (1)$$

with the average offsets for $y_1(i)$ and $y_2(i)$ being $(1/(2\,n_{12}))\,\Sigma\,(y_1(i) - y_2(i))$ and -1 times this value, respectively; n_{12} is the number of overlapping data points between the two time series. Then, we merge together the time series $m_1(i)$ and $y_3(i)$, keeping the weightings equal for all 3 time series (1/3 for each), so that we calculate the new merged time series $m(i)$ via:

$$m(i) = w_m\, m_1(i) + w_3\, y_3(i) = (1/3)\,(y_1(i) + y_2(i) + y_3(i)) \quad (2)$$

which will hold if the weights are $w_m = 2/3$ and $w_3 = 1/3$ (given equation (1) for $m_1(i)$). The average reference value (to which the adjustments of $m_1(i)$ and $y_3(i)$ in the 2nd step are made) is given by $(1/n_m)\,\Sigma\,(\,(2/3)\,m_1(i) + (1/3)\,y_3(i))$, where n_m represents the number of (overlapping pairs of) data values used in step 2. For the HCl and H_2O data merging procedure, we always use the Aura MLS time series as one of the first two series involved in the initial merging step, for example as $y_1(i)$, in order to maximize the overlap between the first two series and obtain more robust offset values. Then, we use the 3rd time series; the order used for HALOE and ACE-FTS (i.e., whether we use HALOE or ACE-FTS for y_2 or y_3) makes very little difference.

Calculation of the standard deviation for the merged data values

The average and standard deviation (square root of variance) for each y_k value (i.e. for each monthly zonal mean in a particular lat/p bin) are calculated from equations (3) and (4) below:

$$\bar{y}_k = \frac{1}{n_{yk}} \sum_j y_{kj} \tag{3}$$

and, for the variance,

$$\sigma_{yk}^2 = \frac{1}{n_{yk} - 1} \sum_j (y_{kj} - \bar{y}_k)^2 \tag{4}$$

where index "*j*" corresponds to individual data values within a month, index *k* represents a given instrument (data source), and *n* is the total number of data values for a given bin and source (instrument) time series point in time (or month). Each value $\overline{y_k}$ above is a monthly average (although we also use instead the simpler notation y_k), with standard deviation about the mean σ_{yk}. Now, given the merged series *u(i)* (where index *i* runs over a large number of months), the standard deviation of each merged data point (for a given month) can be obtained by considering the original datasets y_{kj} that were used to construct ***u*.** Specifically, we have the variance for the merged dataset

$$\sigma_u^2 = \frac{1}{n_u - 1} \sum_j (u_j - u_{ref})^2 \tag{5}$$

where u_{ref} is the merged value (which is not necessarily chosen to be the average value $\bar{u}$) and the u_j values represent the union of adjusted data values that make up the merged product, with the index j for this combined dataset covering all values (up to the total n_u) obtained from the original source values y_{kj}. In practice, we do not keep track of the individual data values that went into making the averages for the series y_k that are being merged, and we need to obtain σ_u based solely on the values $\bar{y}_k$, σ_{yk}, and the original number of points for each dataset y_k, namely n_{yk}. If we consider all the original values, we have a combined dataset with n_u points, such that $n_u = \sum_k n_{yk}$. Now, expanding equation (5), we get

$$(n_u - 1)\, \sigma_u^2 = \sum_j (u_j^2 + u_{ref}^2 - 2\, u_{ref}\, u_j) \tag{6}$$

or

$$(n_u - 1)\ \sigma_u^2 = \sum_j u_j^2 + n_u\, u_{ref}^2 - 2\, u_{ref} \sum_j u_j \qquad (7)$$

Expanding (4) for each individual dataset y_k, we get

$$(n_{yk} - 1)\ \sigma_{yk}^2 = \sum_j y_{kj}^2 + \overline{y}_k^{\,2} - 2\overline{y_k} \sum_j y_{kj} \qquad (8)$$

which leads to

$$\sum_j u_j^2 = \sum_{k,j} y_{kj}^2 = \sum_k (n_{yk} - 1)\, \sigma_{yk}^2 \quad + \sum_k n_{yk}\ \overline{y_k}^2, \qquad (9)$$

so that extracting the variance from equation (7) now leads to

$$\sigma_u^2 = \frac{1}{(n_u - 1)} \left(\sum_k (n_{yk} - 1)\, \sigma_{yk}^2 + \sum_k n_{yk}\ \overline{y_k}^2 + n_u\, u_{ref}^2 - 2 u_{ref} \sum_k n_{yk}\, \overline{y_k} \right) \qquad (10)$$

The adjusted time series are obtained from the original series y_k as Y_k, and we can write Equation (4) in the same manner for the Y_k data values, namely

$$\sigma_{Yk}^2 = \frac{1}{n_{yk} - 1} \sum_j (Y_{kj} - \overline{Y_k})^2 \qquad (11)$$

with $\sigma_{Yk} = \sigma_{yk}$ as the adjustments (offsets) are performed in an additive manner; if these adjustments were performed using multiplicative factors, those factors would also have to be considered in a multiplicative way to get the new σ_{Yk} values. We can thus write (10) for the adjusted datasets as:

$$\sigma_u^2 = \frac{1}{(n_u - 1)} \left(\sum_k (n_{yk} - 1)\, \sigma_{yk}^2 + \sum_k n_{yk}\ \overline{Y_k}^2 + n_u\, U_{ref}^2 - 2 U_{ref} \sum_k n_{yk}\, \overline{Y_k} \right) \qquad (12)$$

Equation (12) for the standard deviation of the merged dataset simplifies if the original datasets are adjusted to exactly the same reference value ref ($\overline{Y_k} = ref$) and the merged value U_{ref} is also equal to that value, as the sum of the last 3 terms in Eq. (10) (with Y_k replacing y_k) then reduces to $n_u\, ref^2 + n_u\, ref^2 - 2\, n_u\, ref^2$, which is zero. In this case, one obtains

$$\sigma_u^2 = \frac{1}{(n_u - 1)} \left(\sum_k (n_{yk} - 1) \sigma_{yk}^2 \right) \qquad (13)$$

However, in general, one should use equation (12) for the standard deviation of the merged dataset, given the adjusted datasets $\overline{Y_k}$ and the merged (or reference) value U_{ref}. Also, we often use a merged value equal to the average of the original data (over a given overlap period), so that

$$U_{ref} = \frac{1}{n_y} \sum_k \overline{y_k} \qquad (14)$$

where n_y is the total number of datasets (y_k), as opposed to having the merged value place more weight on the larger datasets (e.g., for emission-type measurements versus occultation-type), in which case one would consider using $U_{ref} = \frac{1}{n_u} \sum_k n_{yk} \overline{y_k}$. For ozone, we use a particular dataset (SAGE II ozone) as the primary reference, but equation (12) can be used to obtain the standard deviation for the merged dataset (about the SAGE II reference) in that case also. While it is useful to have the formalism above for obtaining the merged dataset standard deviation σ_u, we often find significant differences between the standard deviations of various datasets, so that this effect will have the greatest influence on the results, as opposed to the impact of the last 3 terms in the summation (in (12)). Finally, it is easy to test equation (12) (and we have done so) by using synthetic series and calculating the standard deviation of the combined set. In reality, the standard deviations of the time series monthly mean values are typically larger for MLS than for ACE-FTS, mainly because of the more complete sampling of variability from the daily global measurements acquired by MLS. Sample plots for standard deviations and standard errors in the case of HCl are shown in Fig. A1. As expected, merged standard deviations follow the standard deviations from HALOE HCl before Aug. 2004 and those from MLS HCl after this time. However, the merged standard errors for the MLS time period follow the smaller MLS standard errors, because these values vary inversely with the square root of the number of values sampled, and are therefore made smaller by the significantly larger daily and monthly MLS sampling rate and coverage.

A.3. Procedural details for GOZCARDS HCl, H_2O, and O_3

Data screening procedures for the GOZCARDS source datasets, following previously described methods, are provided (with references) in Table A1, along with certain species-related specifics. Other GOZCARDS data characteristics and details are provided below for each species.

A.3.1. HCl

- The vertical data range for valid HCl merged values is between 0.46 hPa and 147 hPa (inclusive), as a result of data sparseness or data quality issues outside these ranges.
- At 147 hPa, no merged HCl values exist for latitude bins from 35°S to 35°N inclusive, because of unrealistically large Aura MLS HCl values in this region; also, there is not enough data at this level to provide a meaningful product from HALOE and ACE-FTS data alone.
- Because of occasional small negative merged values during southern hemisphere polar winter, we did not apply HCl data offsets in the lower stratosphere for the 65°S through 85°S bins from June through September and for pressures larger than or equal to 15 hPa. For vertical continuity purposes, we applied this method to all lower stratospheric pressure levels, although the small negative merged values only occurred in a small fraction of cases.
- As Aura MLS and ACE-FTS data exist in the 85°N and 85°S bins, but there are no HALOE measurements, we simply extended the offsets from the adjacent bins (at 75°N and 75°S) to these two bins to obtain a merged record after 2004 that exhibits continuity versus latitude.
- At 100 hPa, we used HCl offsets from the 5°S bin for the 5°N bin, as there was insufficient data from the combined data in the latter bin to calculate meaningful offsets. This procedure seems reasonable, given that the time series in these two adjacent tropical latitude bins (during years outside the 2004/2005 overlap period) look continuous and stable enough to justify identical adjustments in both bins and to avoid a data gap in the merged series at 5°N.

A.3.2. H_2O

- The vertical data range for valid H_2O merged values is between 0.01 hPa and 147 hPa (inclusive). While H_2O data exist at 147 hPa for low latitudes, more careful work would be needed to extend the merged data globally in such a region.

- Users should keep in mind the PMC-related caveats mentioned in Sect. 4 for summer at high latitudes in the upper mesosphere, prior to the end of the HALOE dataset (Nov. 2005).
- As for HCl, we could not use our standard merging procedure at the two most poleward latitude bins; we simply extended the offsets from the adjacent bins (at 75°N and 75°S) to these polar bins to obtain a merged record after 2004 that exhibits continuity versus latitude.
- Also as for HCl, at 100 hPa, we used H_2O offsets from the 5°S bin for the 5°N bin, as there was insufficient data from the combined datasets in the latter bin to calculate meaningful offsets and merge the datasets. This procedure avoids a data gap in the merged series at 5°N.

A.3.3. O_3

- The vertical range for valid O_3 merged data is from 0.2 hPa to 215 hPa (inclusive), with the lower altitude bound varying with latitude; the merged product at 147 and 215 hPa has valid data only for the 35° to 85° latitude bins, with values mostly larger than ~ 0.1 ppmv. The upper troposphere is more of a merging challenge, given smaller abundances, more difficult measurements, and a larger impact from different instrument resolutions. Also, while we suggest (see main text) that GOZCARDS merged ozone data should not be subject to a large impact from diurnal variations, the highest altitude region should be treated with caution.

- SAGE I monthly mean source data are used for the merged dataset in the tropical bins (25°S to 25°N) from 1 through 68 hPa only and, at higher latitudes, from 1 through 100 hPa only.
- We omitted the use of UARS MLS at 100 hPa for low latitudes (from 25°S to 25°N), as these monthly values are biased quite high and also exhibit too large a seasonal cycle amplitude, in comparison to HALOE and SAGE II data; this appears to relate to a UARS MLS artifact.

- Since there is no (monthly) overlap between SAGE II and HALOE versus UARS MLS or Aura MLS in the 85°N and 85°S latitude bins, the same offsets as for 75°N and 75°S (respectively) are applied for these bins, in order to minimize discontinuities.

- Because of discontinuities that appeared in merged O_3 at high latitudes above the stratopause, particularly in the 75°S bin, we flagged merged values for 75° and 85° (N and S) as bad, for pressures less than 1 hPa. This issue could be the result of a few bad data points or not enough data overlap. To minimize artifacts, we left the resolution of this issue for future investigations; also, the reduced amount of occultation data at these high latitudes makes the

usefulness of a merged product with poorly sampled seasonal changes somewhat marginal (for certain years at least, the number of monthly values drops significantly at high latitudes).

Table 1. Characteristics of instrument datasets used to create GOZCARDS ESDRs (version ev1.01).

Instrument and Data Versions	Platform	Type of measurement	Time period (GOZCARDS source files)	Vertical Resolution (km)	Retrieved quantity and stratospheric vertical grid spacing
SAGE I V5.9_rev O_3	AEM-2	Solar occultation VIS/UV and near-IR	Feb. 1979 - Nov. 1981	1	Density on altitude grid 1 km spacing
SAGE II V6.2 O3	ERBS	Solar occultation VIS/UV and near-IR	Oct. 1984 - Aug. 2005	0.5 - 1	Density on altitude grid 0.5 km spacing
HALOE V19	UARS	Solar occultation mid-IR	Oct. 1991 - Nov. 2005	2.5	Volume Mixing Ratio on pressure grid with 30 levels per decade (LPD) change in p
MLS V5 O_3 V6 H_2O	UARS	Limb emission microwave / sub-mm	Oct. 1991 - June 1997 (May 1993 end for strat. H_2O)	**H_2O** 3 - 4 (strat.) 5 - 12 (mes.)	Volume Mixing Ratio on pressure grid with 6 LPD in stratosphere
				O_3 3.5 - 5 (strat.) 5 - 8 (mes.)	6 LPD in stratosphere
ACE-FTS V2.2 (V2.2 update for O_3)	SCISAT	Solar occultation mid-IR	Mar. 2004 through Sep. 2010 (2009 for O_3)	3 - 4	Volume Mixing Ratio on 1 km grid spacing (height and p provided)
MLS V3.3 V2.2 O_3	Aura	Limb emission microwave / sub-mm	Aug. 2004 through 2012	**HCl** 3 - 5	Volume Mixing Ratio on pressure grid with 6 LPD
				H_2O 3 - 4 (p > 0.1 hPa) 5 - 9 (0.1-0.01 hPa)	12 LPD
				O_3 3	6 LPD

Table 2. Products and instrument source data making up the available GOZCARDS data records.

Merged Products and pressure range	**Source Datasets** (and years used)
HCl 147 – 0.5 hPa	HALOE (1991-2005), ACE-FTS (2004-2010), Aura MLS (2004 onward) Note: MLS data for p < 10 hPa not used for merged time series
H_2O 147 – 0.01 hPa	HALOE (1991-2005), UARS MLS (1991-1993), ACE-FTS (2004-2010), Aura MLS (2004 onward)
O_3 215 – 0.2 hPa	SAGE I (1979-1981), SAGE II (1984-2005), HALOE (1991-2005), UARS MLS (1991-1997), ACE-FTS (2004-2009), Aura MLS (2004 onward)
HNO_3 215 – 1 hPa	ACE-FTS (2004-2010), Aura MLS (2004 onward)
N_2O 100 – 0.5 hPa	ACE-FTS (2004-2010), Aura MLS (2004 onward)
Temperature 1000 – 0.015 hPa	GMAO MERRA (1979 onward)

1665 **Table A1.** Data screening procedures and related references used for the source dataset generation.

Instrument	Data Screening Issue / Method	Reference
SAGE I (O3)	Aerosol interference issue: Remove values at altitudes below which the 1 μm extinction > 10^{-3} km^{-1}.	L. Thomason (personal communication, 2012)
SAGE II (O3)	Remove entire profile if any error error value exceeds 10% of VMR (for 30 to 50 km altitude); this occurred mainly in 1993 & 1994 (''short events'').	Wang et al. (2002)
	Use aerosol extinctions and extinction ratios to remove data affected by clouds or by aerosols (from Mt. Pinatubo).	
	Remove anomalously low values resulting from very small SAGE II transmittances (errors are capped at 300% as a flag).	
	Remove profiles under high beta angle conditions.	See also Wang et al. (1996)
HALOE	Remove cloud-contaminated values. Also remove profiles that may contain artifacts from faulty trip angle or constant lockdown angle registration.	Hervig and McHugh (1999) haloe.gats-inc.com/user_docs/index.php
	Remove aerosol contamination (O_3 and HCl).	Bhatt et al. (1999)
UARS MLS	Use screening guidelines based on instrument status, retrieval quality flags, and sign of precision values.	Livesey et al. (2003)
Aura MLS	Use screening guidelines based on instrument status, retrieval quality and convergence flags, and sign of precision values.	Livesey et al. (2013)
ACE-FTS	Remove occultations listed as bad.	databace.scisat.ca/validation/data_issues.php
	Remove data when error value > VMR or error value < 10^{-4} xVMR.	K. Walker (personal communication, 2012)
	Use a data screening procedure (see Sect. 2.1) to identify and remove the largest outliers.	
	V2.2 data after Sep. 2010 (2009 for ozone) are not used because of a data processing issue.	

1666

Fig. 1. Merging procedure illustration for HCl. Top left panel shows the HCl monthly mean source data during the overlap period (Aug. 2004 - Nov. 2005) for HALOE, ACE-FTS, and Aura MLS. Top right panel illustrates step 1 in the merging procedure, with the temporary merged data values (orange) resulting from the adjustment of ACE-FTS and Aura MLS values to the mean reference indicated by the black dashed line (time mean of co-located ACE-FTS/Aura MLS points). Also, the cyan dashed line is the mean of the ACE-FTS points and the red dashed line is the mean of MLS points co-located with ACE-FTS. Middle left panel shows step 2 results, namely the merged values arising from merging HALOE data with the temporary merged data; the black dashed line is the new average reference value, obtained from a 2/3 and 1/3 weighting of the dashed orange (mean of orange points co-located with HALOE) and dashed blue line (mean of HALOE) values, respectively. Middle right panel shows all the source data and the final merged values during the overlap period. Bottom panel shows the source and merged time series from 1991 through 2012 after the calculated additive offsets are applied to the whole source datasets, which are then merged (averaged) together wherever overlap between instruments exists.

Fig. 2. Offsets applied to the HCl source datasets (top panels for HALOE, middle panels for ACE-FTS, bottom panels for Aura MLS) as a function of latitude and pressure. The left column gives offsets in ppbv and the right column provides offsets as a percent of the zonal average merged mixing ratios during the overlap period (Aug. 2004 – Nov. 2005) used here to compute the average offsets.

Fig. 3. Example of HCl time series analyses for 50°N-60°N and 32 hPa. (a) HCl monthly mean source data from ACE-FTS and Aura MLS; the MLS dots are filled when there is time overlap with ACE-FTS, and open if no such overlap exists. Simple linear fits are shown as colored lines for ACE-FTS and for Aura MLS (orange line for all red dots and red line for filled red dots only). Correlation coefficient values (R values) for the two time series are provided in the title. (b) Deseasonalized anomalies for both ACE-FTS and Aura MLS, with corresponding linear fits (and R values). (c) Difference of deseasonalized anomalies (ACE-FTS minus Aura MLS), with linear fit.

Fig. 4. Latitude/pressure contours of time series diagnostics obtained from analyses illustrated in Fig. 3 for HCl from Aura MLS and ACE-FTS. Top panel: Correlation coefficient for the deseasonalized time series. Bottom panel: Ratio of the slope of the difference between deseasonalized series over the error in this slope.

Fig. 5. Illustration of GOZCARDS HCl monthly averages with systematic error estimates (grey shading) at 46 hPa for 30°S-40°S; see text for the meaning of this shaded region. The source data from HALOE, Aura MLS, and ACE-FTS are shown in different colors (see legend), along with the merged values.

Fig. 6. Systematic error estimates for GOZCARDS HCl. One error (left panels) is relevant for values lower than (below) the merged values, and one (right panels) for values larger than the merged values; the

top panels give the error estimates in ppbv, and the bottom panel errors are expressed as percent of the average merged values over the relevant time periods (see text). These error bars provide a range within which 95% of the source data values lie.

Fig. 7. Time series of the GOZCARDS monthly-averaged merged HCl abundance for 3 different latitude bin averages (see color legend in panel (a)) for (a) 0.7 hPa, (b) 10 hPa, (c) 32 hPa, and (d) 68 hPa.

Fig. 8. The average rate of change (percent per year) for HCl as a function of pressure for different latitude bin averages (see legend) for time periods corresponding to the appropriate GOZCARDS HCl values (see text) in the upper stratosphere (Jan. 1997 - Sep. 2010) and lower stratosphere (Jan. 1997 - Dec. 2012). Deseasonalized monthly data were used to obtain a long-term trend for these time periods; two-sigma error bars are shown.

Fig. 9. Rates of change for GOZCARDS HCl (connected open circles) are given as a function of latitude in 10° latitude bins for sliding 6-year periods centered on Jan. 1 of each year (e.g., the 1998 point is an average for data from 1995 through 2000, and the 2011 point is for data from 2008 through 2013). (a) is for changes in upper stratospheric HCl at 0.7 hPa and (b) is for the change in the integrated HCl column between 68 hPa and 10 hPa. The two additional curves in (a) represent the rates of change in the estimated surface total chlorine from NOAA data (green is for a 6-year time shift, and purple for a 7-year time shift, to account for transport time to the upper stratosphere); see text for more details. Error bars indicate twice the standard errors in the means.

Fig. 10. Offsets applied to the H_2O source datasets as a function of latitude and pressure, similar to Fig. 2 for HCl.

Fig. 11. Latitude/pressure contours of time series diagnostics for H_2O from Aura MLS and ACE-FTS; this is similar to Fig. 4 for HCl.

Fig. 12. A depiction of the "tape recorder" evolution for tropical water vapor abundances from 147 to 10 hPa for October 1991 through December 2013. This plot was produced from GOZCARDS merged H_2O time series anomalies (differences from the long-term means) for the average of the 4 tropical bins covering 20°S to 20°N.

Fig. 13. Systematic error estimates for GOZCARDS H_2O (similar to Fig. 6 for HCl).

Fig. 14. Variations in stratospheric water vapor from the GOZCARDS H_2O merged data records (1992 through 2013) averaged from (a) 60°S to 60°N and (b) 20°S to 20°N. Monthly average values and annual averages are shown by thin and thick lines (connecting similarly-colored dots), respectively, for the pressure levels indicated in the plot legend.

Fig. 15. Stratospheric water vapor variability on decadal timescales for 1992 through 2013 for tropical (20°S-20°N in black) and mid-latitude (20°N-60°N in red and 20°S-60°S in blue) zonal means, based on the GOZCARDS merged H_2O data record. The variability is expressed here as the difference between maximum and minimum annual average abundances, from 100 to 1 hPa, in ppmv (left panel) and percent (right panel).

Fig. 16. (a) Variations in upper mesospheric (0.01 hPa) water vapor mixing ratios averaged from 60°S to 60°N for Oct. 1991 through Dec. 2013, based on the GOZCARDS merged H_2O data records. Monthly average values and annual averages are shown by connected brown dots and connected black dots, respectively. (b) GOZCARDS merged H_2O annual averages (connected filled symbols) from 60°S to 60°N for 1992 through 2013 at pressure levels between 0.1 and 0.01 hPa. A time series of annually-averaged Lyman α solar flux values (open circles), scaled to arbitrary units, is also displayed (see text).

Fig. 17. Time series of monthly zonal mean O_3 for 10°S - 20°S between 1 hPa and 6.8 hPa (with pressure values given by ″pre″) from SAGE I, SAGE II, HALOE, UARS MLS, Aura MLS, and ACE-FTS, all color-coded following the legend in top left panel.

Fig. 18. Schematic diagram describing the creation of the merged GOZCARDS monthly zonal mean ozone data record from various satellite datasets. Instruments represented in red inside the boxes are used as a reference. Instruments whose measurements have already been adjusted to a reference are indicated with a "*" superscript. AMLS refers to Aura MLS and UMLS to UARS MLS. See text for more details.

Fig. 19. Offsets applied to the O_3 source datasets, similar to Fig. 2 for HCl.

Fig. 20. Latitude/pressure contours of time series diagnostics for O_3 from Aura MLS and ACE-FTS; this is similar to Fig. 4 for HCl. The correlation coefficients (R values) and slope trend diagnostics are provided for HALOE versus SAGE II in the top two panels (for 1993-1999 as the trend issue for converted SAGE II data occurs after mid-2000 and to avoid Pinatubo-related data gaps before 1993) and for ACE-FTS versus Aura MLS in the bottom two panels (for 2005-2009).

Fig. 21. Systematic error estimates for GOZCARDS O_3 (similar to Fig. 6 for HCl).

Fig. 22. Near-global (60°S to 60°N) results for average column ozone (total and stratospheric, from *Ziemke and Chandra,* 2012) compared to GOZCARDS O_3 columns above 68 hPa. Stratospheric columns are offset to better match the total column values, in order to more easily compare relative variations versus time; the black dots and red crosses are referenced to the 1980 total column values, while the cyan

curves are referenced to 2007 to better illustrate the fits in the later years. Also shown (as purple open circles) are yearly-averaged total column data (60°S to 60°N) from the SBUV Merged Ozone (V8.6) Dataset (see text); these values were adjusted upward slightly (by 0.8 DU) to match the ZC12 total column values in 1980.

Fig. 23. Time evolution (Aug. 2004 through 2012) versus latitude of GOZCARDS merged N_2O (ppbv) at (a) 6.8 hPa and (b) 100 hPa.

Fig. 24. Sample results display the time evolution of satellite-retrieved HNO_3 (ppbv) for two different periods, 1992-1997 in (a) and (c) versus 2004-2013 in (b) and (d). Panels (a) and (b) are contour plots at 46 hPa from UARS MLS global data and the merged GOZCARDS global data after 2004, respectively; (c) and (d) show time series at 32 hPa and for the 40°N-50°N latitude bin, with (a) from UARS MLS data, and (d) from ACE-FTS, Aura MLS, and the merged combination (between the two source data sets).

Fig. A1. Illustration of the standard deviations (in (a)) and standard errors (in (b)) for monthly mean GOZCARDS HCl (source and merged records) at 46 hPa for 30°S-40°S. Source data from HALOE, Aura MLS, and ACE-FTS are given by the filled colored dots (see legend); each standard deviation is simply obtained from the range of values measured during the month. The large open brown circles give standard deviations for the merged HCl product; this Appendix provides the formulae to calculate these quantities.

Fig. S1: Illustration of the latitudinal dependence of the HCl offsets for HALOE, ACE-FTS, and Aura MLS at two pressure levels (top panel for 0.46 hPa, bottom panel for 46 hPa). Error bars represent twice the standard error in the derived offsets (based on variability during the overlapping period). Larger standard error values indicate that there were either fewer points of overlap or larger offset variability (standard deviations); we found that both of these factors contribute.

Fig. S2: Latitude/pressure contours of the fitted mean annual amplitudes (ppbv) from HCl time series for HALOE, ACE-FTS, and Aura MLS, based on their respective measurement periods (see text).

Fig. S3: Time evolution (Oct. 1991 through 2013) versus latitude of GOZCARDS merged HCl (ppbv) at 46 hPa.

Fig. S4: HALOE sunrise measurements of H_2O versus the 3.46 μm extinction coefficient for 1992, 1993, and 1999 at 22 hPa. The green vertical line represents the aerosol extinction value ($5x10^{-4}$ km^{-1}) used to screen anomalous HALOE H_2O values. It is apparent that anomalously low H_2O values occurred in 1992 when the 3.46 μm aerosol extinction exceeded about $5x10^{-4}$ km^{-1}. These artifacts were confined to 1991

and 1992; for these years, and for pressure levels at and below 22 hPa, the corresponding H_2O data values were excluded. This screening method eliminates about 10% of the global (lower stratospheric) measurements in 1992.

Fig. S5: Merging procedure illustration for H_2O at 5°N and 22hPa. This is similar to Fig. 2 (for HCl), but an additional step is illustrated for the end of this procedure, whereby stratospheric H_2O data from UARS MLS are adjusted to the early portion of the merged time series that was obtained after the 2nd step; this adds more coverage (more brown dots in the bottom panel for 1991-1993).

Fig. S6: Latitude/pressure contours of the fitted mean annual amplitudes (ppmv) from H_2O time series for HALOE, ACE-FTS, and Aura MLS, based on their respective measurement periods.

Fig. S7: Time evolution (Oct. 1991 through 2013) versus latitude of GOZCARDS merged H_2O (ppmv) at 3.2 hPa (top panel) and 68 hPa (bottom panel).

Fig. S8: Monthly zonal mean ozone differences (%) between SAGE II and (a) HALOE, (b) UARS MLS (UMLS for short), (c) Aura MLS (AMLS for short), and (d) ACE-FTS during their respective overlap periods. Differences are expressed (in percent) as 100 x [(SAGE II - Other) / (Other)]. Shaded areas indicate negative values.

Fig. S9: Monthly zonal mean temperature differences between NCEP (used by SAGE II) and HALOE temperatures relative to MERRA for 10°S - 20°S between 1 and 6.8 hPa, per color-coding indicated in bottom left panel; ‘‘pre‘‘ represents the pressure value. From 1 to 2.1 hPa, differences between NCEP and MERRA are generally within ± 4K before mid-2000. After that time, NCEP temperatures show a sharp increase and are systematically higher than MERRA values by 5 to 10K. However, this divergence and trend are not seen in HALOE temperatures. NCEP temperatures between 3.2 and 6.8 hPa are smaller than MERRA after mid-2000; negative trends (versus MERRA) also occur in the HALOE data at these levels.

Fig. S10: Relative trends (K/decade) in zonal mean temperature differences for NCEP – MERRA and HALOE – MERRA (color-coded as in Fig. S9) in the upper stratosphere. NCEP temperatures show positive trends versus MERRA of ~2-5 K/decade between 2.1 and 1 hPa for all latitudes. However, HALOE temperatures show no significant trends versus MERRA, except at 1.5 hPa in the southern hemisphere. For pressures between 3.2 and 6.8 hPa, the temperature analyses are not conclusive; although NCEP values show negative trends of ~2-3 K/decade versus MERRA, they agree with HALOE.

Fig. S11: Mean differences and standard deviations (horizontal bars) between SAGE II and Aura MLS ozone in three different latitude bins: 20°S to 60°S (left panel), 20°S to 20°N (middle panel), and 20°N to 60°N (right panel). Results based on monthly zonal mean and coincident profiles (see text for coincidence

1822 criteria) during overlap periods are shown in red and blue, respectively. To choose collocated profiles,
1823 coincidence criteria of ±1° in latitude and ±8° in longitude were used; the time difference criterion was
1824 chosen as 12 hours, but only nighttime measurements from Aura MLS were used.

1825 **Fig. S12:** Latitude/pressure contours of the fitted mean annual amplitudes (ppmv) from O_3 time series for
1826 SAGE II, HALOE, ACE-FTS, and Aura MLS, based on their respective measurement periods.

1827 **Fig. S13:** Illustration of the time evolution of the GOZCARDS merged O_3 data field versus latitude at
1828 68 hPa (top panel) and versus pressure for the 40°N-50°N latitude bin (bottom panel).

1829 **Fig. S14:** Offsets applied to the N_2O source datasets (top panels for ACE-FTS, bottom panels for Aura
1830 MLS) as a function of latitude and pressure. The left column gives offsets in ppbv and the right column
1831 provides offsets as a percent of the zonal average merged mixing ratios during the overlap period (Aug.
1832 2004 – Sep. 2010) used here to compute the average offsets.

1833 **Fig. S15:** Latitude/pressure contours of time series diagnostics derived from Aura MLS and ACE-FTS
1834 N_2O data comparisons (and obtained from analyses similar to those illustrated in Fig. 6 for HCl). Top
1835 panel: Correlation coefficient for the deseasonalized time series. Bottom panel: Ratio of the slope of the
1836 difference between deseasonalized series over the error in this slope.

1837 **Fig. S16:** Offsets applied to the HNO_3 source datasets (top panels for ACE-FTS, bottom panels for Aura
1838 MLS) as a function of latitude and pressure. The left column gives offsets in ppbv and the right column
1839 provides offsets as a percent of the zonal average merged mixing ratios during the overlap period (Aug.
1840 2004 – Sep. 2010) used here to compute the average offsets.

1841 **Fig. S17:** Latitude/pressure contours of time series diagnostics derived from Aura MLS and ACE-FTS
1842 HNO_3 data comparisons (and obtained from analyses similar to those illustrated in Fig. 6 for HCl). Top
1843 panel: Correlation coefficient for the deseasonalized time series. Bottom panel: Ratio of the slope of the
1844 difference between deseasonalized series over the error in this slope.

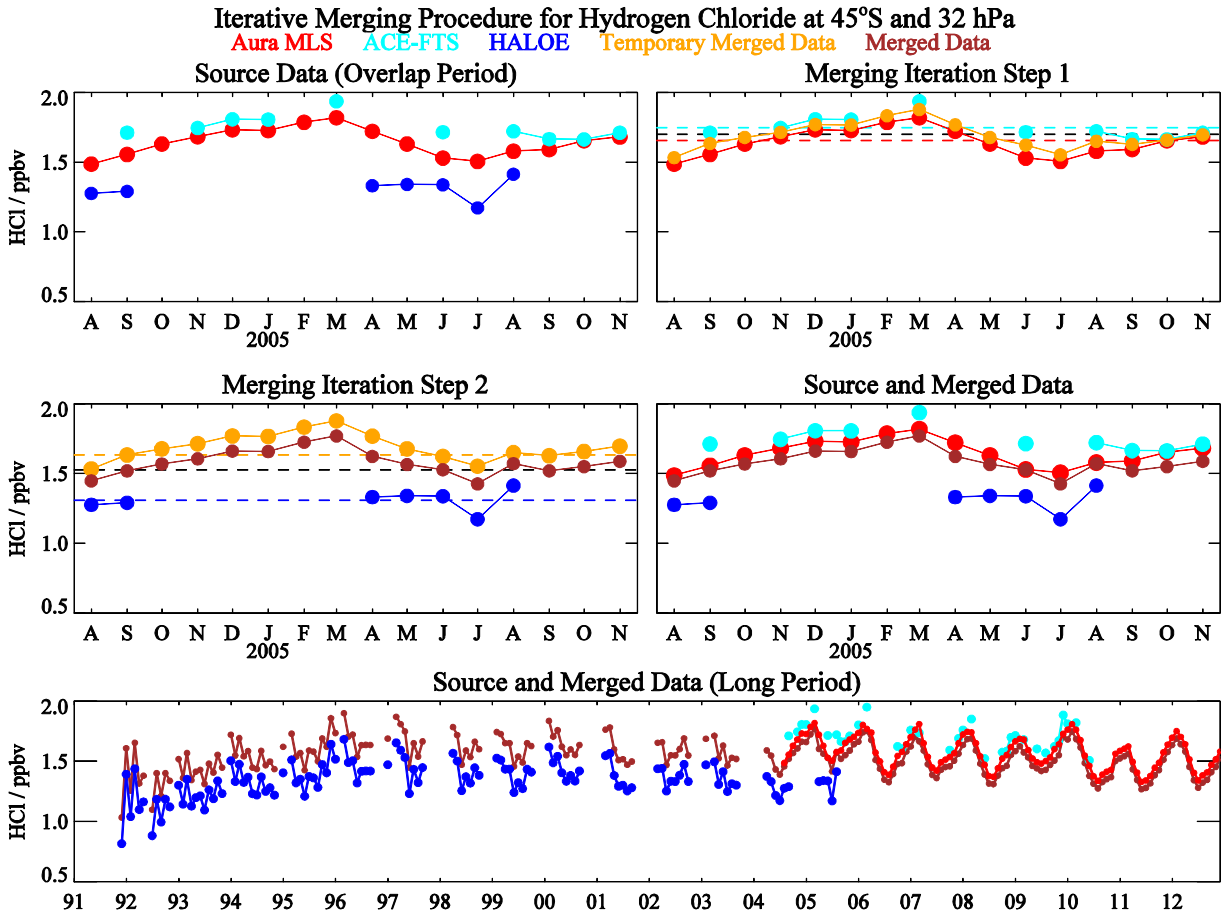

Fig. 1. Merging procedure illustration for HCl. Top left panel shows the HCl monthly mean source data during the overlap period (Aug. 2004 - Nov. 2005) for HALOE, ACE-FTS, and Aura MLS. Top right panel illustrates step 1 in the merging procedure, with the temporary merged data values (orange) resulting from the adjustment of ACE-FTS and Aura MLS values to the mean reference indicated by the black dashed line (time mean of co-located ACE-FTS/Aura MLS points). Also, the cyan dashed line is the mean of the ACE-FTS points and the red dashed line is the mean of MLS points co-located with ACE-FTS. Middle left panel shows step 2 results, namely the merged values arising from merging HALOE data with the temporary merged data; the black dashed line is the new average reference value, obtained from a 2/3 and 1/3 weighting of the dashed orange (mean of orange points co-located with HALOE) and dashed blue line (mean of HALOE) values, respectively. Middle right panel shows all the source data and the final merged values during the overlap period. Bottom panel shows the source and merged time series from 1991 through 2012 after the calculated additive offsets are applied to the whole source datasets, which are then merged (averaged) together wherever overlap between instruments exists.

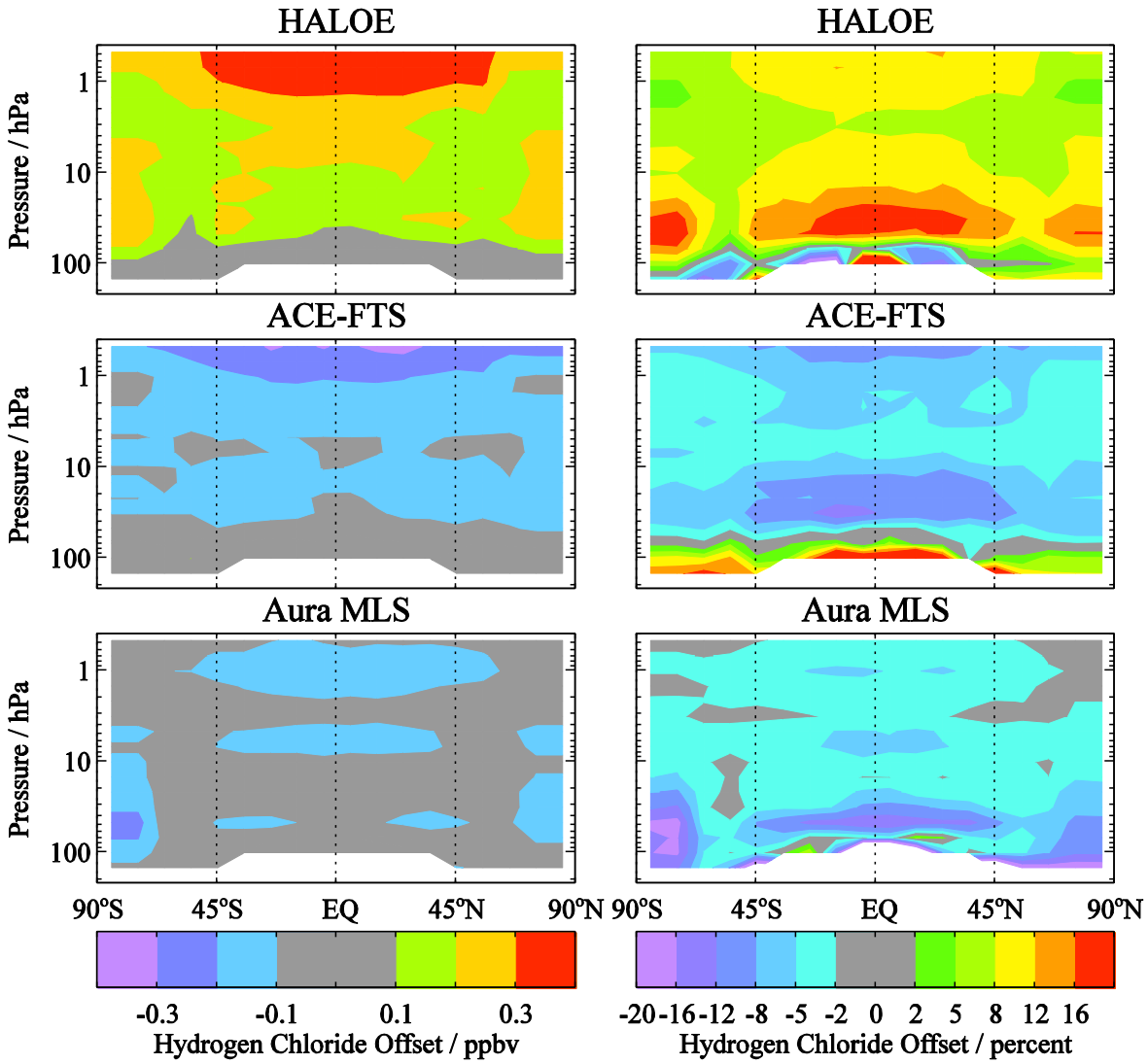

Fig. 2. Offsets applied to the HCl source datasets (top panels for HALOE, middle panels for ACE-FTS, bottom panels for Aura MLS) as a function of latitude and pressure. The left column gives offsets in ppbv and the right column provides offsets as a percent of the zonal average merged mixing ratios during the overlap period (Aug. 2004 – Nov. 2005) used here to compute the average offsets.

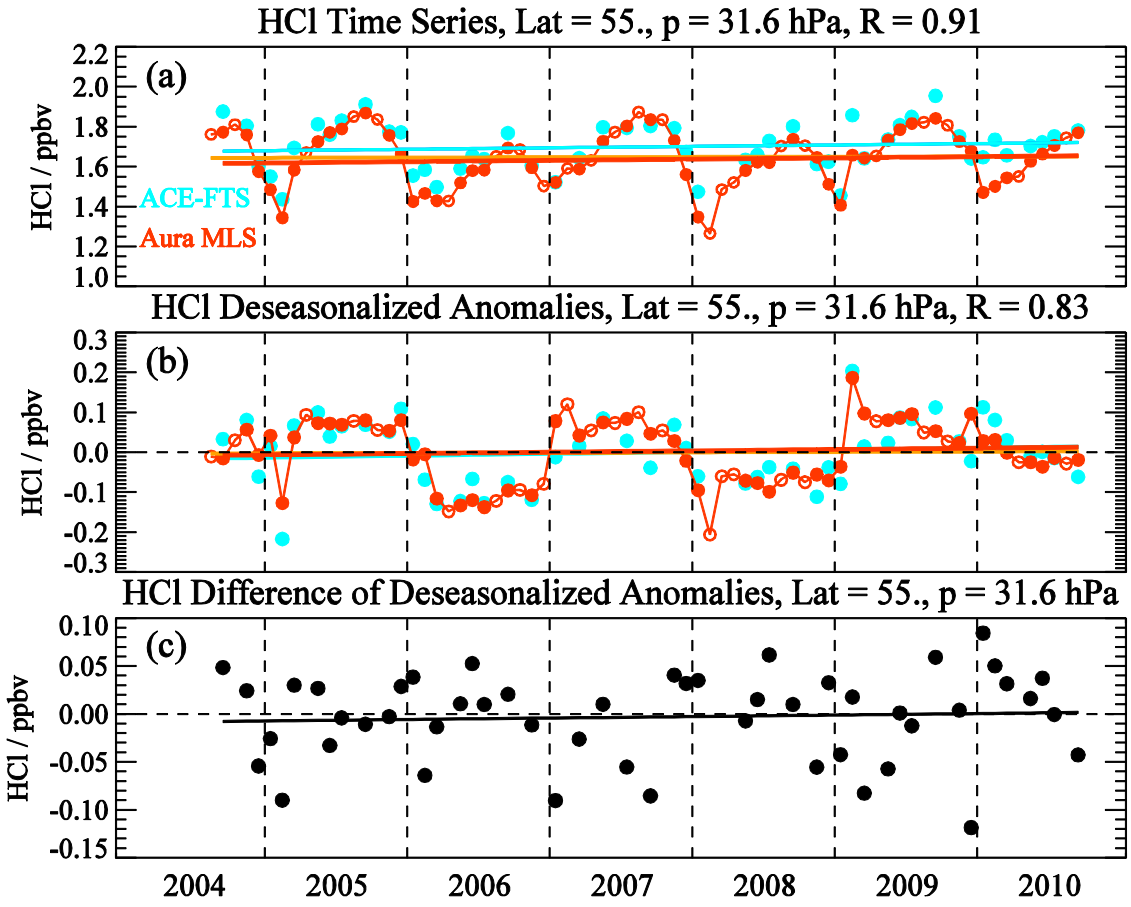

Fig. 3. Example of HCl time series analyses for 50°N-60°N and 32 hPa. (a) HCl monthly mean source data from ACE-FTS and Aura MLS; the MLS dots are filled when there is time overlap with ACE-FTS, and open if no such overlap exists. Simple linear fits are shown as colored lines for ACE-FTS and for Aura MLS (orange line for all red dots and red line for filled red dots only). Correlation coefficient values (R values) for the two time series are provided in the title. (b) Deseasonalized anomalies for both ACE-FTS and Aura MLS, with corresponding linear fits (and R values). (c) Difference of deseasonalized anomalies (ACE-FTS minus Aura MLS), with linear fit.

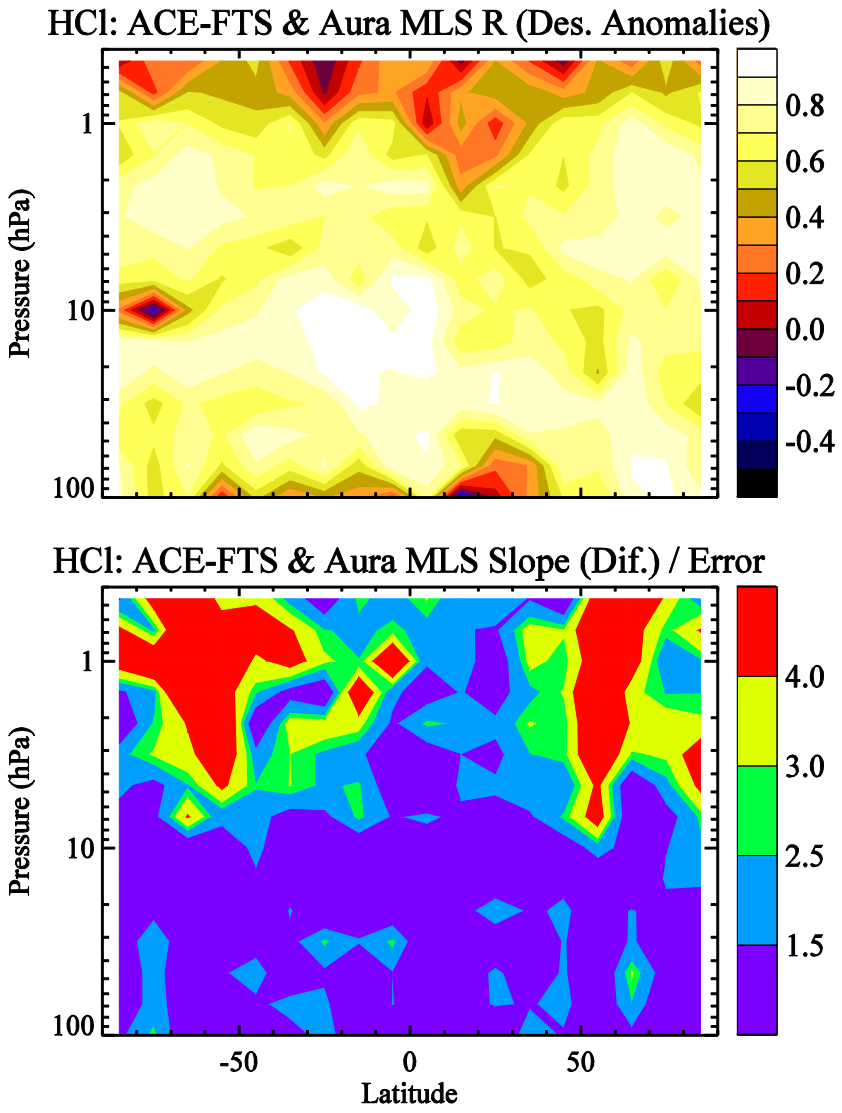

35

36 **Fig. 4.** Latitude/pressure contours of time series diagnostics obtained from analyses illustrated in
37 Fig. 3 for HCl from Aura MLS and ACE-FTS. Top panel: Correlation coefficient for the deseasonalized
38 time series. Bottom panel: Ratio of the slope of the difference between deseasonalized series over the
39 error in this slope.

40

41

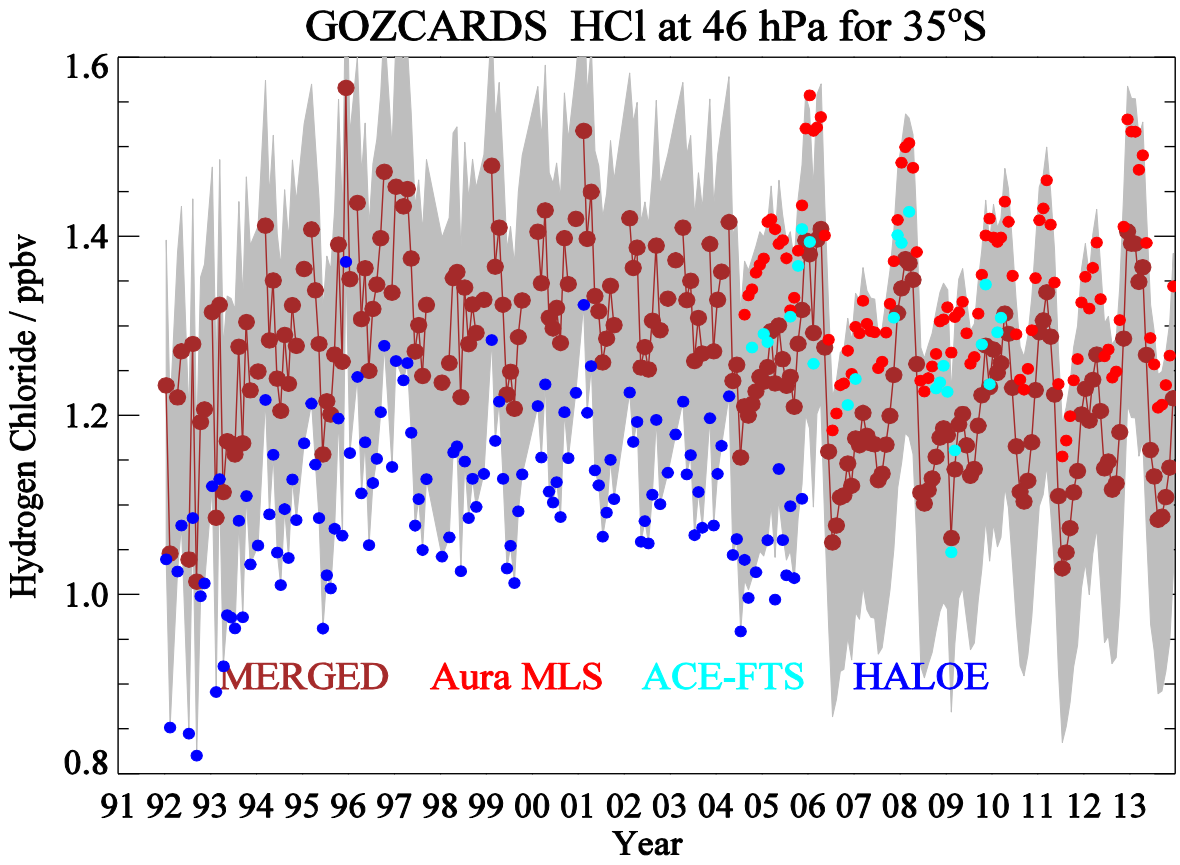

Fig. 5. Illustration of GOZCARDS HCl monthly averages with systematic error estimates (shown as grey shading) at 46 hPa for 30°S-40°S; see text for the meaning of this shaded region. The source data from HALOE, Aura MLS, and ACE-FTS are shown in different colors (see legend), along with the merged values.

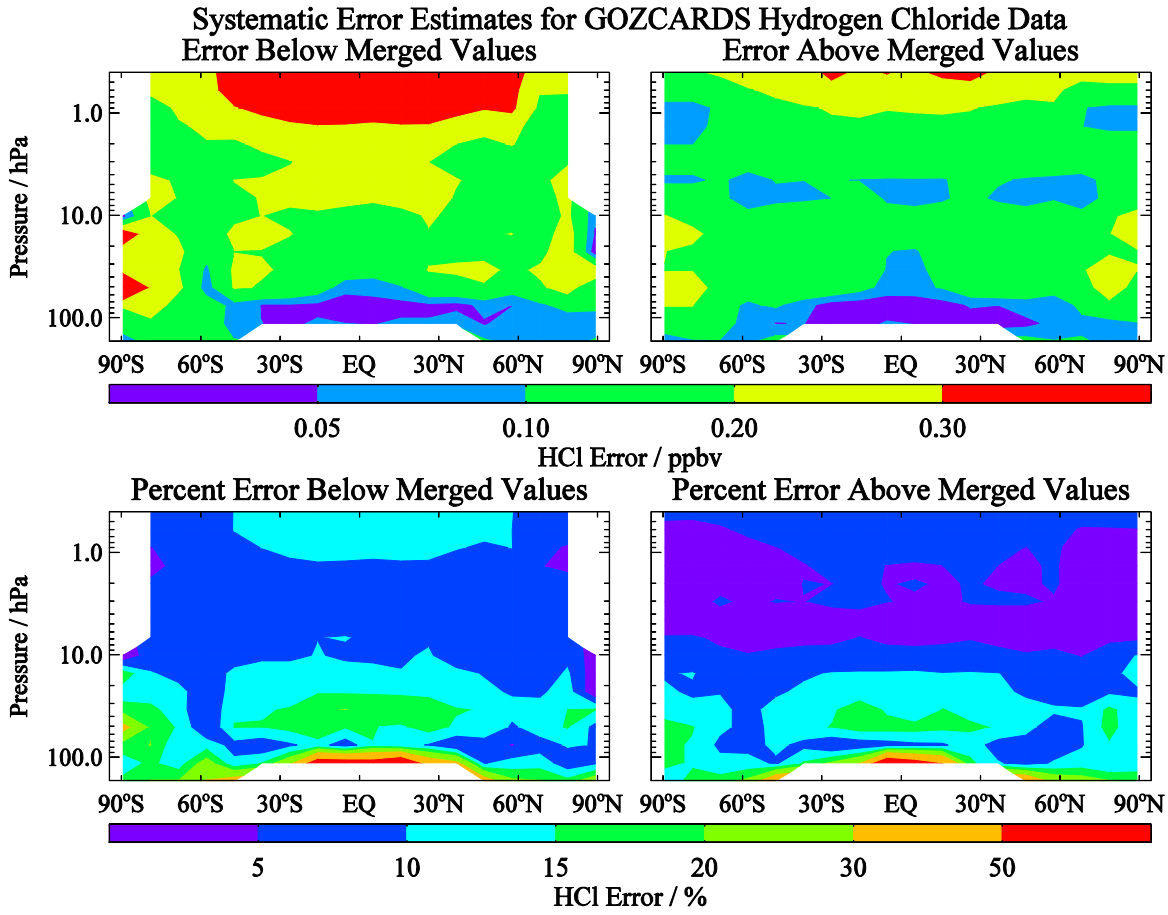

Fig. 6. Systematic error estimates for GOZCARDS HCl. One error (left panels) is relevant for values lower than (below) the merged values, and one (right panels) for values larger than the merged values; the top panels give the error estimates in ppbv, and the bottom panel errors are expressed as percent of the average merged values over the relevant time periods (see text). These error bars provide a range within which 95% of the source data values lie.

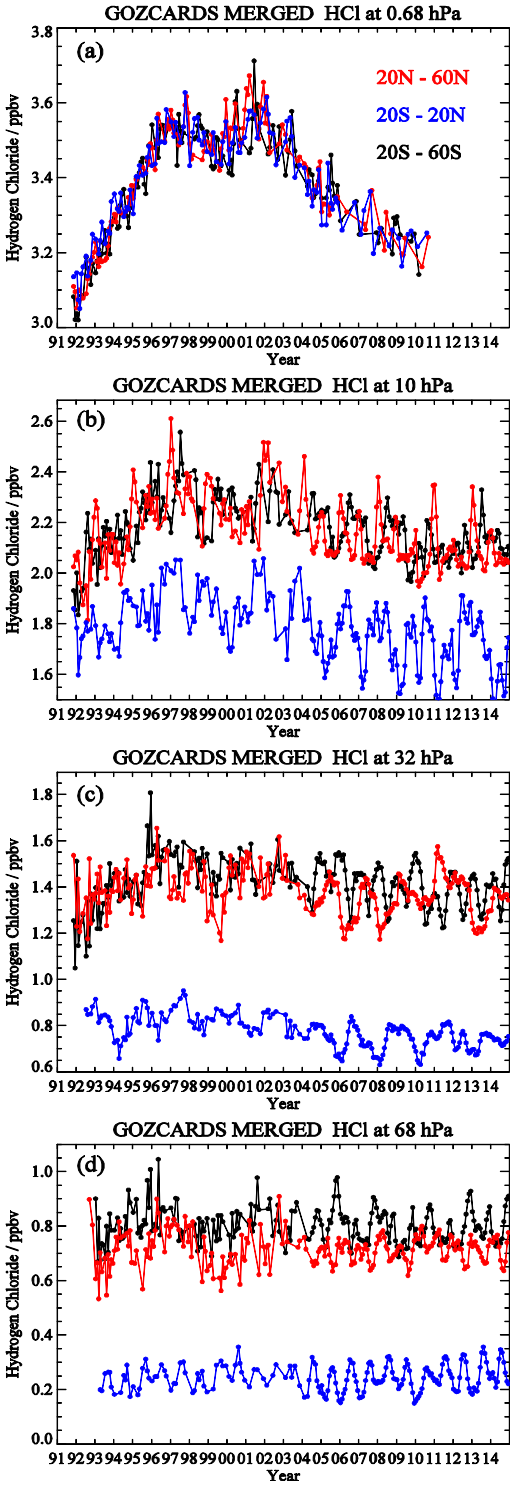

Fig. 7. Time series of the GOZCARDS monthly-averaged merged HCl abundance for 3 different latitude bin averages (see color legend in panel (a)) for (a) 0.7 hPa, (b) 10 hPa, (c) 32 hPa, and (d) 68 hPa.

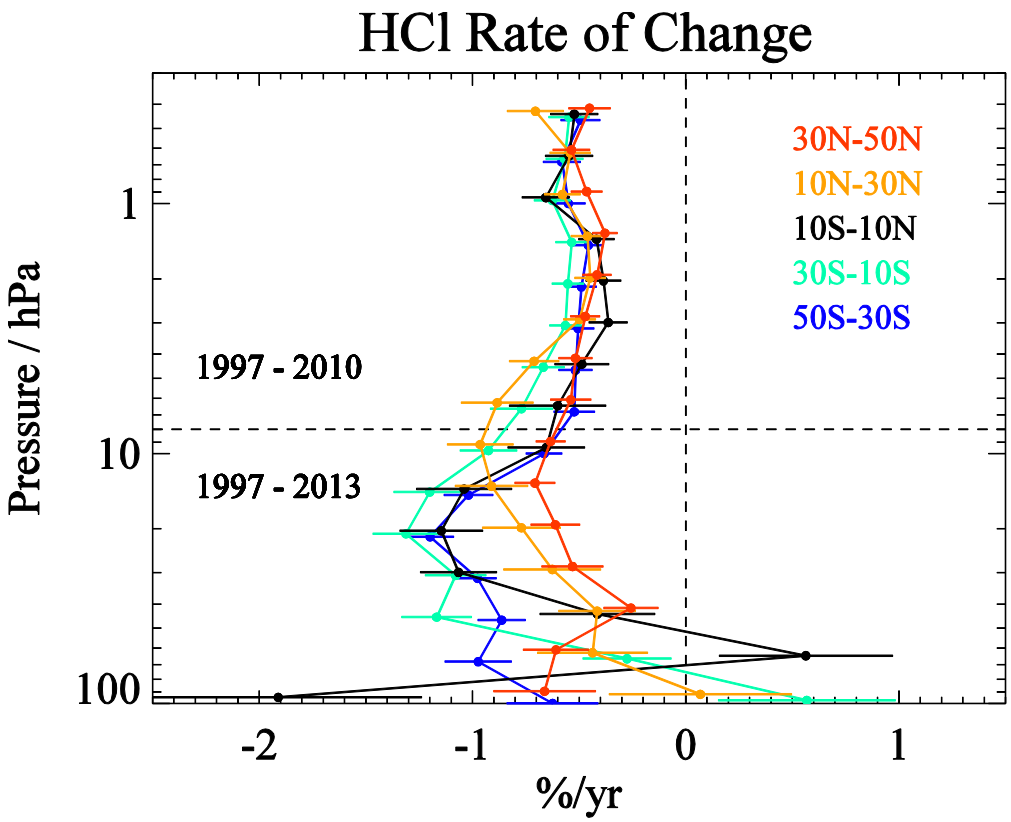

Fig. 8. The average rate of change (percent per year) for HCl as a function of pressure for different latitude bin averages (see legend) for time periods corresponding to the appropriate GOZCARDS HCl values (see text) in the upper stratosphere (Jan. 1997 - Sep. 2010) and lower stratosphere (Jan. 1997 - Dec. 2012). Deseasonalized monthly data were used to obtain a long-term trend for these time periods; two-sigma error bars are shown.

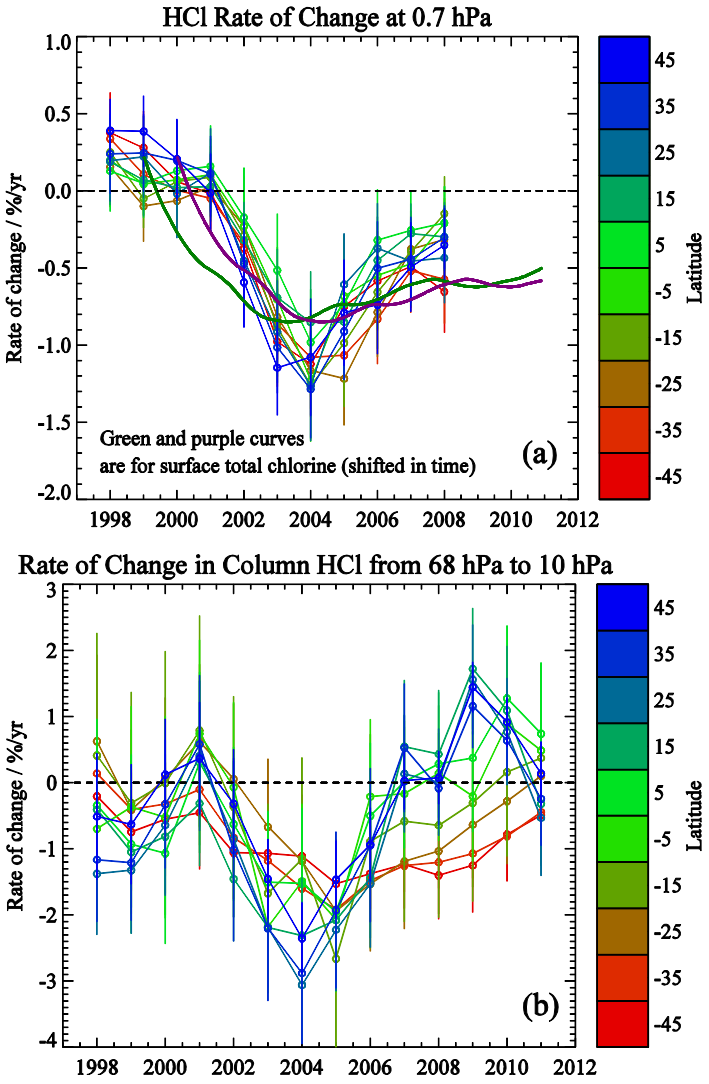

Fig. 9. Rates of change for GOZCARDS HCl (connected open circles) are given as a function of latitude in 10° latitude bins for sliding 6-year periods centered on Jan. 1 of each year (e.g., the 1998 point is an average for data from 1995 through 2000, and the 2011 point is for data from 2008 through 2013). (a) is for changes in upper stratospheric HCl at 0.7 hPa and (b) is for the change in the integrated HCl column between 68 hPa and 10 hPa. The two additional curves in (a) represent the rates of change in the estimated surface total chlorine from NOAA data (green is for a 6-year time shift, and purple for a 7-year time shift, to account for transport time to the upper stratosphere); see text for more details. Error bars indicate twice the standard errors in the means.

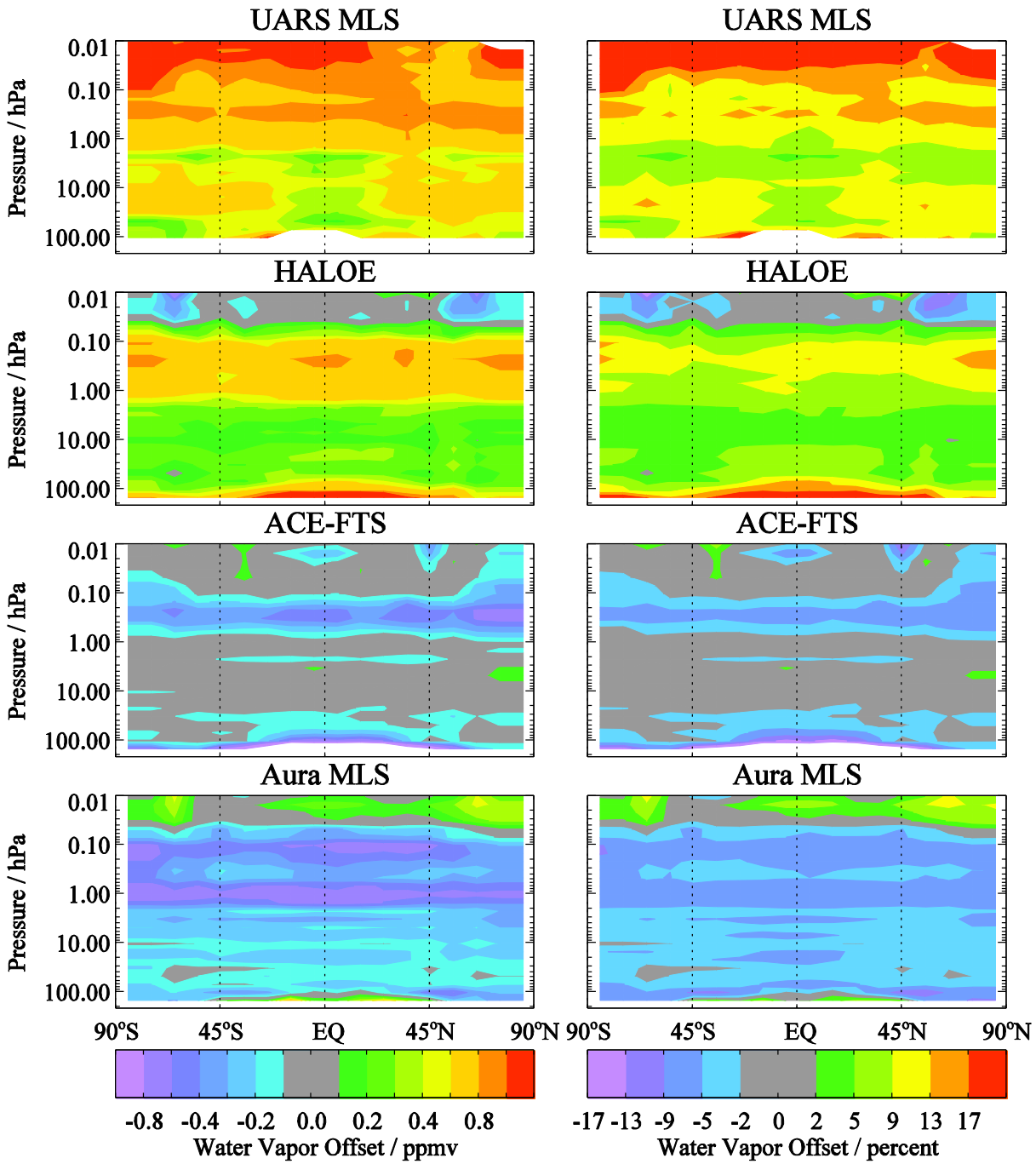

105

106

107 **Fig. 10.** Offsets applied to the H_2O source datasets as a function of latitude and pressure, similar to

108 Fig. 2 for HCl.

109

110

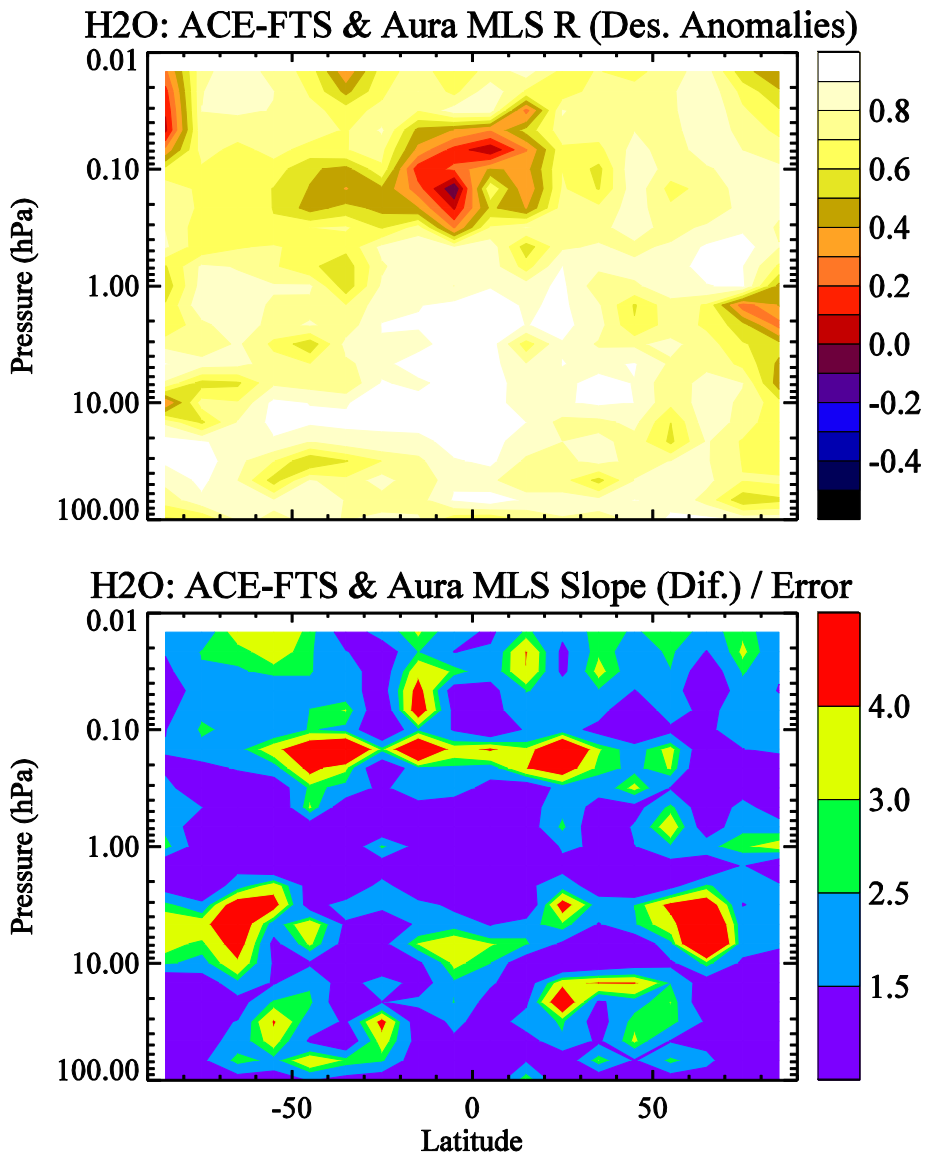

Fig. 11. Latitude/pressure contours of time series diagnostics for H_2O from Aura MLS and ACE-FTS; this is similar to Fig. 4 for HCl.

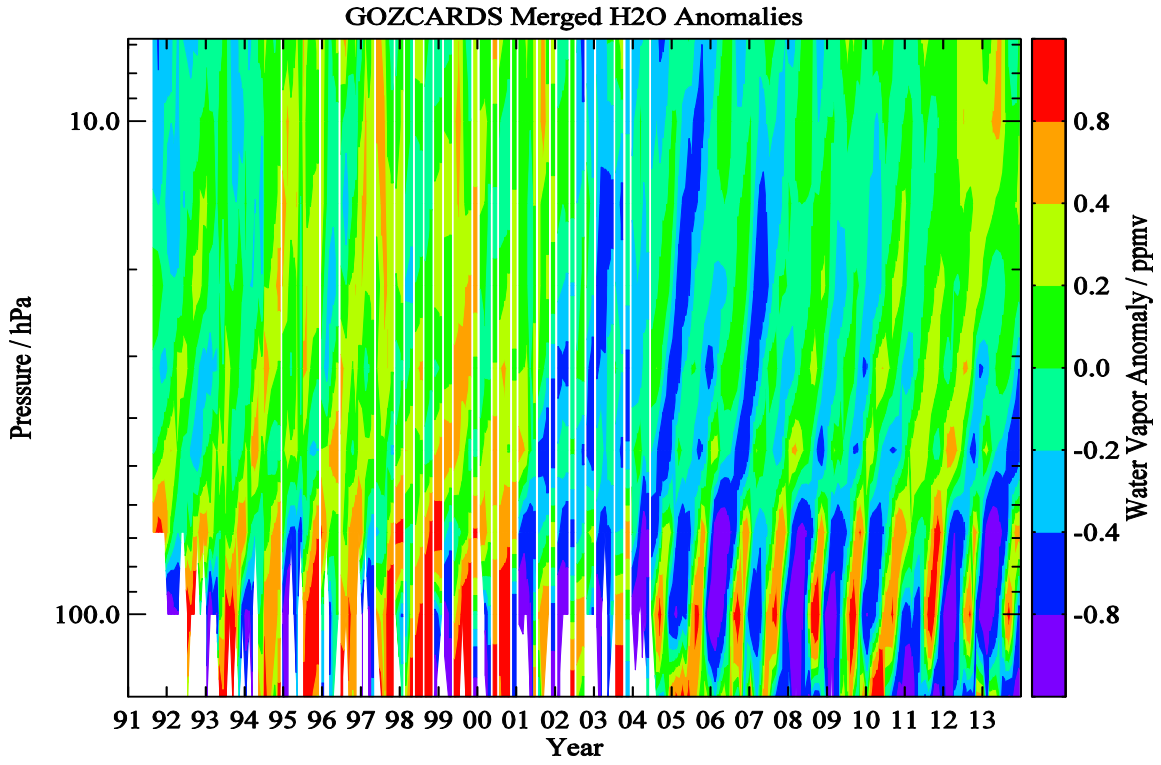

Fig. 12. A depiction of the "tape recorder" evolution for tropical water vapor abundances from 147 to 10 hPa for October 1991 through December 2013. This plot was produced from GOZCARDS merged H_2O time series anomalies (differences from the long-term means) for the average of the 4 tropical bins covering 20°S to 20°N.

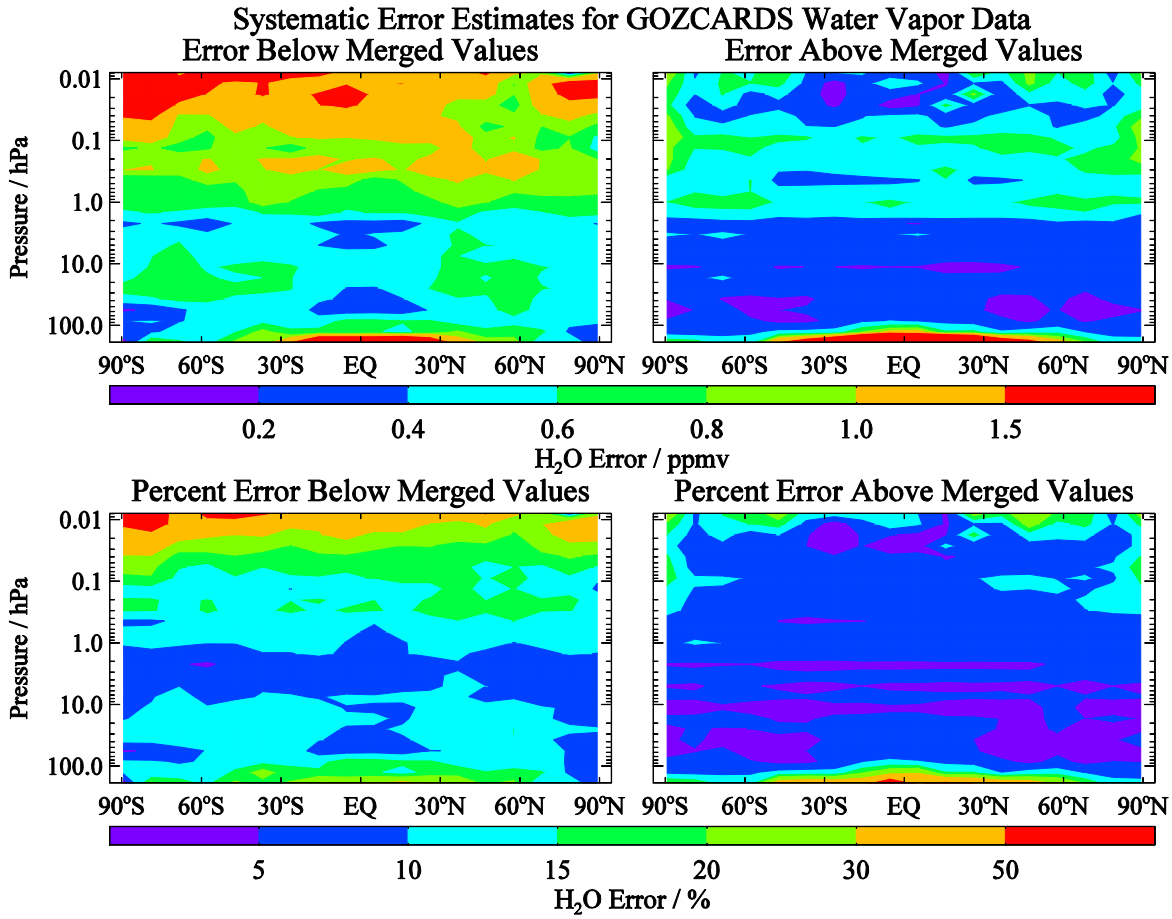

Fig. 13. Systematic error estimates for GOZCARDS H_2O (similar to Fig. 6 for HCl).

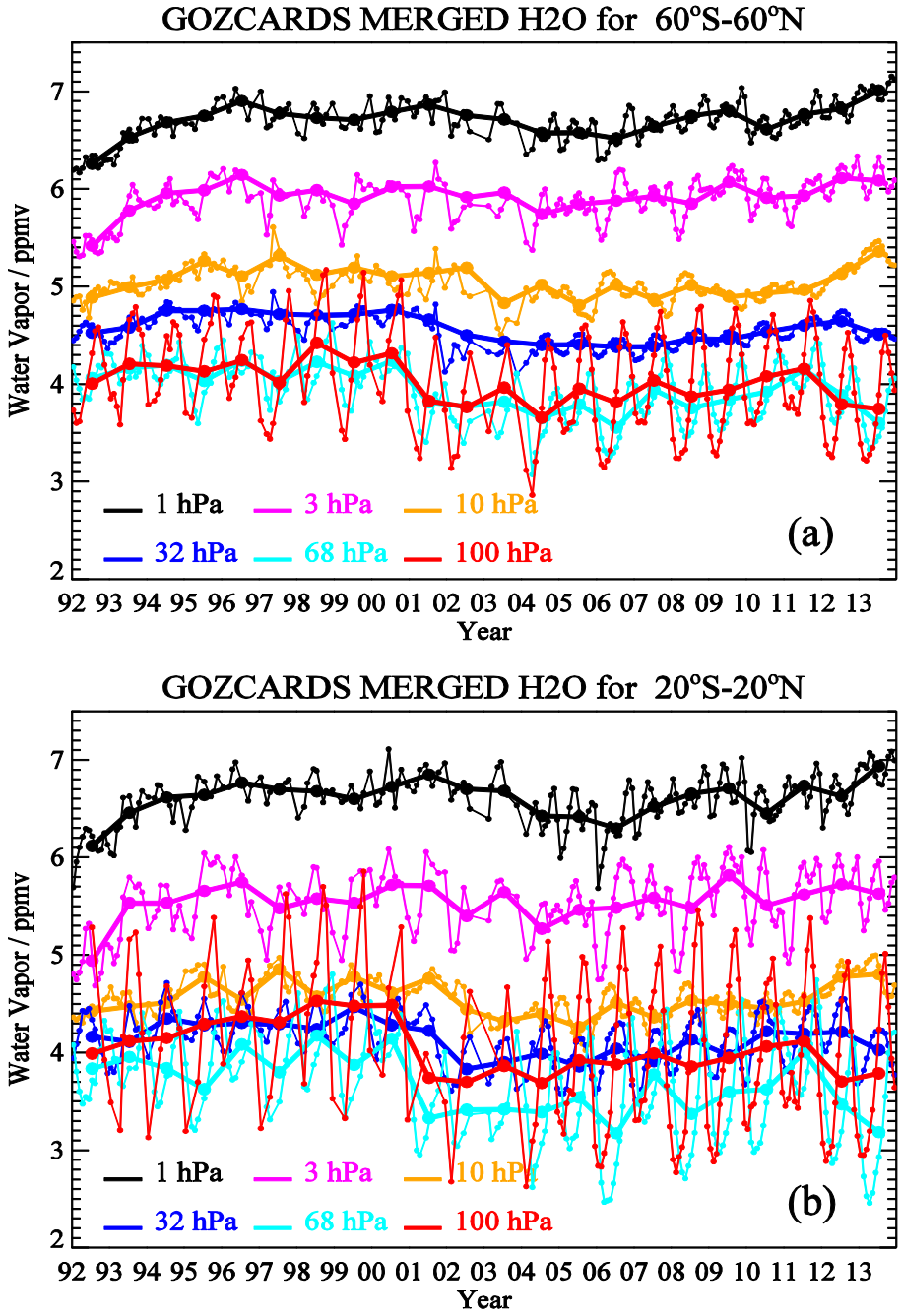

Fig. 14. Variations in stratospheric water vapor from the GOZCARDS H_2O merged data records (1992 through 2013) averaged from (a) 60°S to 60°N and (b) 20°S to 20°N. Monthly average values and annual averages are shown by thin and thick lines (connecting similarly-colored dots), respectively, for the pressure levels indicated in the plot legend.

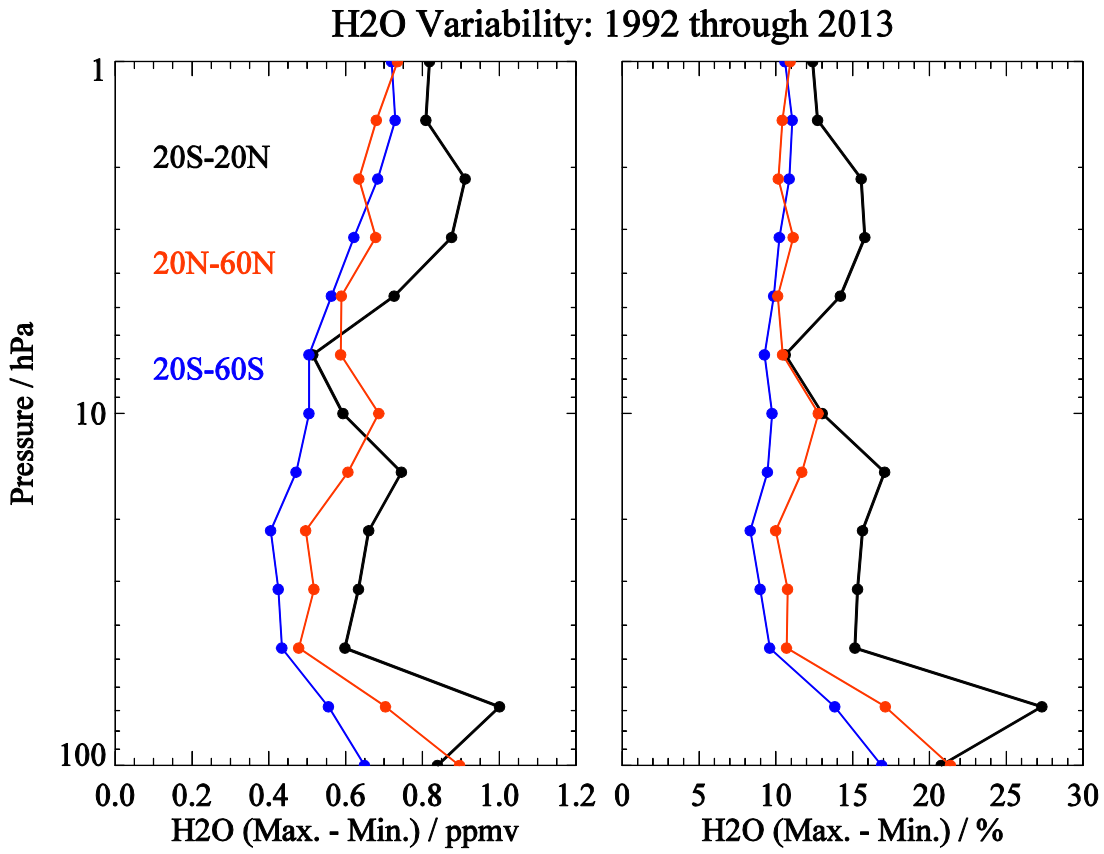

Fig. 15. Stratospheric water vapor variability on decadal timescales for 1992 through 2013 for tropical (20°S-20°N in black) and mid-latitude (20°N-60°N in red and 20°S-60°S in blue) zonal means, based on the GOZCARDS merged H_2O data record. The variability is expressed here as the difference between maximum and minimum annual average abundances, from 100 to 1 hPa, in ppmv (left panel) and percent (right panel).

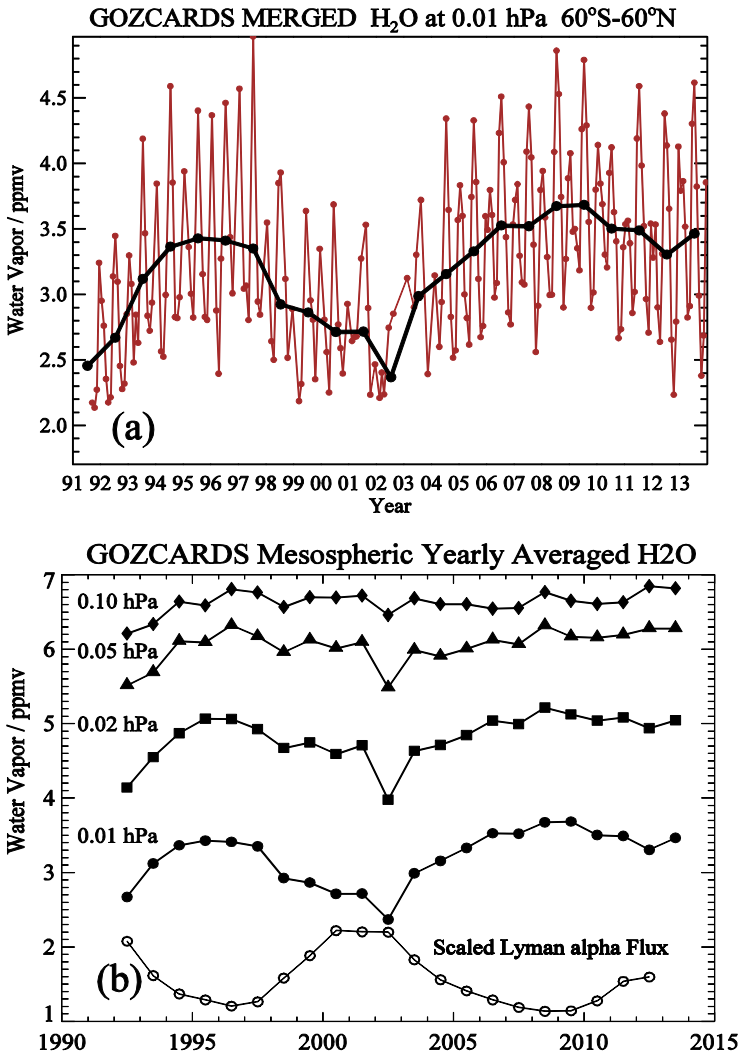

Fig. 16. (a) Variations in upper mesospheric (0.01 hPa) water vapor mixing ratios averaged from 60°S to 60°N for Oct. 1991 through Dec. 2013, based on the GOZCARDS merged H_2O data records. Monthly average values and annual averages are shown by connected brown dots and connected black dots, respectively. (b) GOZCARDS merged H_2O annual averages (connected filled symbols) from 60°S to 60°N for 1992 through 2013 at pressure levels between 0.1 and 0.01 hPa. A time series of annually-averaged Lyman α solar flux values (open circles), scaled to arbitrary units, is also displayed (see text).

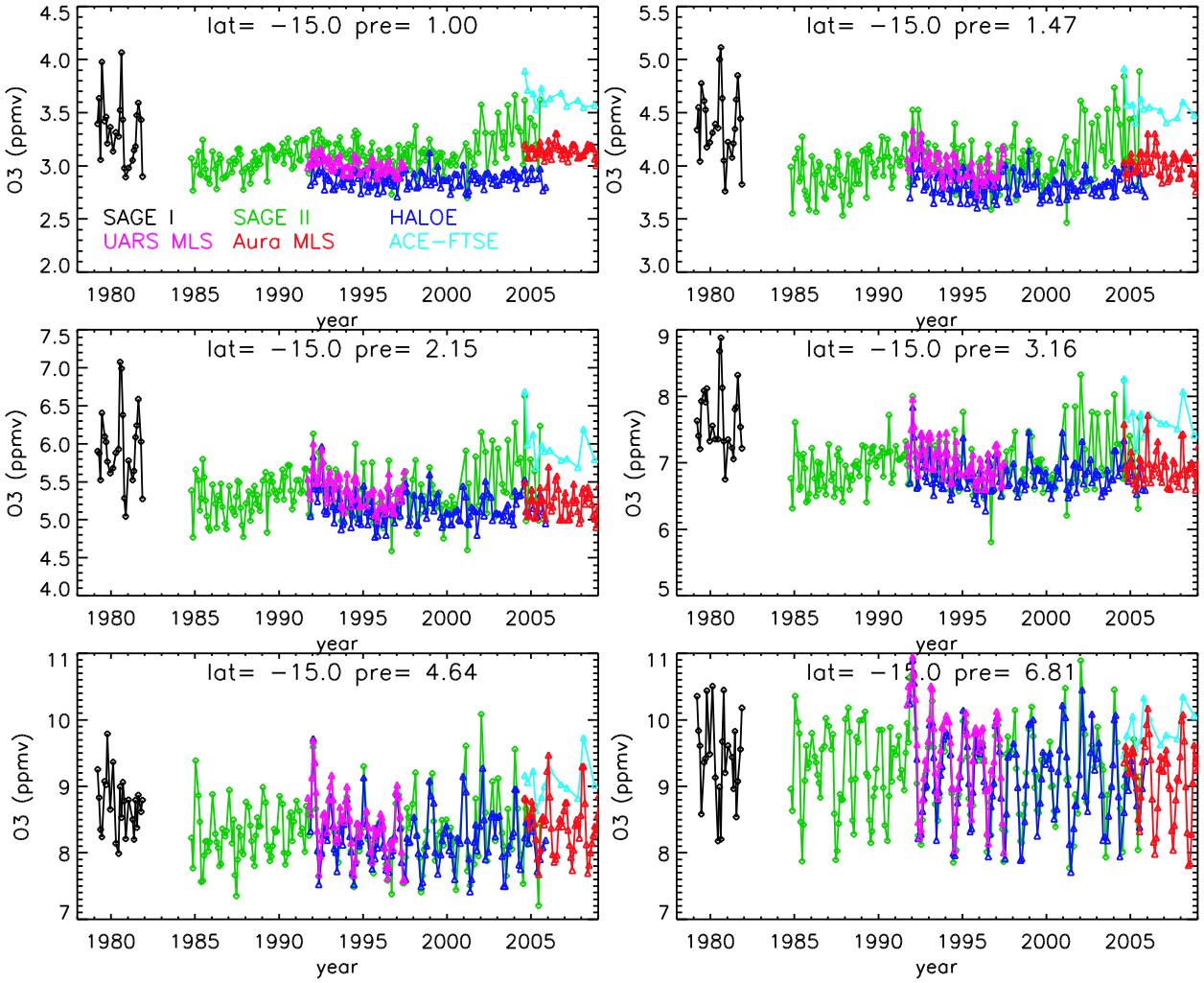

Fig. 17. Time series of monthly zonal mean O_3 for 10°S - 20°S between 1 hPa and 6.8 hPa (with pressure values given by ″pre″) from SAGE I, SAGE II, HALOE, UARS MLS, Aura MLS, and ACE-FTS, all color-coded following the legend in top left panel.

173 .

174

175

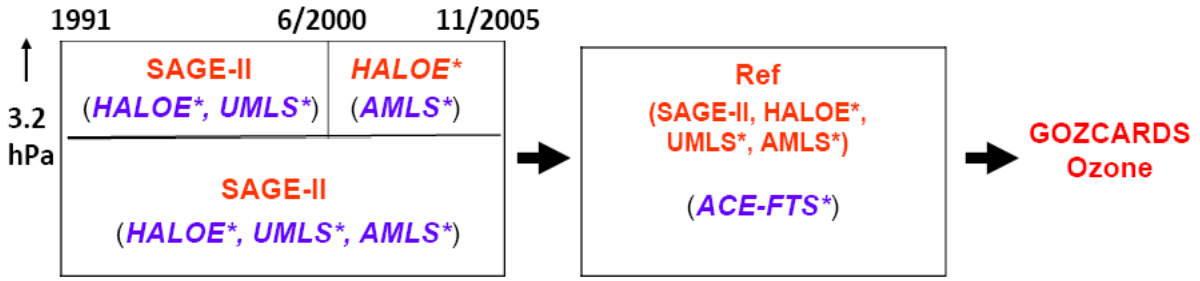

176

177 **Fig. 18.** Schematic diagram describing the creation of the merged GOZCARDS monthly zonal mean
178 ozone data record from various satellite datasets. Instruments represented in red inside the boxes are used
179 as a reference. Instruments whose measurements have already been adjusted to a reference are indicated
180 with a "*" superscript. AMLS refers to Aura MLS and UMLS to UARS MLS. See text for more details.

181

182

183

184

185

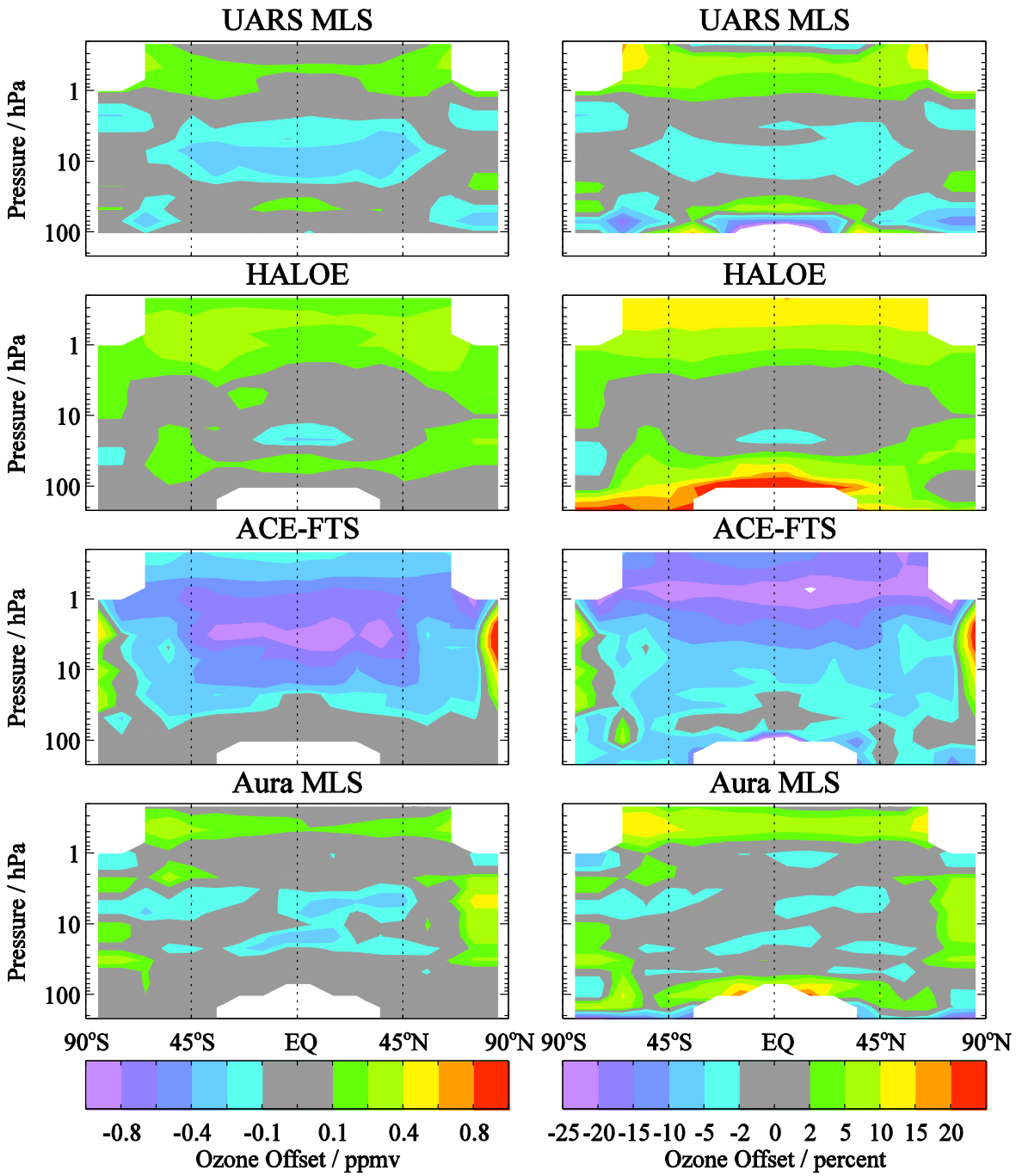

186

187 **Fig. 19.** Offsets applied to the O_3 source datasets, similar to Fig. 2 for HCl.

188

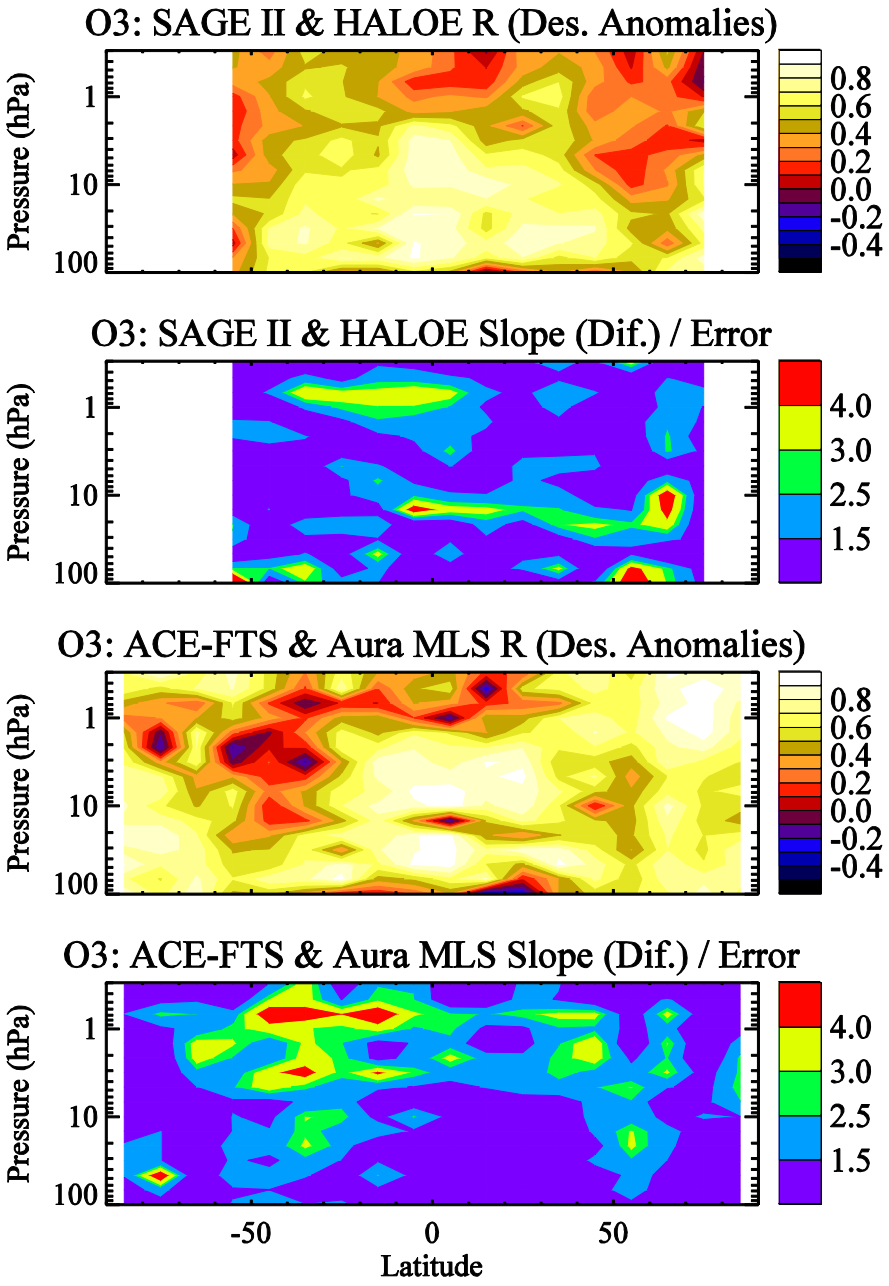

Fig. 20. Latitude/pressure contours of time series diagnostics for O_3 from Aura MLS and ACE-FTS; this is similar to Fig. 4 for HCl. The correlation coefficients (R values) and slope trend diagnostics are provided for HALOE versus SAGE II in the top two panels (for 1993-1999 as the trend issue for converted SAGE II data occurs after mid-2000 and to avoid Pinatubo-related data gaps before 1993) and for ACE-FTS versus Aura MLS in the bottom two panels (for 2005-2009).

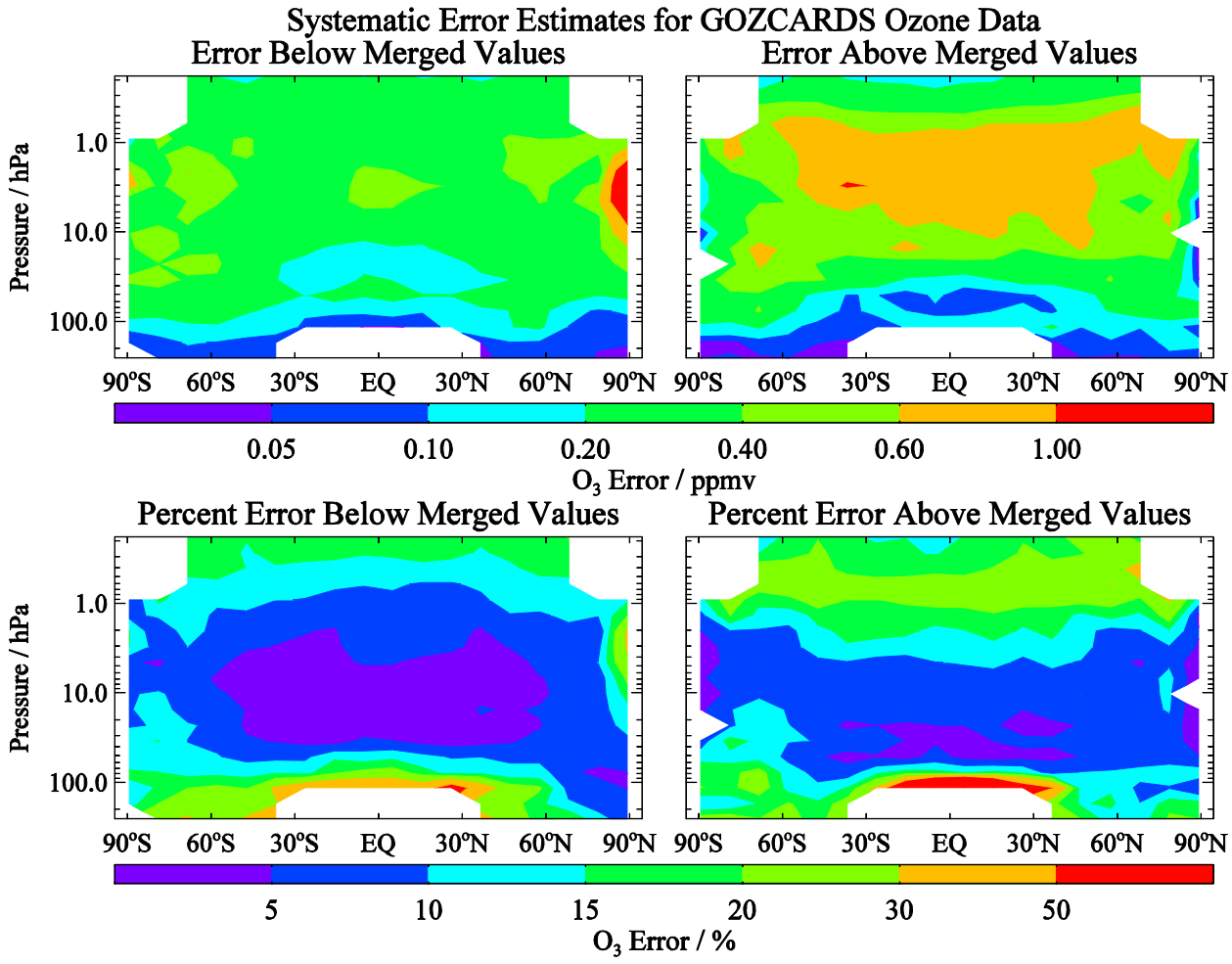

Fig. 21. Systematic error estimates for GOZCARDS O_3 (similar to Fig. 6 for HCl).

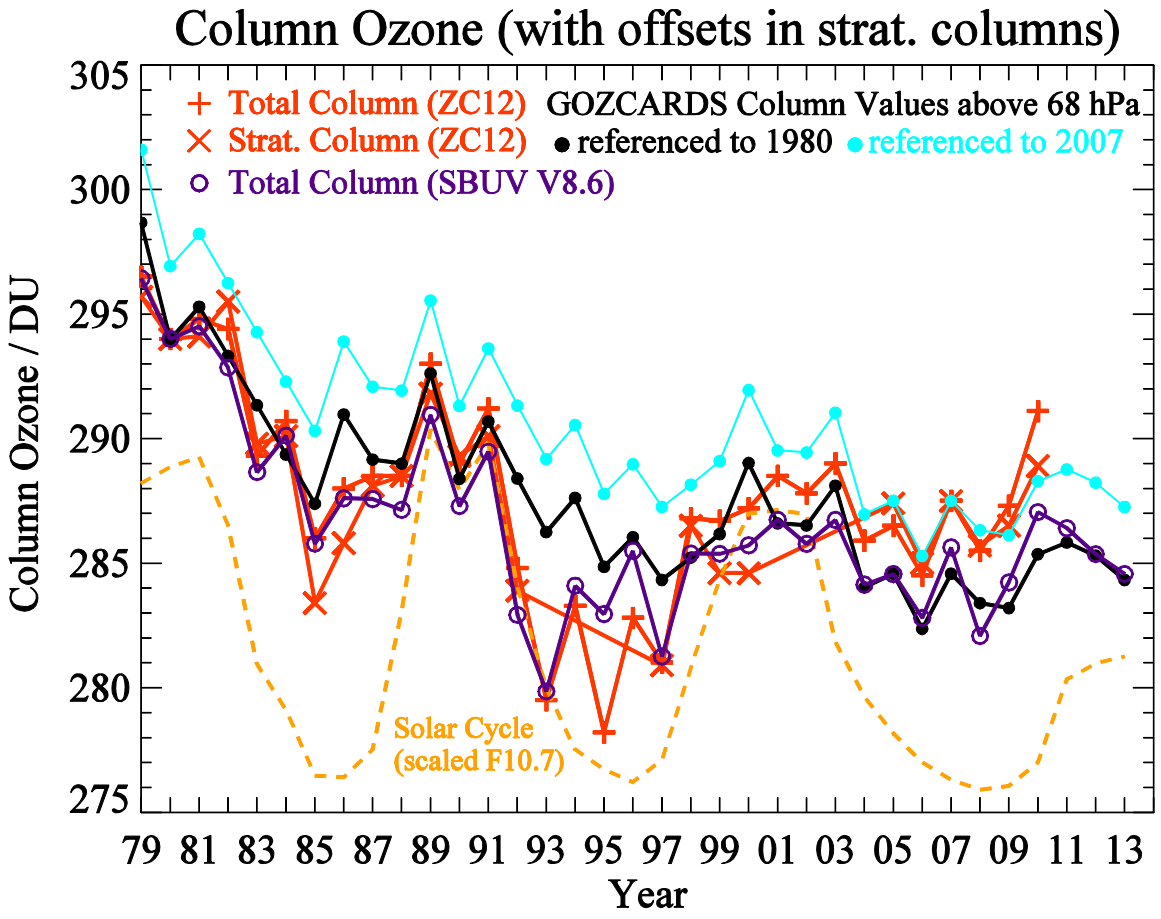

Fig. 22. Near-global (60°S to 60°N) results for average column ozone (total and stratospheric, from *Ziemke and Chandra*, 2012) compared to GOZCARDS O_3 columns above 68 hPa. Stratospheric columns are offset to better match the total column values, in order to more easily compare relative variations versus time; the black dots and red crosses are referenced to the 1980 total column values, while the cyan curves are referenced to 2007 to better illustrate the fits in the later years. Also shown (as purple open circles) are yearly-averaged total column data (60°S to 60°N) from the SBUV Merged Ozone (V8.6) Dataset (see text); these values were adjusted upward slightly (by 0.8 DU) to match the ZC12 total column values in 1980.

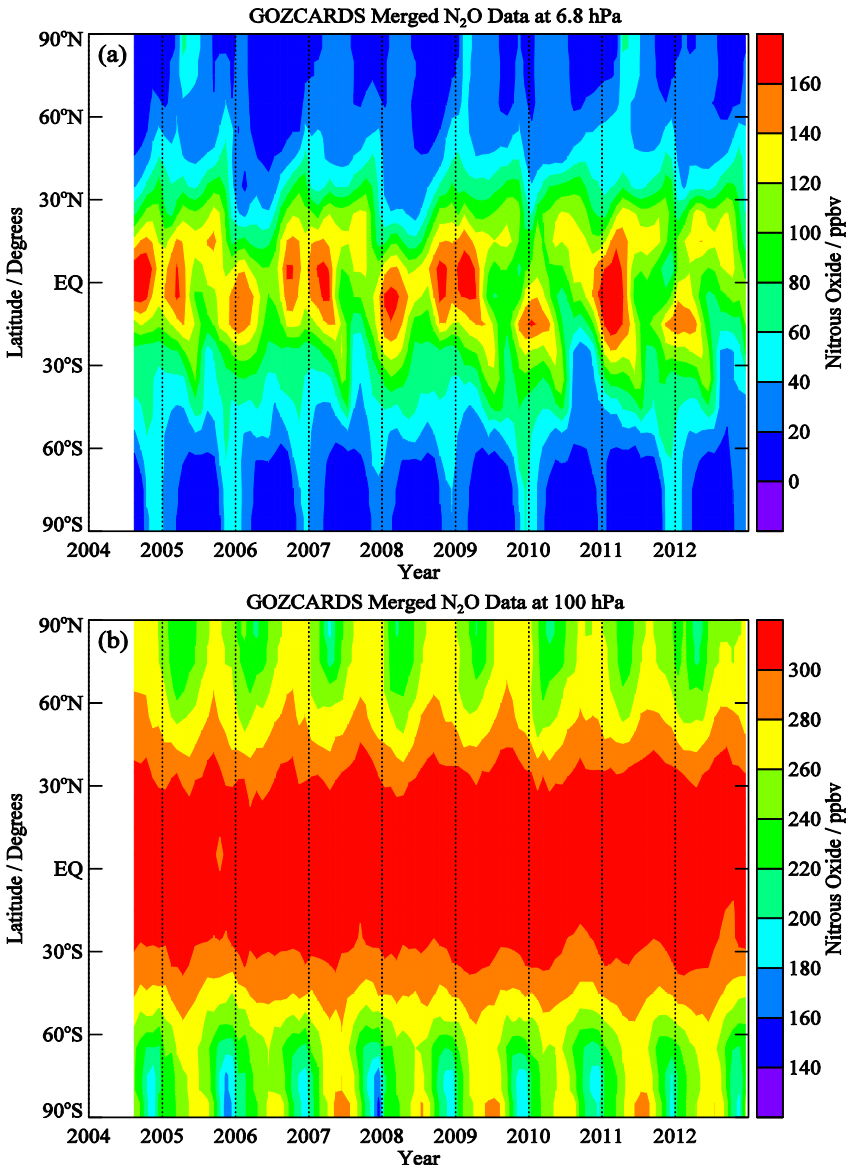

220

221 **Fig. 23.** Time evolution (Aug. 2004 through 2012) versus latitude of GOZCARDS merged N_2O (ppbv) at
222 (a) 6.8 hPa and (b) 100 hPa.

223

224

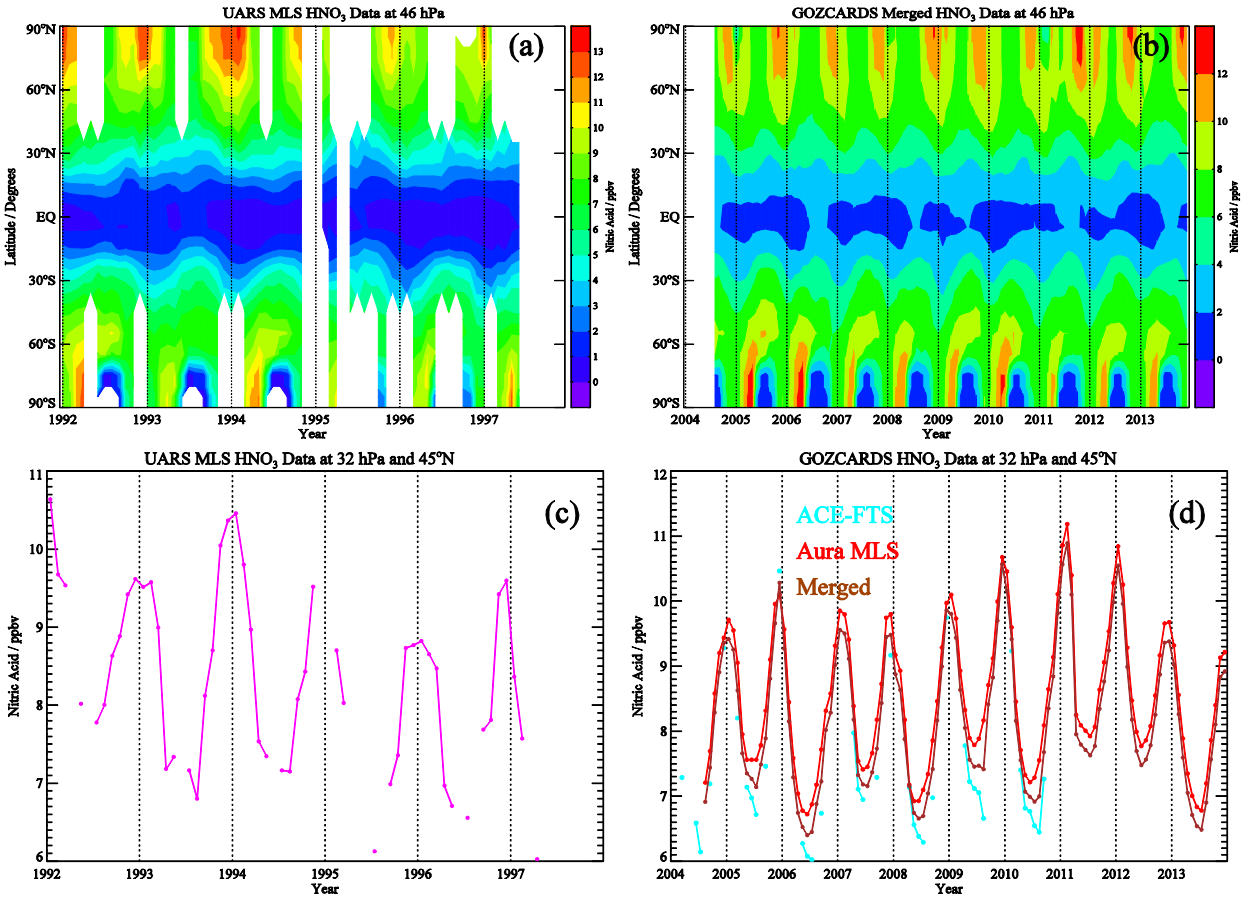

Fig. 24. Sample results display the time evolution of satellite-retrieved HNO_3 (ppbv) for two different periods, 1992-1997 in (a) and (c) versus 2004-2013 in (b) and (d). Panels (a) and (b) are contour plots at 46 hPa from UARS MLS global data and the merged GOZCARDS global data after 2004, respectively; (c) and (d) show time series at 32 hPa and for the 40°N-50°N latitude bin, with (a) from UARS MLS data, and (d) from ACE-FTS, Aura MLS, and the merged combination (between the two source data sets).